Chip-Scale Gas Chromatography

MUHAMMAD AKBAR

Dissertation submitted to the faculty of the Virginia Polytechnic Institute and State University in partial fulfillment of the requirements for the degree of

Doctor of Philosophy

In

Electrical Engineering

Masoud Agah, Chair

Gary W. Rice

Kang Xia

Leyla Nazhandali

Mantu K. Hudait

August 6th, 2015
Blacksburg, Virginia USA

Keywords: MEMS, Gas Chromatography, Nanotechnology, Chemical Detectors, Lab-on-a-Chip, Microfluidics, Separation Column

Chip-Scale Gas Chromatography

Muhammad Akbar

Abstract

Instrument miniaturization is led by the desire to perform rapid diagnosis in remote areas with high throughput and low cost. In addition, miniaturized instruments hold the promise of consuming small sample volumes and are thus less prone to cross-contamination. Gas chromatography (GC) is the leading analytical instrument for the analysis of volatile organic compounds (VOCs). Due to its wide-ranging applications, it has received great attention both from industrial sectors and scientific communities. Recently, numerous research efforts have benefited from the advancements in micro-electromechanical system (MEMS) and nanotechnology based solutions to miniaturize the key components of GC instrument (pre-concentrator/injector, separation column, valves, pumps, and the detector). The purpose of this dissertation is to address the critical need of developing a micro GC system for various field-applications. The uniqueness of this work is to emphasize on the importance of integrating the basic components of µGC (including sampling/injection, separation and detection) on a single platform. This integration leads to overall improved performance as well as reducing the manufacturing cost of this technology. In this regard, the implementation of micro helium discharge photoionization detector (µDPID) in silicon-glass architecture served as a major accomplishment enabling its monolithic integration with the micro separation column (µSC). For the first time, the operation of a monolithic integrated module under temperature and flow programming conditions has been demonstrated to achieve rapid chromatographic analysis of a complex sample. Furthermore, an innovative sample injection mechanism has been incorporated in the integrated module to present the idea of a chip-scale µGC system. The possibility of using µGC technology in practical applications such as breath analysis and water monitoring is also demonstrated. Moreover, a nanotechnology based scheme for enhancing the adsorption capacity of the microfabricated pre-concentrator is also described.

Acknowledgements

Over the past four years, I have received great support and encouragement from many individuals. Dr. Masoud Agah, being my advisor deserves special appreciation for providing me this wonderful opportunity. I have learnt many valuable lessons from him that I believe will be a valuable asset for my future professional endeavors. I am grateful to Dr. Agah for his guidance and making this a thoughtful and rewarding journey. I was also lucky enough to have collaborated with Dr. Gary Rice (Associate Professor in the Department of Chemistry, College of William and Mary, Williamsburg) and Dr. Randy Heflin (Professor in the Department of Physics and Associate Dean for Research, College of Science, Virginia Tech). I benefited a lot from their experience, insight and scientific approach. I am extremely grateful to my PhD Advisory Committee- Dr. Gary Rice, Dr. Kang Xia, Dr. Mantu Hudait and Dr. Leyla Nazhandali for their time, advice and invaluable feedback to accomplish several research milestones.

Additionally, a big thank you is owed to the current members and alumni of VT MEMS Laboratory, Dr. Hamza Shakeel (NIST), Dr. Phillip Zeller (Department of Defense), Dr. Shree Narayanan (Intel) Mr. Apoorva Garg (Bloomberg), Mr. Alperen Ketene (Boeing), Mr. Michael Restaino, Mr. Yahya Hosseini, Mr. Hesam Babahosseini, Mr. Mohammad Mehdi Alemi, Ms. Sarah El-Helw, Ms. Vaishnavi Srinivasaraghavan, Ms. Diana Nakidde (Intel) and Ms. Sepeedah Soltanian-Zadeh.

I am grateful to Mr. Donald Leber of the Center for MICroelectronics, Optoelectronics, and Nanotechnology (MicrON) for his availability and readiness to help whenever needed when it came to equipment malfunction in the clean room. Another thank you goes to the Department of Electrical and Computer Engineering staff, specifically Ms. Kim Medley, Ms. Becky Semones, and Mr. John Harris, for their administrative support throughout my research. I would like to also thank all the faculty and staff I interacted with during my residency at Virginia Tech for making this experience a gratifying, enjoyable and highly educational one.

I am thankful to all good friends including Mr. Tamoor Gandapur, Dr. Awais Khawar, Mr. Shafiq Ur Rahman and Dr. Waseem Ansar Malik for their encouragement and friendship.

I am eternally grateful to my father Muhammad Akhtar and my mother, my father-in-law, my mother-in-law, and my wife Dr. Iqra Binte Saeed for their endless support and prayers during my PhD studies. I appreciate the continuous support of my elder brothers Muhammad Asghar and Muhammad Afsar, my sisters, my brothers-in-law Dr. Imran Khan, Dr. Shahid Iqbal, Naveed, Usama and Talha, and my sisters-in-law. I would particularly like to mention the great support of my elder brother Flying Officer Muhammad Afzal who embraced martyrdom in 2005. He motivated me to work harder and become a better student. This dissertation is dedicated to him.

Table of Contents

List of Figures

List of Tables

Chapter 1: Introduction

I. Gas Chromatography

Over the past several decades, the progress in micro fabrication technology has revolutionized the world through the mass production of integrated circuits (IC) in large scale foundries. This development has powered the advancements in the field of computing, signal processing, communications and automobile industry. The important processes utilized in this technology involve thin film deposition, pattern transfer and etching techniques. Since the early days of this technology, there was a growing interest to extend it to non-IC world, particularly in miniaturizing the well-established analytical instruments [1].

One such paradigm of instrument was the gas chromatography (GC) system which emerged as the standard method for the analysis of complex volatile organic compounds (VOCs) mixture. The instrument was widely accepted by the analytical chemists after discovering that it could provide simple, fast and reliable solution for screening VOCs. This led to the increase in the demand for the instrument which was responded effectively by developing new gas chromatographs with improved features.

A typical bench-top GC system is shown in Fig. 1.1. It mainly includes five key components including 1) flow controller unit, 2) sample introduction module (injector/pre-concentrator), 3) separation column, 4) detector, and 5) data handling system. The flow controller unit provides the carrier gas (mobile phase) at user defined flow rate conditions. The carrier gas is usually an ultra-high purity gas (helium, nitrogen air or hydrogen) that moves the sample through the GC system. Depending on the application, the sample injection unit can involve either an injector or a pre-concentrator step. The injector is kept at an elevated

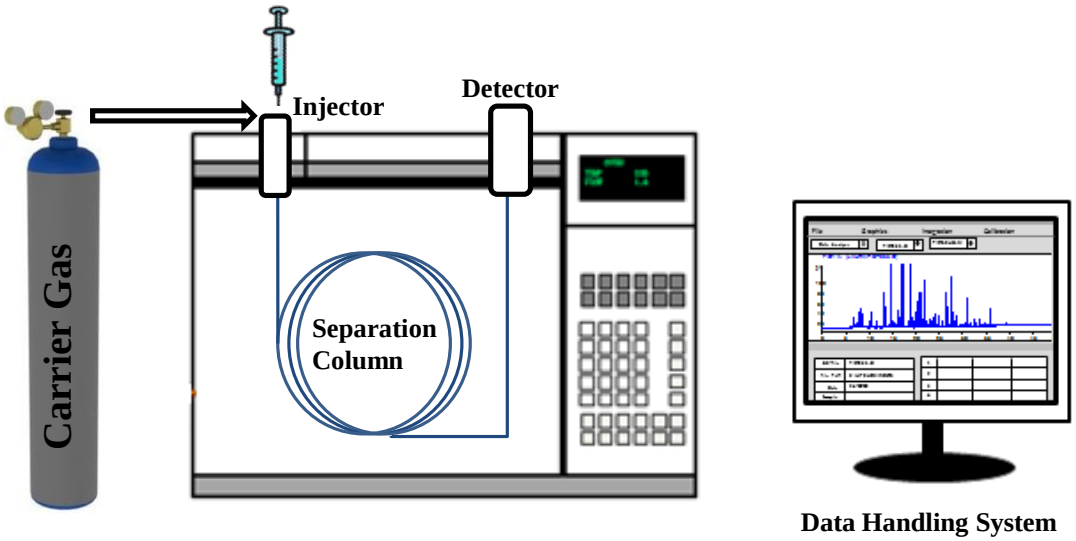

Figure 1.1 *A typical gas chromatograph.*

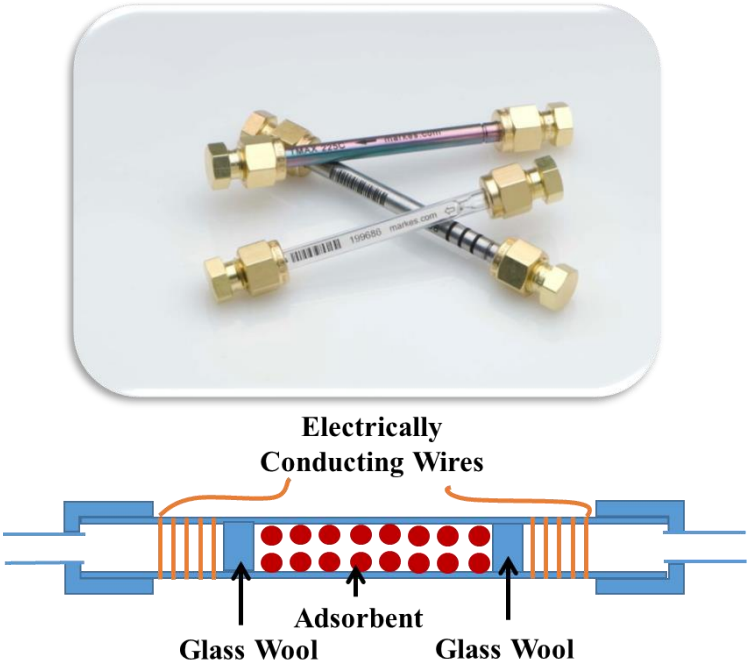

Figure 1.2 *Conventional pre-concentrators employed in gas chromatography.*

temperature to vaporize the sample which is introduced using a gas tight syringe. Normally, an injector is employed for the analysis of concentrated samples which can be easily sensed by the detector. Alternatively, if the application requires the analysis of a dilute or trace-level sample; a pre-concentration step is added to meet the detection limit of the detector. The pre-concentrator is a stainless steel tube (Fig. 1.2) which contains adsorbent material and is solely used for the collection of trace-level volatile organic compounds (VOCs) over a certain period of time. After sufficient amount of VOC collection, the pre-concentrator is thermally desorbed using electrical wire coiled around it to introduce the sample into the separation column as a concentrated plug. The column is made up of fused silica tubing whose inner walls are coated with immobilized solid or liquid phase polymer known as the stationary phase. The sample partitions between mobile and stationary phase depending upon their relative solubility and vapor pressure in the stationary phase and separates into individual components. The detector finally detects the separated compounds generating an electrical signal known as the chromatogram. The data handling system automatically integrates the peak area based on the quantity of the sample. The compounds can be easily identified by the retention times (t_r), the traverse time for each of them as they pass through the GC system.

II. GC Microfluidic Components

Although commercially available GCs were highly sophisticated instruments, the size, cost and power consumption requirements restricted the use of this technology to only laboratory-based analysis. For

instance, the heating of capillary GC column was carried out in an oven using a turbulent fan and was primarily based on convective heat transfer mechanism. This provided an excellent mean to achieve uniform heating of the column; nevertheless, heating a large size oven was extremely power-intensive. Additionally, the gas supplies (carrier or makeup gas for the detector) were supported by large size cylinders which made GC less desirable for the portable applications. These factors encouraged the interest in shrinking down the GC analytical tool to enable analysis in off-grid locations for various applications including homeland security, space and fossil fuel exploration, biomedical diagnostics and food processing.

Several research groups utilized microtechnology to revise the primary components of GC including the injector/pre-concentrator, separation column and the detector. Different materials, device designs and fabrication methodologies were investigated for each entity to improve their individual performance criteria. Most studies have used silicon as a substrate material owing to its high thermal conductivity, easy availability and convenience in fabrication by adopting already developed procedures from the semiconductor industry. In the following, we describe each entity of μGC system in detail.

A. Micro Thermal Pre-concentrator

Three mechanisms can be employed to achieve pre-concentration including absorption into the solution, cryogenic trapping and adsorption on a solid or thick polymeric surface. The former most can be useful for low volatility compounds while cryogenic trapping helps in capturing wide range of compounds and also facilitates selective adsorption. Nevertheless, the flexibility in the choice of adsorbent and simplicity makes the latter one an attractive approach to achieve pre-concentration in miniaturized devices.

A MEMS-based pre-concentrator is one of the key components of μGCs. Interest in micro thermal pre-concentrator (μTPC) continues to grow in response to ever increasing demand for more sensitive and selective micro sensing systems. Generally, μTPC consists of a micro cavity or a channel etched in silicon which is used to hold the adsorbent material. The silicon chip is then bonded to a glass substrate for packaging the device. Thin film heaters and temperature sensors are deposited on the backside of silicon and fused silica tubes are inserted into the fluidic ports of the chip to externally access the device. The sample to be concentrated is allowed to pass through the chip at a certain flow rate using a micro pump. The sampled volume (V_{sample}) can be calculated from the product of loading time and the flow rate of the micro pump. The compounds are retained on the surface of the adsorbent mainly due to the weak intermolecular interactions known as Van der Waals forces. It is worth mentioning that the electronic structure of the atom or molecule is hardly changed in the adsorption process which makes it an easily reversible process. After sufficient amount of adsorbate has been collected, thermal energy is provided to

overcome the Van der Waals bonding and to release the compounds as a concentrated plug. This thermal energy is provided by using the on-chip heaters and monitored by the on-board temperature sensors. The performance of the µTPC is evaluated in terms of a parameter known as pre-concentration factor (PF). It is the ratio of volume sampled (V_{sample}) during the process to the desorbed volume ($V_{desorbed}$),

$$PF = \frac{V_{sample}}{V_{desorbed}} = \frac{V_{sample}}{W_h \times u}$$

where desorbed volume ($V_{desorbed}$) is the width of the concentrated plug, W_h (min) multiplied by the desorption flow rate, u (ml/min).

µTPCs can be divided into three broader categories. This classification is based on the method used to deposit the adsorbent inside the cavity. The first one consists of micro-cavities or micro-channels filled with granular forms of adsorbent material [2-9]. In these devices, channels and cavities formed in silicon are filled by the adsorbent beads and then sealed (bonded) by (to) another substrate. For instance, Zellers' group [4] fabricated silicon membrane compartments that served as micro-heaters and packed them with three different carbon adsorbent granules (Carbopack B, Carbopack X and Carboxen 1000) in a multi-stage configuration. The Virginia Tech MEMS Laboratory developed, for the first time, divinylbenzene (DVB) packed µTPCs [9] for the analysis of volatile organic compounds in breath. DVB was mixed with polydimethylsiloxane (PDMS) to immobilize the 100µm particles within the 7mm x 7 mm × 0.38 mm etched cavity in silicon. The device successfully concentrated lipid oxidation products in human breath and allowed for GC/MS analysis that distinguished control breath from treated breath produced after the

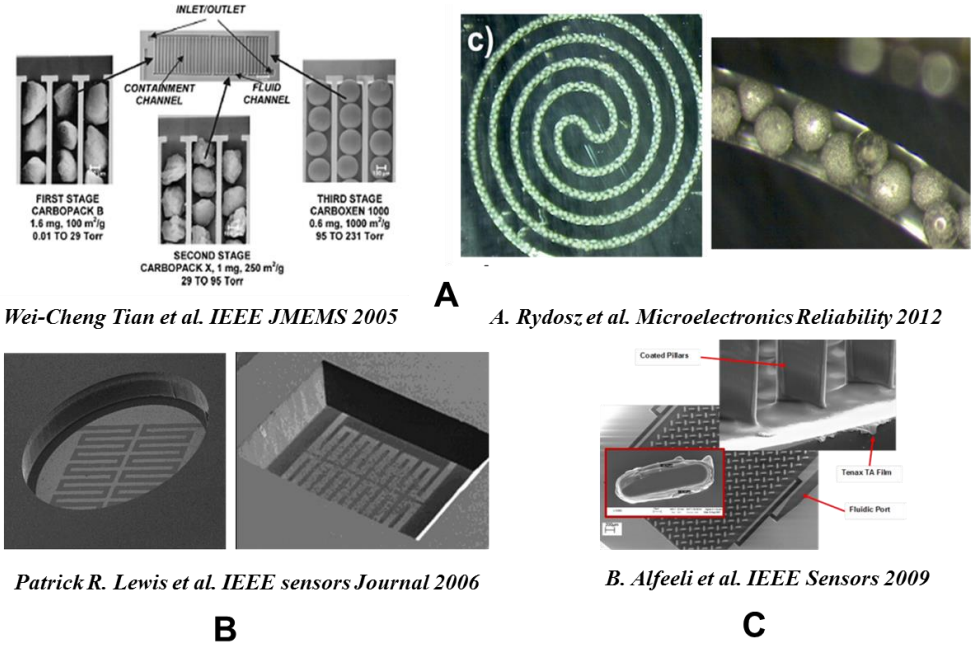

Figure 1.3 *Classification of µTCP into three categories (Adapted with permission from above mentioned sources).*

subject was dosed with iron to stimulate production of lipid oxidation products that are often used as biomarkers for disease. The second type of μTPCs utilizes adsorbent materials in thin film form [10-16] deposited on a membrane or inside microfabricated channels/cavities. Sandia National Laboratories [16] used a free-standing micro machined hotplate spray coated with sol-gel as a pre-concentrator achieving very narrow desorption peaks (~0.2 s) but having very low surface area. Spiral-shaped 30 cm-long micro channels with 1.8 μm constrictions were also studied for concentration of non-polar compounds by combining adsorption and capillary effects [11].

Packed structures can provide high adsorption capacity but they suffer from high pressure drops and high power consumption. In addition, packing μTPCs with granular adsorbents is not a batch fabrication process (resulting in higher costs) and extra care needs to be taken to ensure that the beds are inside the cavity and not preventing the chip sealing process (resulting in lower yield). The devices in the second category, on the other hand, have low power consumption and are typically manufactured with a MEMS-compatible process; however, they have limited capacity due to small surface areas. In addition, long path lengths in the microchannel structures are likely to result in partial re-adsorption (during the cooling cycle) of the desorbed sample before reaching to the end of the channel or require excessive pressure for elution. An innovative approach (third μTPC category) for increasing adsorbent sites (concentration factor) is to form closely-spaced high-aspect-ratio embedded micro pillars and to coat them with a thin film adsorbent layer. This approach has been used by researchers at the University of Illinois, Urbana Champaign (UIUC) [17] and has been extensively explored and established at VT MEMS Laboratory for both enhancing the adsorption capacity and improving the flow distribution in the microchip [18-21]. The devices in this category combines the advantages of previous two categories i.e. provide high sample capacity at the expense of low pressure drop. An example of this kind of μTPC is discussed in Chapter 2 where thin film of electroplated gold is used for breath analysis application. The μTCP devices from each category are shown in Fig. 1.3.

B. Micro Separation Columns

Separation column is the most important part of a GC system. Like their conventional counterparts, micro separation columns (μSC) consist of a channel which holds the stationary phase. This channel is mostly fabricated on silicon substrate and packaged with a Pyrex wafer. Unlike conventional columns which requires a large size oven to heat the μSC, thin film resisters and temperature sensors can be integrated on the substrate for temperature programming of μSC. μSCs can be categorized into three types, open tubular (OT), packed and multi capillary columns. The stationary phase in open tubular columns is only supported by the column wall whereas in packed columns, the stationary phase is supported by small adsorbent particles packed throughout the entire column volume. OT capillary

columns typically exhibit high efficiencies with minimal pressure drops and are the most common type of columns used in GC. Packed columns produce larger pressure drops and more eddy diffusion, thereby reducing the separation efficiency [22]. The separation efficiency of chromatographic columns can be quantified by the height-equivalent-to-a-theoretical-plate (HETP) and is expressed by following equation:

$$\mathrm{HETP} = \mathrm{A} + \frac{\mathrm{B}}{\overline{\mathrm{u}}} + \mathrm{C}\,.\,\overline{\mathrm{u}} \qquad (1)$$

where $\overline{\mathrm{u}}$ is the average linear carrier gas flow velocity. Since HETP is inversely proportional to the number of theoretical plates (N=L/HETP) which describes the column efficiency, each of the three constants A (eddy diffusion), B (longitudinal molecular diffusion in carrier gas) and C (mass transfer in stationary phase) should be minimized in order to maximize the column efficiency. For OT columns, the A term is insignificant and HETP reduces to

$$\mathrm{HETP} = \frac{\mathrm{B}}{\overline{\mathrm{u}}} + (\mathrm{C}_s + \mathrm{C}_m)\,\overline{\mathrm{u}} \qquad (2)$$

The B term, which is a measure of natural diffusion through the column decreases with increasing carrier gas velocity [22] or using a carrier gas with larger molecular weights like nitrogen or argon. The C term, which is the dominant factors in the operation of GC columns, comprises the mass transfer coefficients of the eluents between the mobile (C_s) and stationary (C_m) phases. To minimize C_s term, stationary phase with smaller thickness and larger value of diffusion coefficient should be preferred. Furthermore, the mass transfer in the mobile phase (C_m term) is due to the laminar flow and a parabolic velocity profile inside the μSC. This means the velocity of the gas molecules in the center of the column is greater than molecules near the walls, resulting in solute molecules in the center of the column moving ahead of those at the wall and causing band broadening. Capillaries with smaller diameters decrease this broadening because the mass transfer distances are shorter (a compound proximity to the column wall and stationary phase increases). The efficiency of conventional GC columns can thus be enhanced by reducing the internal diameter (I.D.), but at the price of reduced sample capacity and increased pressure drop across the column. Sample capacity is defined as the maximum amount of an eluting species that can be injected into a column without saturating the stationary phase and overloading the column [23]. The biggest advantage of packed columns is that they support more stationary phase, which provides a larger sample capacity. In OT columns, the sample capacity can be improved by increasing the coating thickness, but this can cause more band-broadening and can reduce the separation efficiency. Multicapillary columns provide high-sample capacity and higher high number of theoretical plates [24-26] compared to a corresponding single channel narrow width columns. At VT MEMS Laboratory, we have also invented a new type of column referred to as semi-packed by incorporating the properties of open channel (high efficiency) and packed columns (high sample capacity) into a single chip [24]. In semi-packed columns, the A term is minimal as the paths are fairly uniform due to the symmetrical distribution of the posts

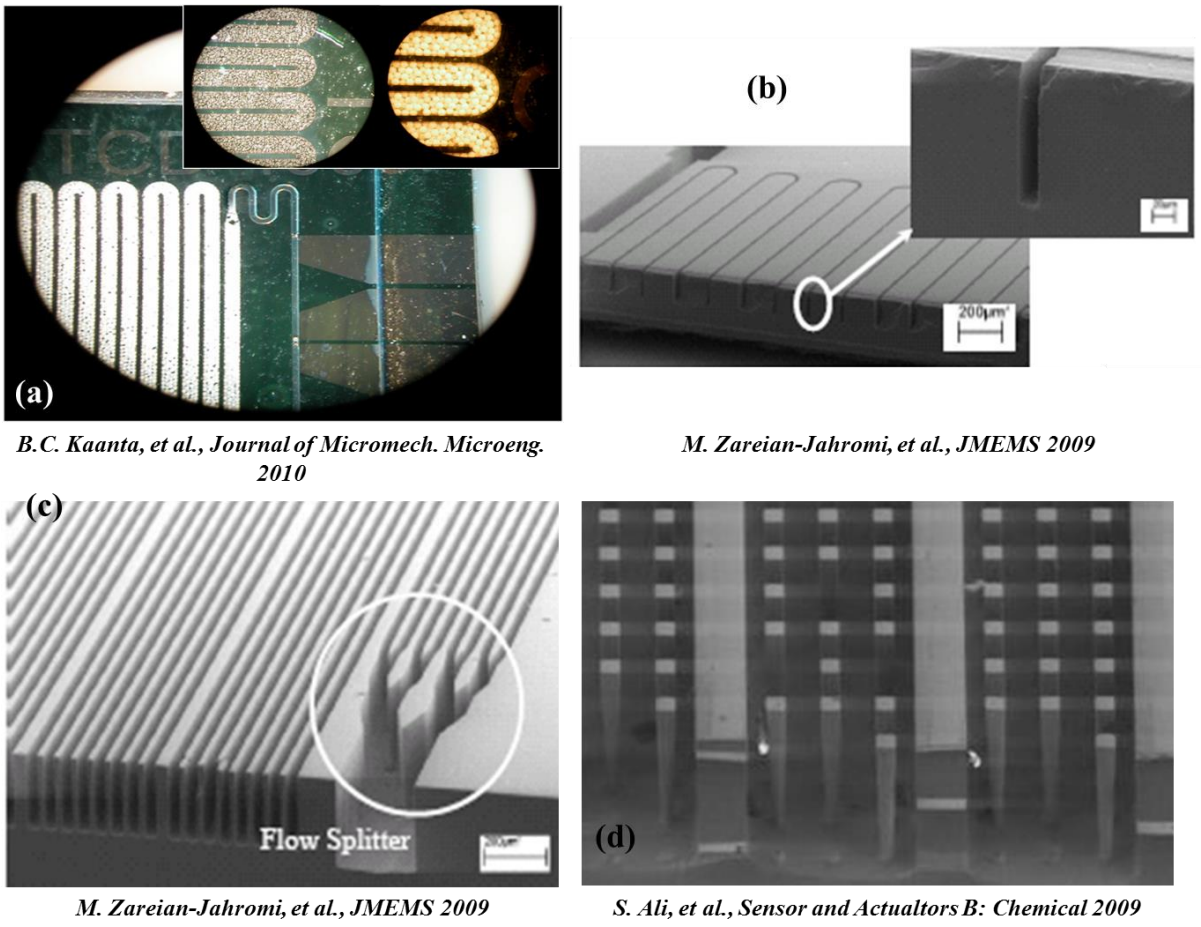

B.C. Kaanta, et al., Journal of Micromech. Microeng. 2010

M. Zareian-Jahromi, et al., JMEMS 2009

M. Zareian-Jahromi, et al., JMEMS 2009

S. Ali, et al., Sensor and Actualtors B: Chemical 2009

Figure 1.4 *Different types of microfabricated separation columns (a) packed column, (b) open tubular rectangular column, (c) multi capillary column and (d) semi-packed column (Adapted with permission from above mentioned sources).*

enabled by MEMS fabrication [27]. These columns also alleviate the high pressures required in narrow-width single-capillary and multi-capillary columns [26, 28, 29]. Since their introduction in 2009 by our group, semi-packed columns have garnered interests in the micro analytical chemistry community [25, 30-32]. Different types of μSC are shown in Fig. 1.4.

C. Miniaturized Gas Detectors

The selection criteria for a gas detector in GC applications include sensitivity, response time, linearity, chemical selectivity, complexity of required external accessories, and stability under fluctuations in temperature and flow conditions. Some common types of portable electrochemical sensors include chemi-resistors (CRs), chemical field-effect-transistor (Chem-FET), surface acoustic wave (SAW), metal-oxide-semiconductor (MOX) sensors, and quartz crystal microbalance (QCM) [33-38]. These standalone detectors if employed in tandem with separation columns can provide sensitive and often selective detection capabilities. CR-based array sensors have been used for chip-based GC systems [34]. CRs are

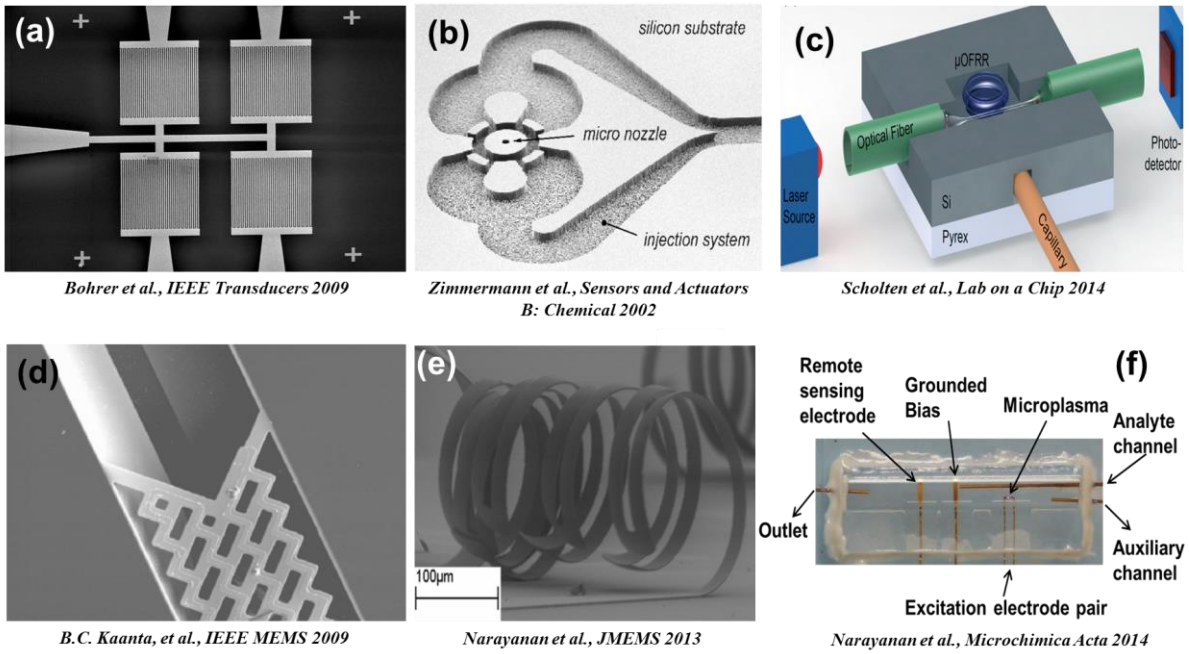

Figure 1.5 *Different types of micro machined detectors used in μGC system. (a) chemi-resistors, (b) micro-FID, (c) ring resonator detector, (d) anchored TCD, (e) suspended TCD and (f) photo ionization detector (Adapted with permission from above mentioned sources).*

simple resistors, with each resistor typically coated with a different chemically selective material, normally employed in an array configuration to detect the change in impedance upon analyte exposure. CRs, while facing difficulty in array coating, are characterized by slow time responses, sensitivity to electromagnetic interferences, and being prone to flow and temperature variations. Their optical counterpart including Fabry-Perot and ring resonator detectors [39-41] are immune to electromagnetic interference and do not generate any electric field that could be undesirable in sensitive environments; however, they are not suitable for portable instruments since they require a complex testing setup (a laser, spectrometer/photodetectors, and beam splitter/collimator) [42, 43]. The conventional GC systems employ detectors that are typically non-selective such as thermal conductivity detectors (TCDs), flame ionization detectors (FIDs), and photoionization detectors (PIDs). The first μGC system by Terry et al. [44] and the subsequent manifestation by Reston et al. [45] utilized a microfabricated TCD for sample detection. The research at VT MEMS Laboratory also demonstrated two generations of μTCDs (anchored and suspended) [46, 47]. While having simple fabrication and operation, μTDCs (and TCDs in general) have a poor detection limit (100pg-1ng) and are prone to temperature and flow rate variations of the carrier gas. Zimmerman et al. produced the first micro-FID [48] for measuring organic compounds, utilizing a glass-silicon-glass stack configuration. However, the need to provide additional hydrogen and air supplies makes it less desirable for portable applications. Moreover, reduction in the flame size also decreases the ionization power and, subsequently, the efficiency of detecting higher molecular weight

analytes. Recently, Bulbul et al. introduced a non-traditional bubble-based gas sensor for a GC system [49]. A very recent miniaturization effort based on plasma-based PIDs referred to micro-discharge photoionization detector (μDPID) has been demonstrated [50]. This detector is suitable for μGC applications and can be monolithically integrated with a separation column as will be discussed in Chapter 6. Fig. 1.5 shows the images of few detectors employed for micro-scale gas chromatography. Apart from improving the individual components of μGC, few groups have also attempted to develop a fully integrated μGC system. These efforts have been summarized in the following section.

III. Integrated μGC Systems

The history of integrated μGC system dates back to the late 1979 when Terry and colleagues demonstrated the revolutionary work on miniaturized gas analysis system (Fig. 1.6) [44]. Due to the lack of sophisticated technology, the μGC system was developed using lithography and wet etching techniques. The complete system consisted of a monolithically integrated sample injection valve and a 1.5 m-long separating capillary column (200 μm wide and 30 μm deep) packaged with a Pyrex wafer. An off-chip thermal conductivity detector (TCD) fabricated using nickel as a resistor was coupled to the system for sample detection. The system provided poor separation efficiency resulting from non-uniform

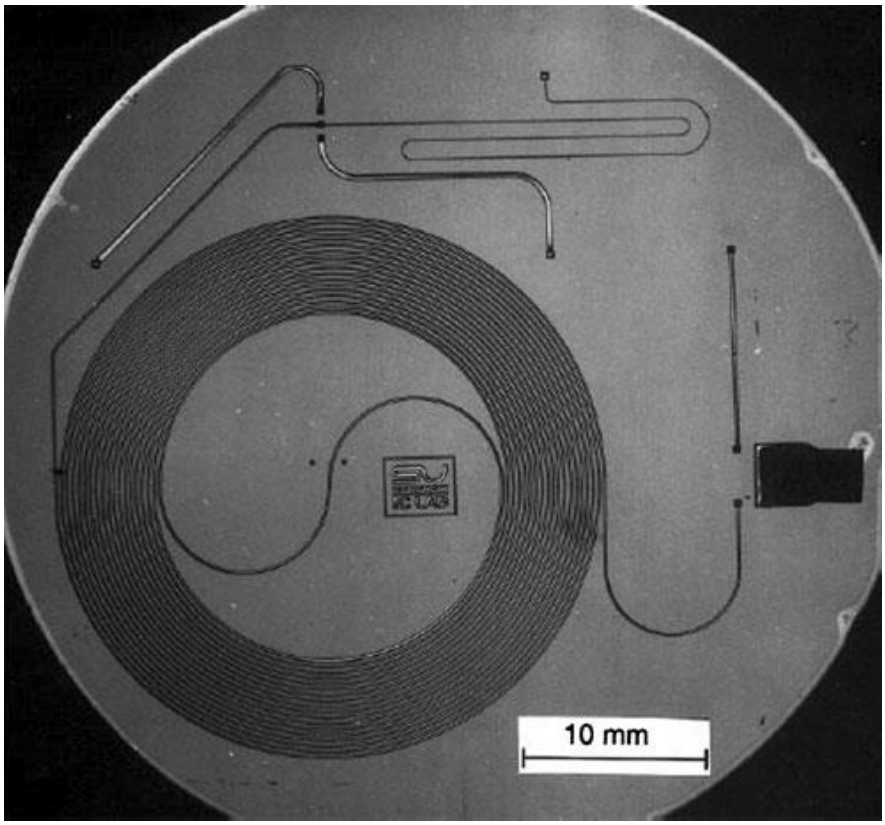

Figure 1.6 *Photograph of first gas chromatograph integrated on silicon (Reprinted with permission from ref [44]).*

stationary phase coating. The separation of a simple hydrocarbon mixture was demonstrated in 10 s utilizing OV-101 as the stationary phase. The minimum detection limit of 10 parts-per-million (ppm) was achieved with the TCD.

Afterwards, the µGC research was shelved for almost a decade with very little work reported between 1980s and 1990s. During this time, the successful proliferation of the micro fabrication technology to other applications demonstrating the fluid manipulation on micro-scale revived confidence in developing the miniaturized gas chromatography (µGC) system. Notable among them was the groundbreaking paper by Manz et al. reporting first high-pressure liquid chromatography (HPLC) column using Si-Pyrex technology [51]. This paper demonstrated the first true manifestation of a concept called the miniaturized total chemical analysis system that has since been established as µTAS (micro total analysis system). Furthermore, the fabrication of micro-valves [52] and micro-pumps [53, 54] by silicon micromachining had also been presented by the end of 1980s. These events revived the hope in developing a miniaturized GC system. In the following years, few groups reported the integrated µGC system.

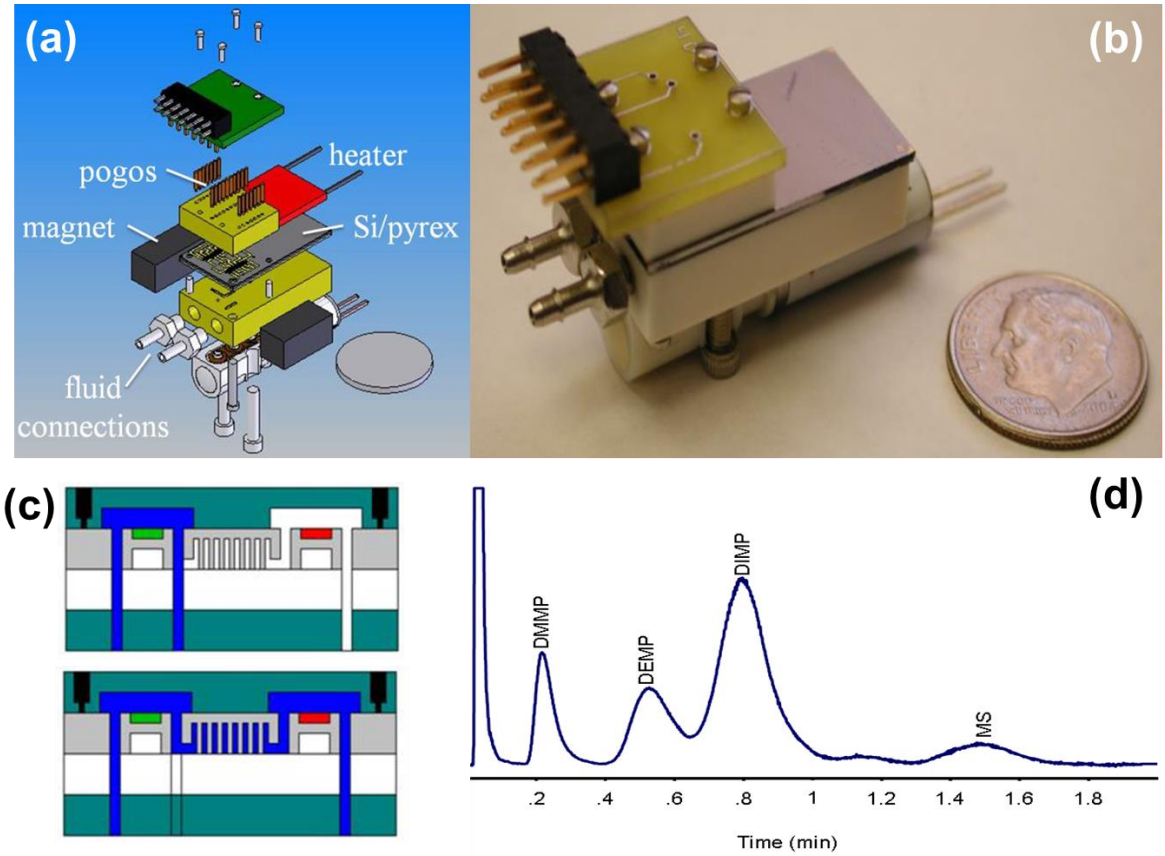

Figure 1.7 *(a) Schematic showing the device packaging (b) photograph of actual device developed by Sandia National Laboratories(c) schematic showing the flow of carrier gas (blue color) during the sampling and analysis mode through the monolithic integrated chip (d) chromatogram showing the separation of four chemical warfare agents (CWA) with FID used as a detector (Reprinted with permission from ref [56]).*

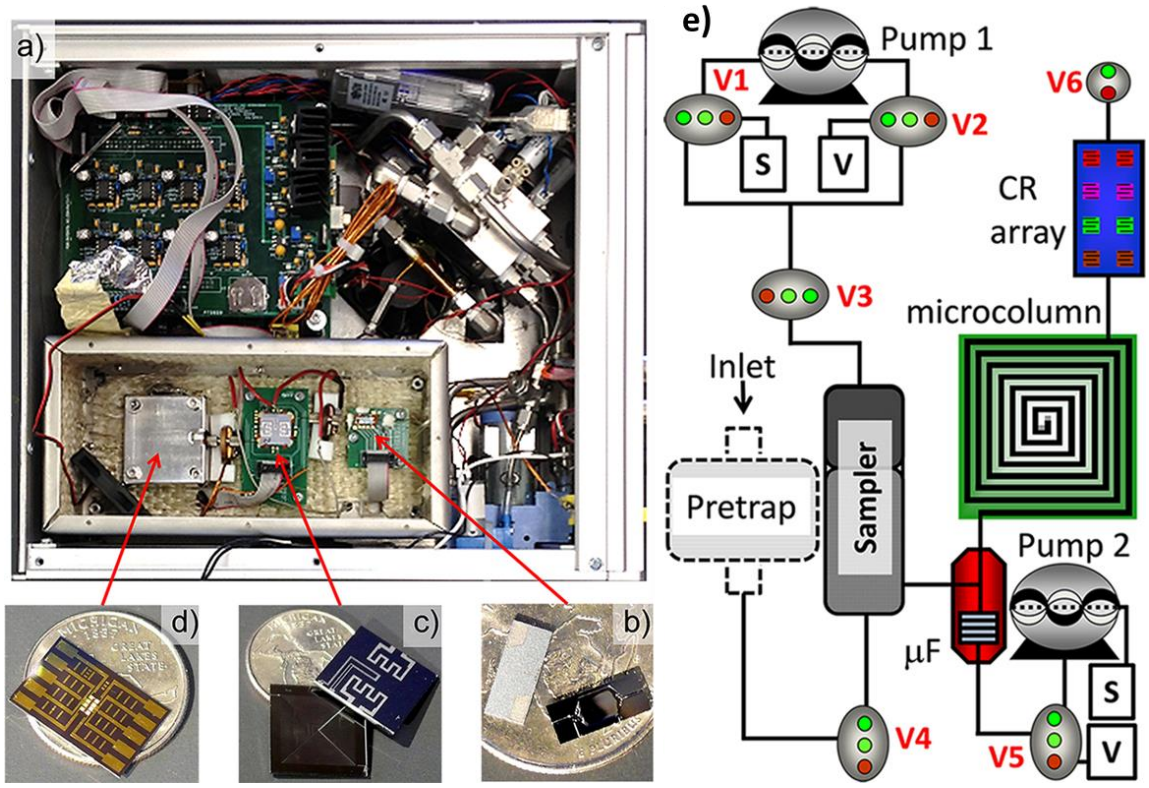

Figure 1.8 *(a) Schematic showing the device packaging (a)INTREPID µGC system (b)µF chip (c) µSC (d) CR array (e) schematic showing the configuration of microfluidic components (Reprinted with permission from ref [64]).*

Sandia National Laboratories launched µChemLab™ targeting the homeland security applications in 1998. Novel micro pre-concentrators (µPC), micro separation columns (µSC) and detectors were employed with an aim to limit the size of the overall system to a small football [36, 55]. The unique aspect of their effort was that it was centered towards the development of a truly monolithic integrated µGC system. Such integration of microfluidic components (chemical pre-concentrator, µSC, detector, valves and pumps) along with the electronic components could potentially lead to a dramatic size and cost reduction. Fig. 1.7 shows the images of the actual monolithic integrated chip produced as a result of their research effort [56]. The system was comprised of a pre-concentrator, a separation column (86 cm long, 100 µm wide and 400 µm deep) and a magnetically-actuated pivot plate resonator (PPR) fabricated on a silicon on insulator (SOI) wafer. Chromium and gold layer (15nm/75nm) patterned through liftoff process were utilized as heater and transducer line for pre-concentrator and detector respectively. Post-fabrication coating of pre-concentrator and the detector with silica sol gel was performed using spray coating system. The column was coated dynamically with a solution of polydimethylsiloxane (PDMS). Although the fabrication and subsequent coating mechanism for the integrated chip was demonstrated, it is interesting

to note that no chromatogram was published. The chromatogram shown in Fig. 1.7d was generated by connecting the integrated chip in series with the conventional FID.

The National Science Foundation (NSF) Wireless Integrated MircoSystems (WIMS) Center established at the University of Michigan in 2000 continued research to improve performance of the individual elements of µGC [57-62]. The WIMS group significantly advanced the field by implementing several prototypes of the integrated µGC system [63-66]. Their recently reported INTREPID µGC system (Fig. 1.8a) was comprised of a conventional pre-trap (a stainless-steel tube packed with a dual-adsorbent

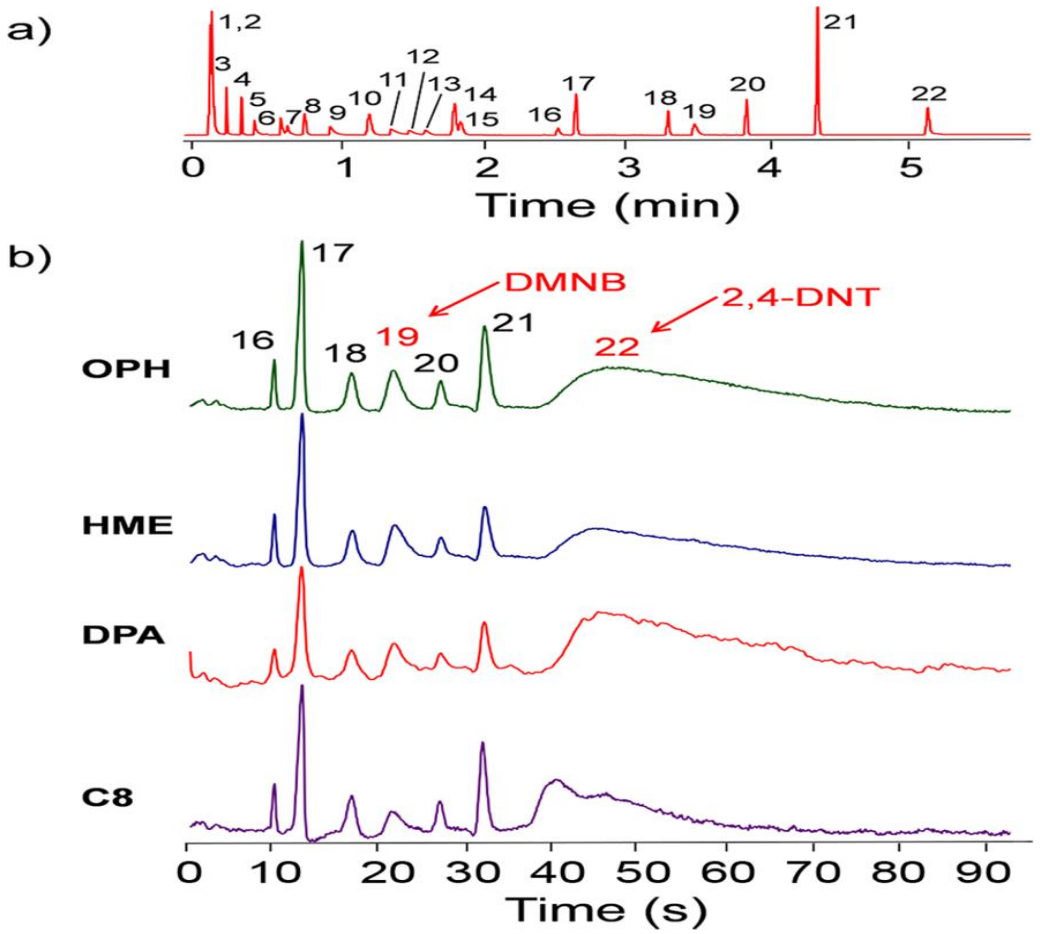

Figure 1.9 *Reference chromatogram of a 22-component mixture (including DMNB and 2,4-DNT) obtained with a commercial 6-m long capillary column with a PDMS stationary phase (0.25 mm i.d., SPB-1, 0.25 µm thickness, Supelco) and an FID (He carrier gas, 3 mL/min). (b) Chromatograms from the four CR sensors generated with the INTREPID prototype from the automated analysis of a 1-L air sample containing the 22-component mixture. Fifteen (15) of the interferences were (intentionally) not trapped by the sampling module and therefore do not appear in the chromatograms. Compounds: 1, benzene; 2, 1-propanol; 3, n-heptane; 4, toluene; 5, n-octane; 6, hexanal; 7, 2-hexanone; 8, isoamyl alcohol; 9, m-xylene; 10, 2-methyl 2-hexanol; 11, 2-heptanone; 12, n-nonane; 13, cumene; 14, heptanal; 15, 1-hexanol; 16, octanal; 17, decane; 18, n-undecane; 19, DMNB; 20, n-dodecane; 21, n-tridecane; and 22, 2,4-DNT. (Temperature program: 20-s hold at 70 °C, ramp at 8 °C/s to Tmax = 120 °C; hold.) (Reprinted with permission from ref [64]).*

bed) and a Si/Pyrex micro-focuser (μF) chip (Fig. 1.8b) for sampling purposes [64]. The reason for using a pre-trap was to enable high-volume sampling in a shorter period of time. The μF served as an injector and contained an etched cavity packed with a granular adsorbent and integrated with backside heater. The μSC (1-m, spiral channel, 150 μm × 240 μm) was made in Si/Pyrex and coated with PDMS (Fig. 1.8c). The μSC was equipped with on-chip temperature programming capabilities. Furthermore, four pairs of interdigital metal electrodes of chemiresistor (CR) array (Fig. 1.8d) were coated with one of the four types of thiolate-monolayer protected gold nanoparticle (MPN) by drop casting from solution. The airflow was provided by two commercial mini diaphragm pumps and controlled by set of commercially available solenoid valves. The configuration of microfluidic components is shown in Fig. 1.8e. The aim of this study was to enable rapid determination of two explosive marker including 2,3-dimethyl-2,3-dinitrobutane (DMNB) and 2,4-dinitrotoluene (2,6-DNT) from a matrix of 20 or more interfering compounds. Selective pre-concentration and temperature-programmed chromatographic separation facilitated the determination of primary markers from 20 interfering compounds within 2 min (Fig. 1.9). Estimated LODs of 2.2 and 0.86 ng were achieved for DMNB and 2,4-DNT respectively.

In another effort, Zampolli et al. developed a prototype μGC system (Fig.1.10a) having a micro machined pre-concentrator, μSC and a commercially available highly sensitive metal oxide semiconductor (MOX) detector [67]. Pre-concentrator and μSC were fabricated in Si/Pyrex with platinum heater together with platinum thermistor positioned on backside of silicon wafer. New adsorbent was used including Quinoxaline-bridged cavitand (QxCav) for pre-concentrator and Carbograph 2 + 0.2% Carbowax^{TM} for stationary phase inside the μSC. A micro machined filter was provided at the outlet of the pre-concentrator and μSC, shown in the inset of Fig. 1.10c, to prevent the phase from being pushed out by the gas flow. The operation of the μGC platform is shown in Fig. 1.10b. The μGC platform operated in two modes namely in idle mode and injection mode. In idle mode, the sampling pump provided a constant rate flow of sample (~50 mL min^{-1}) through the pre-concentrator. During this time, GC pump flushed the μSC with clean air. In injection mode, the multiway valve was activated, connecting the pre-concentrator unit to the GC pump. The pre-concentrator was heated to 100 ˚C to release the adsorbed aromatics. This step was referred to as injection and typically lasts between 5 and 30 s. After injection, the flow was returned to the idle mode. The signal from the MOX detector was acquired as the aromatic compounds exit the GC column outlet. Fig. 1.10d shows the chromatogram generated by the μGC system using four-compound mixture for five different concentrations. The minimum detection limit of 0.1 parts-per-billion (ppb) was noted for benzene with the sampling time of ~55 min.

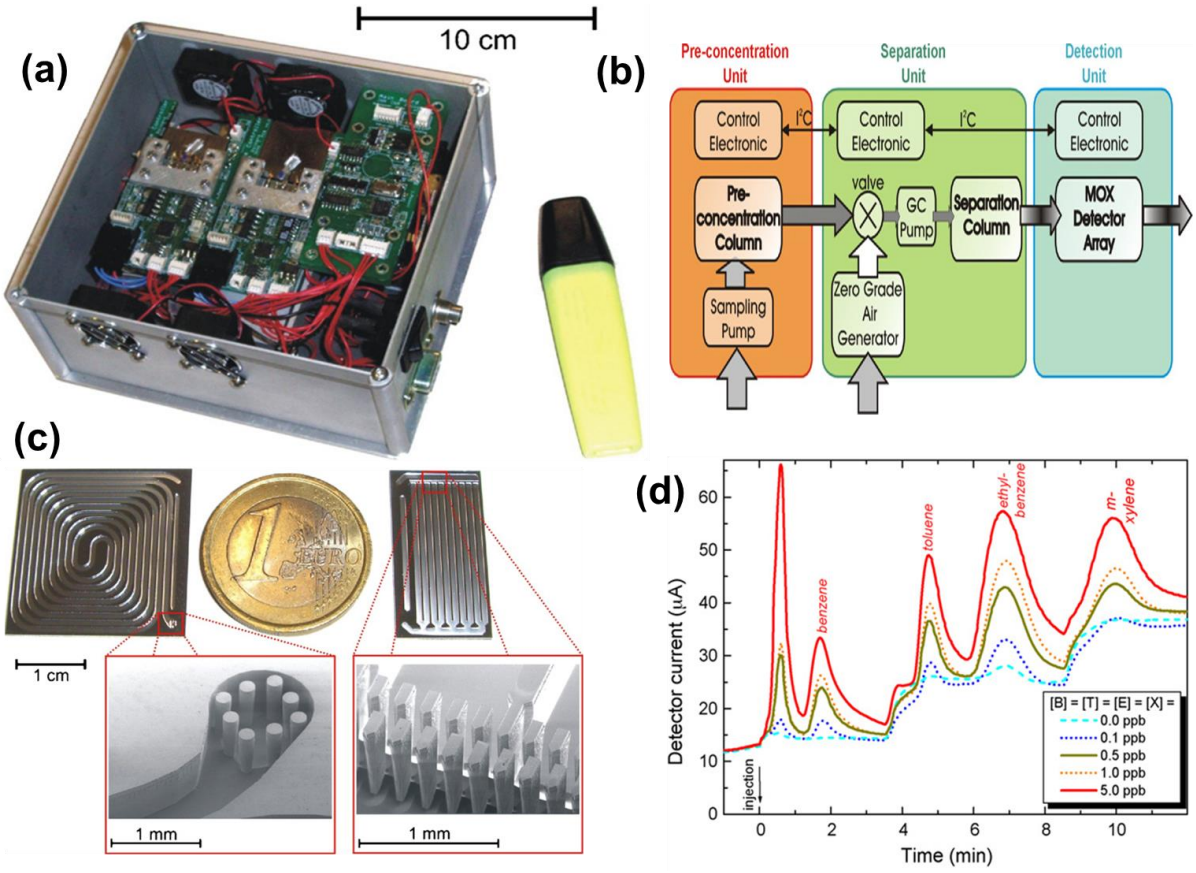

Figure 1.10 *(a) complete packaged μGC system (b) architecture of μGC (c)separation column (left) and pre-concentrator (right). Inset shows micro machined filters (Reprinted with permission from ref [67]).*

Recently, our group has also developed a fully integrated μGC system. The unique aspect of our μGC system is that the major components of the system including pre-concentrator, μSC and detector have been microfabricated. Furthermore, separation and detection is performed on a monolithic integrated chip. The prototype μGC system developed by our group has been discussed in Chapter 5. Moreover, monolithic integrated μGC chip will be demonstrated in Chapter 7.

Chapter 2: A Microfabricated Propofol Trap for Breath-Based Anesthesia Depth Monitoring

(Part of this chapter reproduced from [160] with permission from IEEE JMEMS)
M. Akbar and M. Agah, "A microfabricated propofol trap for breath-based anesthesia depth monitoring," Journal of Microelectromechanical Systems, vol. 22, pp. 443-451, 2013.

Anesthetic agents can be administered into the body of human patients by different methods. In conventional methods, the vaporized inhalants are introduced into the body through oral or nasal means. The anesthesia depth is reflected in the change of the partial pressure of the anesthetics in the brain [68]. One of the disadvantages using this method is the requirement of special apparatus (anesthetic vaporizer) to deliver a specific amount of anesthetic dose to the patient [69]. On the other hand, the intravenous technique relies on injecting the anesthetic agents (propofol, ketamine, and etomidate) directly into the vein. The agents gain access to the blood, after being administered by one of these methods, and become part of the circulatory system through which they are transported to the desired location in the central or autonomic nervous system [70-73].

The accurate amount of dose necessary to induce anesthesia is very critical and is a persistent challenge for anesthesiologists [20, 74, 75]. An inadequate amount of anesthesia may result in acute pain and accidental awakening during the surgery and is extremely traumatic. Moreover, the patient may recall conversation and other unpleasant events that occurred during the process of surgery. Similarly, overmedication of anesthetic agent can lead to serious consequences such as permanent brain damage and even mortality.

Propofol (2,6-diisopropylphenol) is widely used for general sedation in intensive care units. It has a phenolic chemical structure with a distinct smell and a molecular weight of 178.27 g mol^{-1}. Monitoring the quantity of propofol injected into the blood of the patient undergoing anesthesia is very critical and usually is carried out by high-performance liquid chromatography and gas chromatography (GC) [76, 77]. These methods are time consuming, expensive, and labor intensive. Moreover, after the injection of anesthetic agent into the patient body, 97%–99% of propofol is bound with albumin and red blood cells, and the remainder exists in blood as free type. Only free type is detected by these techniques, which makes them inaccurate for the quantification of propofol [78, 79]. Furthermore, almost 88% of the propofol dose can be monitored in urine sample as hydroxylated and conjugated metabolites [80, 81].

Currently, there is no medical device that can directly determine the level of anesthesia based on effect-site concentration in blood [82, 83]. Therefore, anesthesiologists presently rely on observation and indirect monitoring methods, including monitoring the blood pressure, patient pulse, pain response, heart rate, and rhythm [84, 85].

Analysis of the exhaled breath provides a noninvasive method to quantify/monitor the compound of interest in the breath sample. Recent studies have revealed that there is correlation between the amount of

propofol injected into the blood and that present in the exhaled breath of patients [86-89]. However, analyzing breath is not a trivial task for several reasons. First, volatile organic compounds (VOCs) are present at very low concentration, usually in the parts-per-billion range in the breath sample. Analyzing analytes at such low level of concentration is extremely difficult and cumbersome. Second, the high level of breath complexity containing more than 1200 VOCs, including ketones, aldehydes, and alcohols, makes it difficult to identify the compound of interest from the rest of the breath biomarkers found in human breath. In addition, the background level of these compounds must be accounted for in a consistent reliable manner because of their presence in ambient air at the similar concentration. In addition, the trace level of these compounds makes it difficult to detect by conventional sensors.

Currently, breath-based propofol monitoring is performed in the analytical laboratory by highly trained technicians. First, the breath sample is collected in the sampling tube typically filled with Tenax TA polymer, which is subsequently separated and identified from the complex compound present in human breath [90, 91]. The separation and detection is usually carried out by instruments such as GC–flame ionization detector (GC–FID), GC–mass spectrometry (GC–MS), ion-molecule-reaction MS, and proton-transfer-reaction MS [92, 93]. These instruments are large, expensive, require extensive maintenance, and need highly trained technicians to work with them [20], making them unsuitable for breath-based anesthetic depth monitoring (ADM) in operating rooms.

Miniaturization of analytical instruments using microelectromechanical systems (MEMS) technology can address some of the aforementioned issues and can lead into small, energy efficient, and less expensive systems. Our group has reported the development of MEMS-based pre-concentrators (μPCs) [20, 94], separation columns [29, 95] and detectors [47] for micro-GC (μGC) with applications focused on environmental monitoring and breath analysis. This paper stems from our previously reported microfabricated pre-concentrators consisting of an array of pillars embedded in a silicon cavity and coated with Tenax TA. The purpose of μPC is to concentrate and thus facilitate trace level detection of a wide range of analytes [74]. Similarly, under certain circumstances, interest may lie in capturing and analyzing certain compounds from a complex sample. This necessitates for deployment of a device in the analysis system, which selectively captures and concentrates the desired analytes of interest. The golden microtrap reported here is able to trap and concentrate the low concentration of the propofol compound over a period of time in the breath sample. The chip is coated with electroplated gold and is capable of eliminating the unwanted species from the breath sample while capturing only the propofol compound alleviating the need for chromatographic and/or spectroscopic analysis. The chip can be integrated with a detector such as a thermal conductivity detector (TCD) in order to realize a handheld propofol sensor [47]. The proceeding sections describe the chip design and fabrication and its performance for selective propofol trapping from human breath samples.

I. Chip Overview and Device Fabrication

Fig. 2.1 shows an optical image along with a scanning electron microscopy (SEM) image of a fabricated device. The 12-mm^2 chip consists of a 7 mm × 7 mm × 0.24 mm cavity etched in silicon and includes embedded parabolic pillars. The interior surfaces of the chip can be coated with an adsorbent material to trap the analytes introduced through the inlet by an inert carrier gas such as helium or nitrogen. The configuration and geometry of the pillar are chosen to maximize the interaction between gas molecules and the adsorption bed, as reported earlier [20]. The deactivated fused silica tubing is connected to the inlet and outlet ports using a high-temperature silica-based bonding agent. The gas molecules interact with the adsorbing material depending upon its affinity and the surface topography, including the pore size and surface area provided by the adsorbing material. The entrapped molecules can be then released by the thermal desorption process for subsequent analysis.

In this paper, four chips were considered, including the one coated with Tenax TA, electroplated gold, evaporated gold, and bare silicon without any adsorbent. The former most has been widely used as an adsorbent for breath analysis [96, 97], whereas the latter one is used as our reference chip. The electroplated gold was employed to selectively capture the propofol compound. The evaporated chip has been considered to study the effect of changing the gold surface profile on the selectivity of the propofol compound. Fig. 2.2 shows the fabrication process for all the four chips.

A. Silicon Chip

The fabrication of our reference chip comprises standard photolithography and patterning of photoresist, anisotropic etching of micro channels and fluidic ports, and anodic bonding of a silicon wafer to the Pyrex 7740 substrate and then dicing the wafer to release the individual devices. The process starts by photolithography of parabolic structures and fluidic ports using AZ9260 on a standard 4-in wafer. The wafer is then subjected to deep reactive-ion etching (DRIE) to achieve an etching depth of 260 μm. The device is then sealed with the Pyrex 7740 wafer using anodic bonding with temperature, pressure, and voltage set to 340 ˚C, 22 kPa, and 1250 V, respectively. Finally, the fused silica capillary tubes (220-μm O.D. and 100-μm I.D.) are attached to the inlet and outlet of the device.

B. Cobweb Tenax TA Chip

The fabrication process for our Tenax TA devices has been already reported elsewhere [94] and has been used for pre-concentration of VOCs for breath analysis and environmental monitoring.

The fabrication starts by utilizing DRIE to form the parabolic structures and the fluidic ports according to the process described earlier. Then, Tenax TA particles are dissolved in dichloromethane (50 mg/ml) concentration to create a solution that fills the cavity. Few drops of 2-propanol are added to the solution

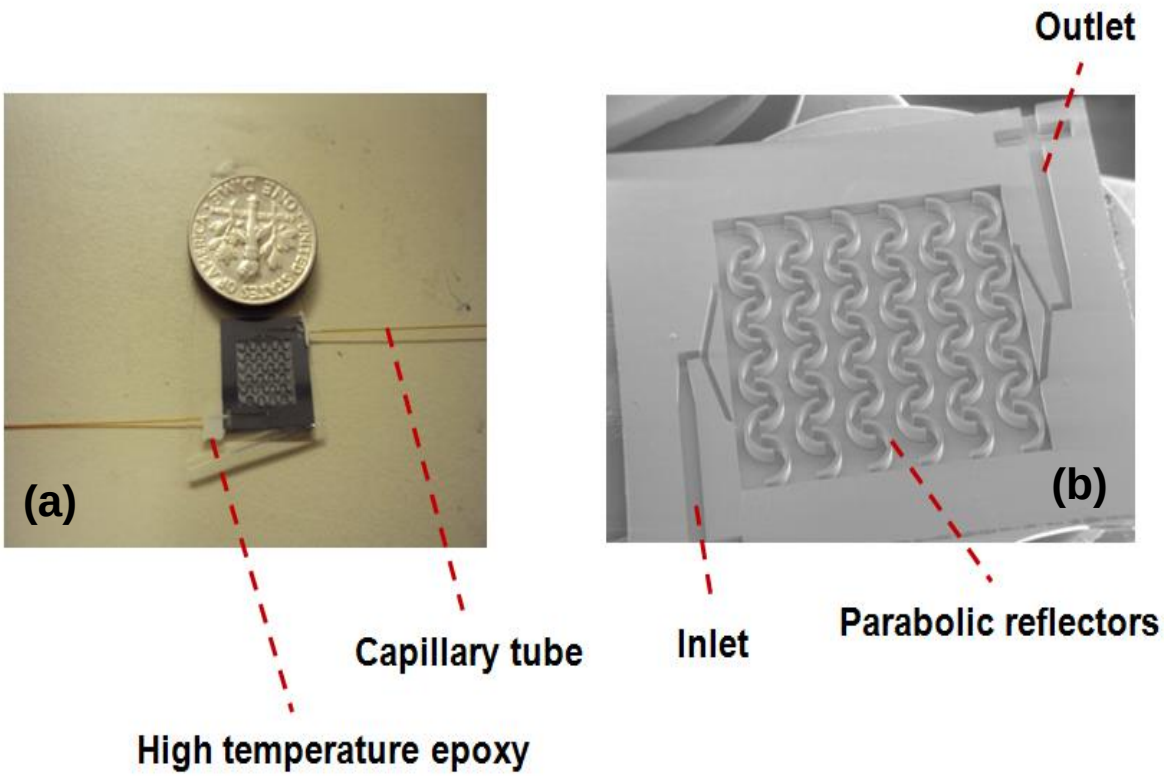

Figure 2.1 *Optical and SEM image of the fabricated chips (a) optical image of the chip (b) SEM image to show device overview.*

before it evaporates. This results into the formation of a cobweb pattern of the polymer providing a high surface-to-volume ratio and increased VOC trapping capacity. The device is then sealed with Pyrex 7740 using anodic bonding. The bonding temperature is selected lower than the conventional 350 ˚C–400 ˚C to avoid damaging the polymer. Finally, the fused silica capillary tubes (220-µm O.D. and 100-µm I.D.) are inserted inside the fluidic channels to make the inlet/outlet of the device.

C. Golden Microtrap Chip

The fabrication process for the golden microtrap chip can be divided into four major steps, namely, anisotropic etching of silicon to form microstructures, phosphorous doping, thin-film deposition using electroplating, and anodic bonding.

The fabrication starts by utilizing DRIE to form the parabolic structures and the fluidic ports according to the process described earlier. Then, phosphorous doping is performed at 950 ˚C for 6 h. The wafer is then diced into individual devices for the subsequent electroplating process. The gold layer is deposited using the DC electroplating technique. The gold solution is maintained at 55 ˚C with a stirring rate of 200 rev min^{-1} to provide uniform distribution of the gold ions during the process. The circuit is completed using a platinized Ti grid (anode) that has to be much larger in size compared with the cathode to provide

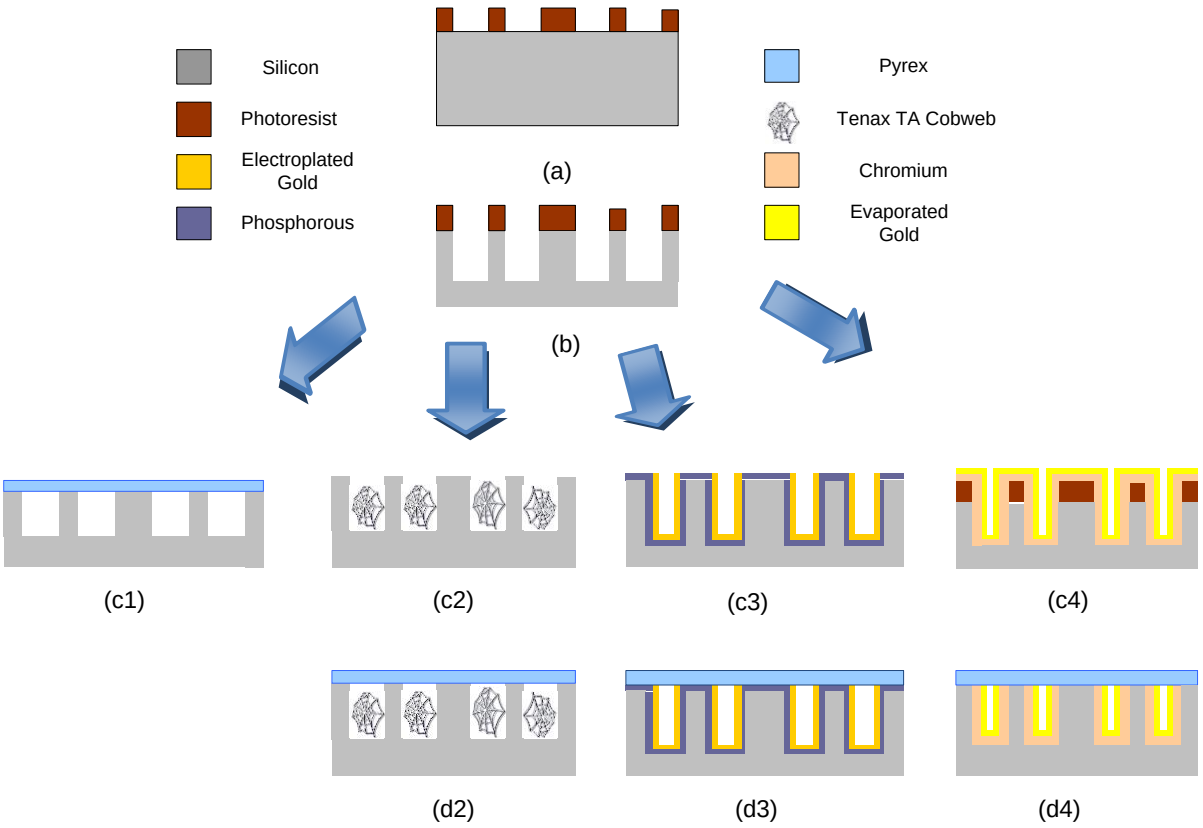

Figure 2.2 *Process flow for fabrication for silicon, Tenax TA cobweb, golden micro-trap and evaporated gold chip. (a) photolithography and patterning (b)deep reactive ion etching (c1) anodic bonding of Pyrex wafer with silicon chip (c2) deposition of Tenax TA cobweb structure inside channels (d2) sealing the device with Pyrex by anodic bonding (c3)phosphorous doping, DC electroplating and patterning the gold on the top surface of the structures (d3) sealing the chip with the Pyrex (c4) evaporation of chromium and gold using physical vapor deposition (d4) patterning of the evaporated gold using lift-off process and sealing the device with Pyrex.*

a uniform electric field. The anode is kept at a distance of ~2 cm from the cathode. The dc current is maintained at 4 mA for 1 min to deposit a thin gold layer. As discussed in [95], the weak gold-to-silicon adhesion is advantageous as it allows the manual post deposition removal of gold from the top boundary using acetone and cotton swab assisting in the subsequent anodic bonding process. The device is then sealed with Pyrex 7740 using anodic bonding. The bonding temperature is selected to be less than Si–Au eutectic temperature, and it also serves to provide stability to the deposited gold layer by the thermal annealing process. Finally, the fused silica capillary tubes (220-µm O.D. and 100-µm I.D.) are inserted inside the fluidic channels to make the inlet/outlet of the device.

D. Evaporated Gold Chip

Figure 2.3 *Experimental setup for the adsorption phase with arrows showing the direction of the sample flow.*

To fabricate these chips, after etching silicon and forming parabolic structures, a layer of 25-nm/150-nm Cr/Au is deposited using electron beam evaporation to cover the interior surfaces of the chip. The evaporated gold layer is removed from the top surfaces of the chip through the liftoff process by dipping the wafer inside acetone for approximately an hour. The device is then diced and sealed with Pyrex 7740 wafer using anodic bonding.

II. Material Characterization

A. Surface Profilometry

Surface topography was characterized with a Veeco Dektak 150 surface profilometer using a 12.5-μm stylus with 1-mg stylus force in “Hills and Valley” profile mode. For each sample, the 250-μm length was

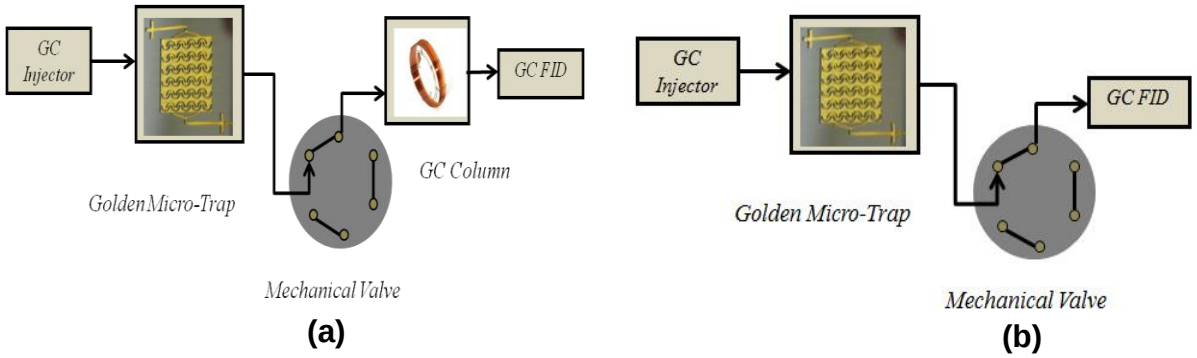

Figure 2.4 *The desorption setup inside the GC oven (a) using the separation column and (b) without the separation stage*

scanned in 40 s along four parallel lines separated approximately by 0.5-mm distance. The results for four scans were averaged for both the electroplated and evaporated gold. Veeco MultiMode atomic force microscopy (AFM) in "contact mode" was also used to evaluate surface roughness of two different 1 μm × 1 μm and 10 μm × 10 μm size square fields.

B. Surface and Compositional Analysis

Adsorbent surface structures were imaged using a field emission scanning electron microscope (LEO 1550, Zeiss) equipped with an X-ray energy dispersive spectrometer (EDS). EDS analysis was made at 5-kV accelerating voltage with data processed using the embedded INCA system. At least two random points were selected from each sample for EDS analysis.

III. Experimental Setup

The complete experimental setup for the adsorption phase is shown in Fig. 2.3. It comprises a Tedlar bag for collecting the breath sample [98] and the vial in which propofol has been diluted to the desired concentration found in human breath (4.3–33.5 ng) and maintained at 250 ˚C [99]. The subject is provided with a Tedlar bag and a nose clip. The subject is asked to take a deep breath before sample collection and, when ready, to place the nose clip on his nose. After holding the breath for approximately 30 s, the subject breath sample is collected in the Tedlar bag. A T-junction is used to connect the Tedlar bag and the vial to the device. A vacuum pump is employed to draw both the breath sample and the propofol compound for 6 min through the chip. As the propofol compound is heated to its boiling point (250 ˚C) in the vial, it condenses to the walls of the vial [100]. The condensation process can be avoided by heating the vial long enough such that its walls are essentially at the same temperature as the bottom, leading to an accurate quantification of the propofol compound.

The golden microtrap was experimentally evaluated by comparing its performance with the e-beam gold-coated, cobweb Tenax TA, and silicon chips. Before introducing the breath sample, the chips were

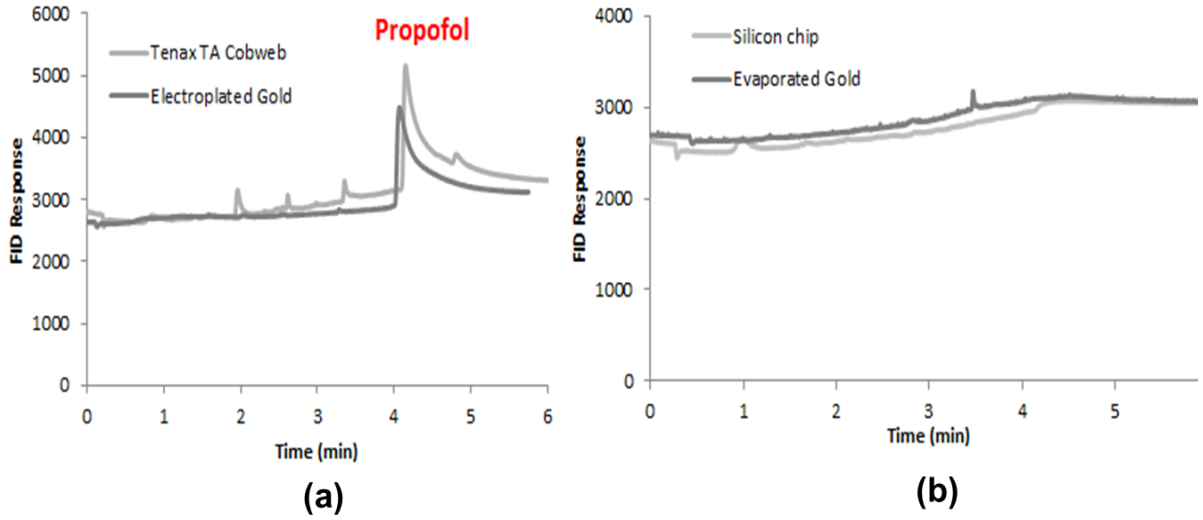

Figure 2.5 *Chromatograms overlaid (a) for Tenax TA cobweb and golden micro-trap and (b) for silicon chip and evaporated gold under the same testing conditions.*

taken to a higher temperature (250 ˚C) to remove any possible adsorbed analyte from previous experiments or from the environment. By exploiting a thermal desorption mechanism, cross contamination between experiments can be effectively eliminated. Subsequently, the devices were loaded with breath samples by employing the setup described earlier. The desorption tests of the extracted samples were carried out using an HP 5890 GC system. The testing setup was completed by connecting the commercial methylpolysiloxane phase GC column to the chip using the six-port zero-dead-volume valve, as shown in Fig. 2.4(a). The isothermal conditions were maintained by installing the setup inside the GC oven. Nitrogen was used as a carrier gas, and the pressure was adjusted to 10 lbf in^{-2} to achieve a flow rate of 1 mL min^{-1}. The chip was quickly heated to 250 ˚C at the rate of 100 ˚C s^{-1} using an off-board high-performance ceramic heater, and the GC oven was programmed from 35 ˚C to 150 ˚C at the rate of 30 ˚C min^{-1}.

IV.Results and Discussion

The chromatograms of the golden microtrap, evaporated gold, Tenax TA, and silicon chips were compared, as shown in Fig. 2.5. The retention time of the propofol in the column under the aforementioned temperature programmed conditions is about 4 min. The ability of Tenax TA cobweb to adsorb more compounds in the breath sample is attributed to the high surface-to-volume ratio provided by the cobweb structure inside the cavity. This particular formation allows more interaction of the adsorbent film with the gas molecules, thus enhancing chances of adsorption. It is noteworthy that the adsorption process for a particular compound on the chip depends upon different factors, including the number of

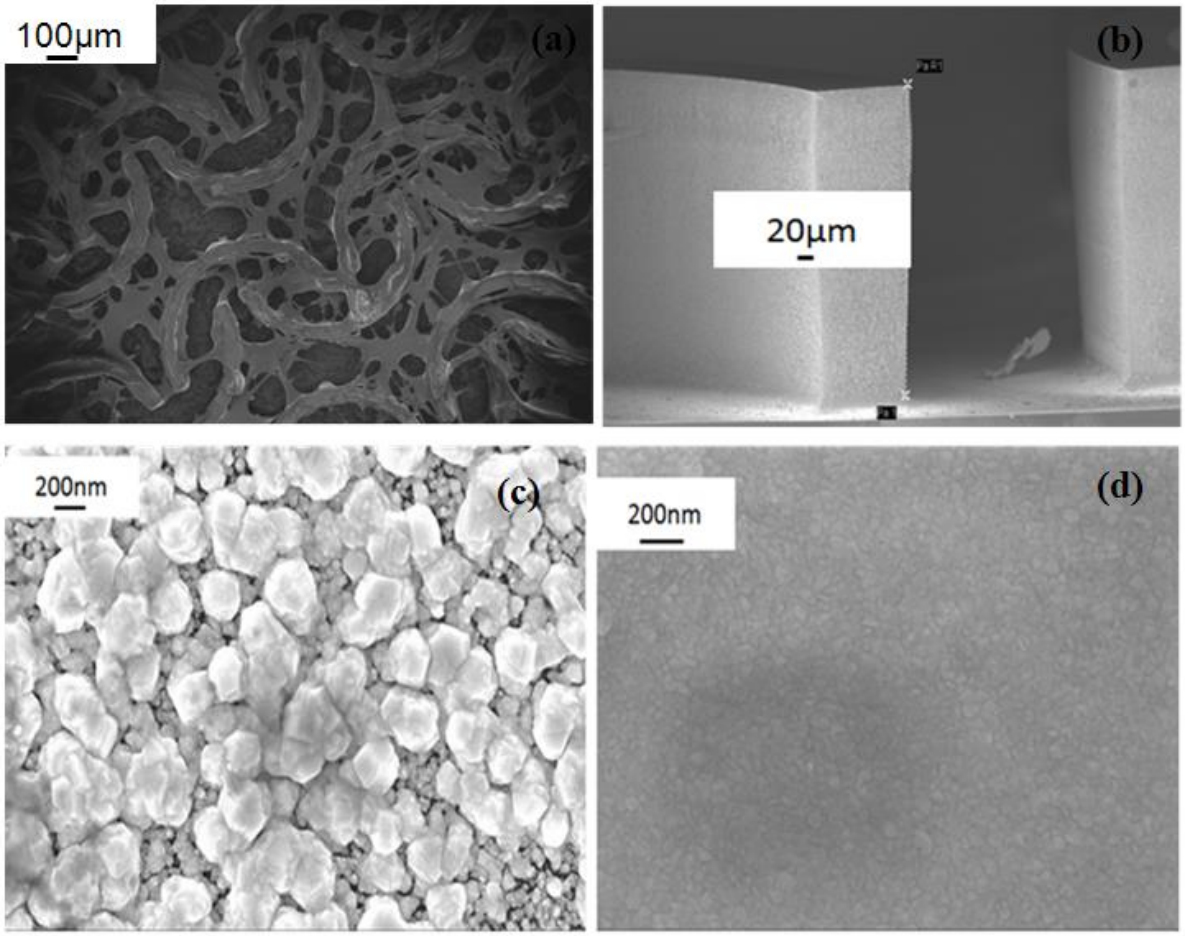

Figure 2.6 *SEM images of (a) cobweb structure of Tenax TA inside the fabricated chip, (b) electroplated gold on micropillar surface, (c) electroplated gold surface, and (d) evaporated gold surface.*

available adsorption sites (surface area) offered by the adsorbent material, the flow of the carrier gas through the chip, micro-pillar configuration, and the adsorption temperatures. The experimental conditions and the pillar configuration in all these chips are identical. Thus, the difference in the chromatograms shown in Fig. 2.5 stems mainly from the difference in the adsorbent material.

One interesting observation is the inability of evaporated gold to adsorb propofol, whereas that deposited by electroplating captures propofol very effectively. From the SEM images shown in Fig. 2.6, it is obvious that porosity inherited by the electroplated gold has been replaced with a completely smooth surface in case of evaporated gold. This proves that, owing to changed surface texture, a different method for gold deposition results in different affinity for the propofol compound. We anticipate this is mainly due to the difference in surface morphology, including porosity and roughness, of the electroplated gold compared with its evaporated counterpart. Generally, evaporation of metals is conducted at slow rates and low pressure resulting in layer-by-layer growth, providing smooth film deposition [101]. Conversely, mass transfer limitations of a solid–liquid interface during the electroplating process cause roughness to

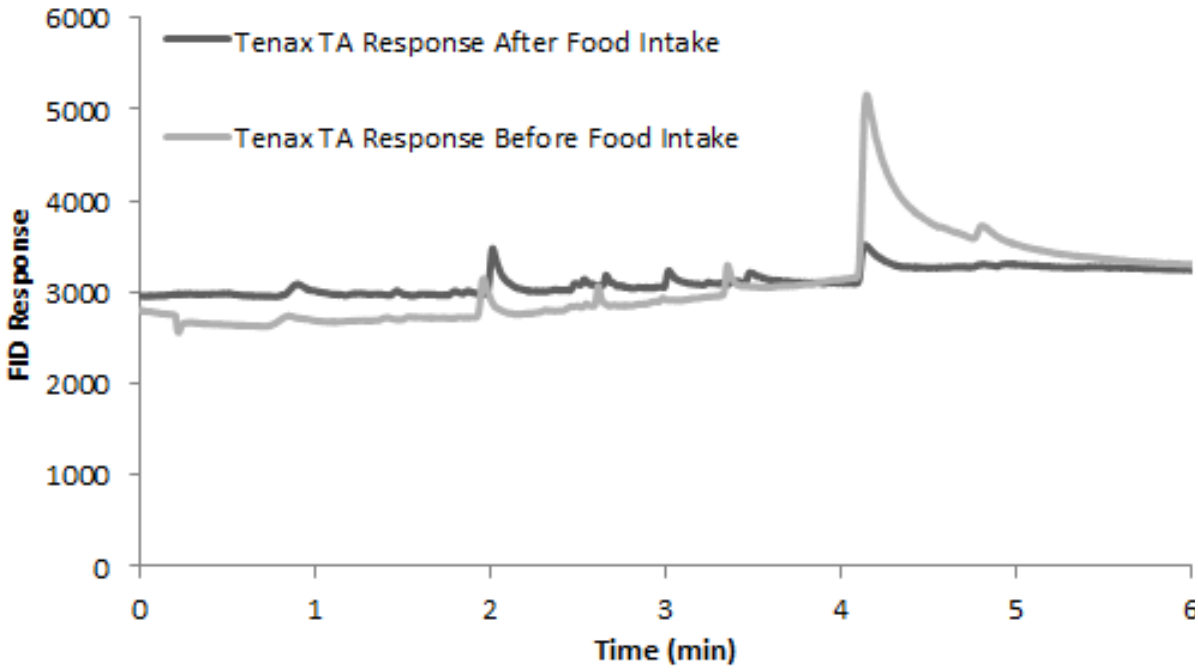

Figure 2.7 *Chromatograms showing the Tenax TA response before and after food intake.*

increase [102]. The electroplating conditions reported herein result in gold grain sizes ranging from 250 to 450 nm with pore sizes around 20–40 nm. In addition, average roughness (Ra) measured for the electroplated gold film using the profilometer is about 590 nm, whereas that for the evaporated gold is around 13 nm, showing approximately an order of magnitude difference in surface roughness. Although the absolute numbers measured by the two methods are significantly different due to the scanned length, the trends in both cases are in good agreement. The average roughness and the scanned surface area for both films using AFM are listed in Table 2.1. Due to increased roughness and porosity, electroplated gold yields more surface area as compared with evaporated gold [101-103]. The compositional analysis performed using EDS shows 100% gold content presence on the electroplated gold film. These studies reveal that, despite the identical chemical composition, the gas sorption properties for the two films vary according to their morphology. This is in agreement with previous studies suggesting that, for the same adsorbent material, the effect of altering surface morphology has a profound influence on its adsorption capacity [104-108].

It is important to mention that our group has demonstrated before that the propofol compound can be selectively adsorbed through the manipulation of adsorption temperatures in two cascaded microfabricated pre-concentrators coated with Tenax TA [74]. The selective pre-concentration of propofol was carried out by eliminating low and high boilers (1-propanol, C_{10}, C_{12}, C_{14}, and C_{16}) while retaining only mid boiler (propofol compound) through variation in adsorption temperature and reversing

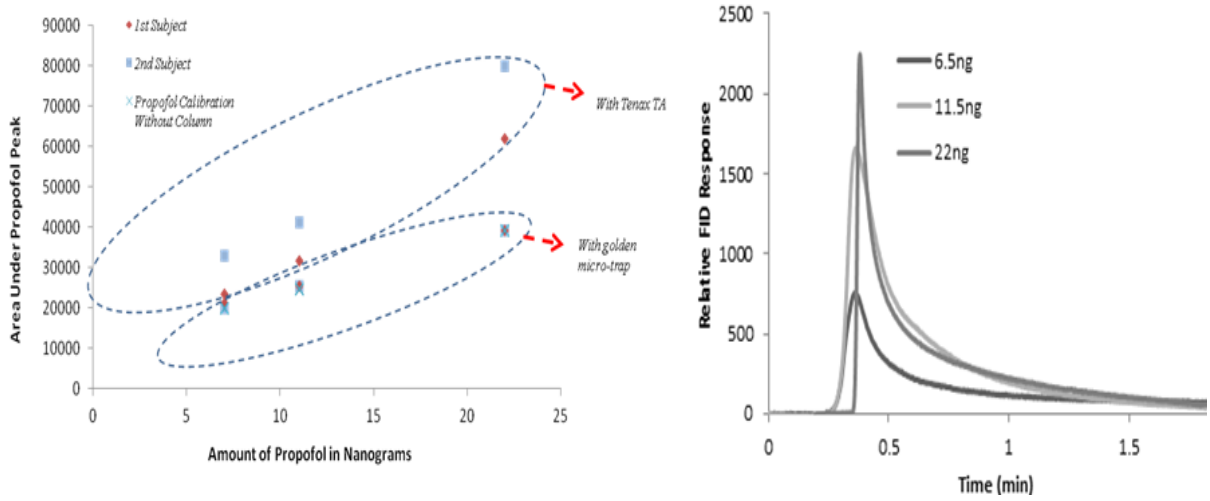

Figure 2.8 *(a) Calibration data for different quantities of propofol in gas phase for Tenax TA and golden chips. It is notable that the propofal signal changes less than 3% for the golden micro-trap when no column (separation stage) is used clearly demonstrating the highly selective nature of the chip, (b) graph showing the change of FID signal with propofol concentration.*

the carrier gas flow direction. Compared with the work presented in this paper, our previous approach does not fully remove the other compounds in the breath and has the potential of trapping compounds whose boiling point is close to that of propofol. In addition, it relies on a more complicated cascaded method resulting in a cumbersome and time consuming approach. The presented golden microtrap is able to capture only the propofol compound in human breath by a more frequent and cost-effective manner, eliminating the need for maintaining specific adsorption temperature or adapting a cascaded approach.

Anesthesiologists rely on the precise quantification of the propofol compound. Hence, reproducibility in terms of quantification of propofol is one of the important issues in ADM. As shown earlier, the Tenax TA chip is capable of adsorbing propofol and, hence, can be potentially used in conjunction with GC for propofol identification among the other breath analytes adsorbed by this polymer. However, the amount adsorbed can be influenced by the other analytes due to competitive adsorption, making quantification of the propofol concentration present in breath very challenging. To prove this point, we demonstrated the effect of food intake on the adsorption of the propofol compound by the cobweb Tenax TA chip. The chromatograms for the breath samples before and after the food intake are shown in Fig. 2.7. The difference in chromatograms is due to the change in pattern of VOCs in exhaled breath because of food consumption and metabolism . The increased amount of VOCs in the exhaled breath generated after food intake compete for the limited adsorption sites varying the adsorption of propofol on the polymer surface. Our group has previously shown that adsorption of a compound on Tenax TA is influenced by the presence of other compounds [109]. It is obvious that there is a significant difference in the area under the propofol peak in the two cases, making the Tenax TA polymer subjected to inaccurate quantification of

propofol for the same subject under different breath conditions. This can be the case for the breath of two different subjects containing the same propofol amount. To demonstrate this point, the chip was tested with breath of two different subjects. Three different quantities of propofol in the gas phase were used to evaluate the reproducibility and reliability of the device. The results for Tenax TA show that propofol adsorption on the available surface site is subject dependent and significantly varies. The golden microtrap, however, allows quantification of the propofol within ±3%, as shown in Fig. 2.8(a). This is due to its high selectivity toward absorbing propofol and its inability to adsorb other breath compounds. This has a very important practical outcome. That is, the golden microtrap can be independently used without any separation stage, which leads to a simple and faster analysis. As demonstrated in Fig. 2.8(a) for different propofol concentrations, when the desorbed sample is directly injected to FID using the desorption setup shown in Fig. 2.4(b), the area under the FID signal is within ±3% compared with the case in which the same goes through the separation column. The desorbed FID response versus the propofol concentration is shown in Fig. 2.8(b) revealing the dependence of the desorbed propofol to the initial propofol concentration in the sample. It is important to mention that at least three golden microtrap chips have been tested. The standard deviation in the FID signal for a given propofol concentration has been less than 10% when considering the response of all the different chips. The results presented herein demonstrated the ability of the microchip with electroplated gold to provide an accurate quantification of the propofol amount in breath, one that can serve anesthesiologists in the operating room.

Gold Deposition Method	Surface Area	Average Roughness
Electroplated Gold	1μmx1μm	6.82nm
	10μmx10μm	8.86nm
Evaporated Gold	1μmx1μm	0.63nm
	10μmx10μm	0.49nm

Table 2.1 *Surface area and average roughness of the deposited gold surface using atomic force microscopy.*

V. Conclusion

A unique golden microtrap chip, which is efficient for breath-based propofol monitoring, has been reported in this paper. The chip has been compared with those coated with Tenax TA, which is a commonly used adsorbent material for breath analysis. The golden microtrap chip has highly selective affinity for the propofol compound in human breath samples. Furthermore, the chip can be employed for accurate quantification of propofol in contrast to Tenax TA chips that adsorb different amounts of propofol depending on the breath sample. The golden microtrap was successful to deliver a subject independent result, which is imperative for accurate ADM. The selective property of electroplated gold is ascribed to the surface roughness by comparing it with the evaporated gold chip. In future work, by varying the deposition conditions, the effect of the surface texture of the electroplated gold on selective propofol trapping and its adsorption capacity will be thoroughly studied. In addition, the chip will be integrated with a TCD to develop the first stand-alone MEMS-based propofol sensor. The TCD incorporates two evaporated thin-film resistors located at the inlet and outlet fluidic ports, as already demonstrated by our group [47]. By differential measurement, the TCD embedded in the golden microtrap generates an electric signal indicating the presence of the selectively trapped propofol and its concentration.

Chapter 3: Improved Performance of Micro-Fabricated Pre-concentrators using Silica Nanoparticles as a Surface Template

(Part of this chapter reproduced from [161] with permission from Journal of Chromatography A)
M. Akbar, D. Wang, R. Goodman, A. Hoover, G. Rice, J. R. Heflin, et al., "Improved performance of micro-fabricated preconcentrators using silica nanoparticles as a surface template," Journal of Chromatography A, vol. 1322, pp. 1-7, 2013.

Micro scale gas chromatography (GC) is considered to be one of the leading techniques for the separation and analysis of volatile organic compounds (VOCs). It has a wide range of applications including on-site environmental monitoring, homeland security, and real-time toxic industrial chemicals detection [110-112].

Such systems typically consist of an injector/pre-concentrator, a separation column and a detector all fabricated using microelectromechanical system (MEMS) technology. A MEMS-based thermal pre-concentrator (μTPC) is one of the key components of μGC system for the collection of trace level VOCs in air over a fixed time period to concentrate the analytes before introducing them into a GC column for separation. It consists of an etched cavity in a silicon chip which is filled with adsorbent material. The chip cavity is then sealed by bonding it to another substrate, with heaters and sensors deposited or attached on the backside of the chip afterwards. Analytes are typically desorbed from a μTPC in the form of a sharp sample plug, usually via thermal desorption.

Three different categories of μTPC have been reported in the literature. They are distinguished from each other based on the cavity layout (empty or either encompassing channels or microposts) or by the adsorbent profile (granular or thin film). In the devices using granular adsorbent material, channels and cavities formed in silicon are filled with adsorbent beads and then sealed (bonded) to another substrate [3, 60, 113-118]. The second type of μTPCs utilizes adsorbent materials in the thin film form deposited on a membrane or inside microfabricated channels or cavities [15, 36, 119-123]. There are trade-offs with both types of devices. The first type can provide high sample capacity but suffers from high pressure drops and power consumption during the thermal desorption process. In addition, the difficulty in restricting the beads inside the cavity makes the bonding process extremely cumbersome and can lower the fabrication yield. The devices in the second category significantly reduce the pressure drop, though they have limited sample capacity due to less surface area interacting with the analytes. A third type of μTPC addresses the limitations of the previous types by embedding closely-spaced high-aspect-ratio (HAR) microposts inside an etched cavity and coating them with a thin film adsorbent layer. This approach has been extensively explored and established in our previous work for both enhancing the adsorption capacity and improving the flow distribution in the microchip devices [20, 124-126].

There are a variety of commercially available adsorbents for μTPC depending on the chemical properties of VOCs to be concentrated. For example, there is significant literature available on the

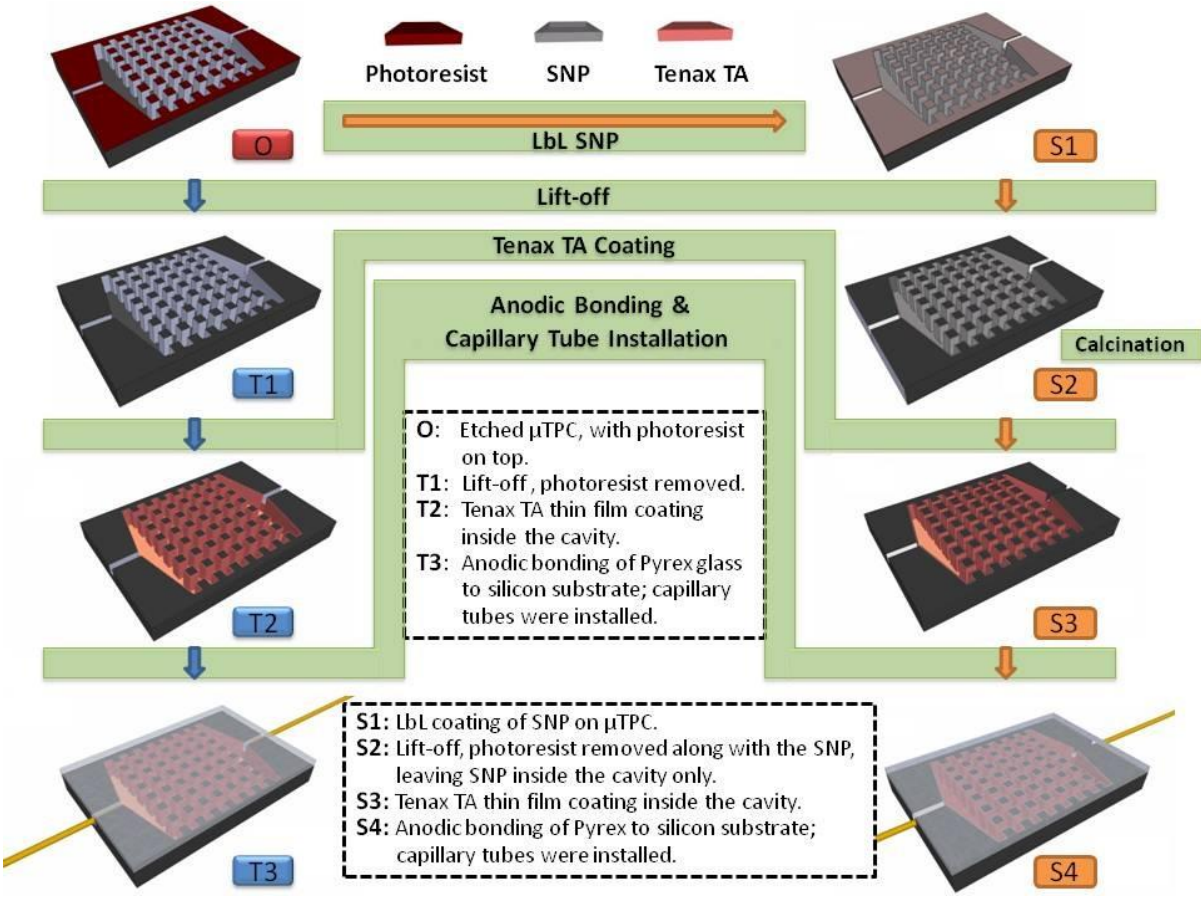

Figure 3.1 *Fabrication process for µTPCs coated with three different adsorbents. For uncoated µTPC and the one coated with SNP (not shown in the figure), the anodic bonding and capillary tube installation is performed after the lift-off "T1" and calcinations "S2" process, respectively.*

adsorption properties of Tenax TA in the granular form [127-135], with a few describing the VOCs adsorption mechanisms [136-138]. Our group has published systematic fundamental study of this polymer in the thin film form with regard to surface topography, crystal structure, thermal stability, modes of adsorption, and adsorption/desorption characteristics [139, 140].

Nanotechnology appears to offer the possibility of producing better controlled films which exhibit unique chemistry compared with more established adsorbents. Because of its high thermal stability (up to 800 ˚C) and large surface area, silica nanoparticle (SNP) coatings would be a good candidate for an adsorbent material, if they could be evenly and conformably deposited on the inner surface of µTPC devices. Very recently, by utilizing the layer-by-layer (LbL) self-assembly technique, our group successfully deposited SNP coatings as a stationary phase for micro GC separation columns [141]. In this paper, we combine the two adsorbents (SNP and Tenax TA) previously used by our group to improve the device performance. The results obtained indicate that the SNP coating as a surface template for Tenax TA polymer can significantly enhance the adsorption capacity of the latter. In addition, the SNP adsorbent alone is found to be able to provide some selectivity in analyte adsorption. These developments provide a

novel approach in enhancing the morphology and increasing the surface area of the adsorbent material to improve the overall performance of the μTPC devices.

I. Experimental

A. Materials and Instruments

Reagent grade VOC compounds, solvents, and Tenax TA (80/100mesh) used in this work were purchased from Sigma Aldrich (St. Louis, MO) in > 99% purity. Polyallylamine hydrochloride (PAH) and colloid SNP (40–50 nm in diameter, 20–21 wt. % in water) used for LbL deposition were purchased from Sigma Aldrich (St. Louis, MO) and NISSAN Chemical (Houston, TX) respectively. Single-side polished silicon wafers (4 in., 500 μm thick, n-type) and double-sided polished (4 in., 500 μm thick) Pyrex Wafers were purchased from University Wafers (South Boston, MA). Ultrapure gases (> 99% purity) including helium and air were purchase from Airgas (Christiansburg, VA). Fused silica capillary tubing (220 μm O.D., 100 μm I.D.) used as fluidic interfaces were purchased from Polymicro Technologies (Phoenix, AZ). Agilent 5890 and 6890 GC systems used for adsorption/desorption tests and a 30-m long, 320 μm-I.D., 0.25 μm film thickness fused silica capillary GC column with dimethypolysiloxane as the stationary phase were purchased from Agilent Technologies, Inc. (Palo Alto, CA). A high performance ceramic heater was purchased from Power Module Inc. (Havertown, PA). Atomic Force Microscopy (Bruker Dimension Icon, ScanAsyst mode) and Field Emission Electron Microscopy (LEO 1550, Zeiss) were used for surface roughness evaluation and imaging purposes respectively.

B. μTPC Chip Fabrication/Adsorbent Coating

1. μTPC Chip Fabrication

The fabrication of μTPC chips starts with the photolithography of micro-posts and fluidic ports using AZ9260 photoresist on a standard 4’’ wafer. The wafer is then subjected to deep reactive ion etching (DRIE) to achieve an etching depth of 240 μm. After dicing the etched wafer into individual devices, the chips are ready for adsorbent deposition as described below and in Fig. 3.1.

2. Coating Thin Film Tenax TA

After stripping photoresist with acetone, the etched device was filled with Tenax TA solution (10 mg/ml in dichloromethane) and allowed to evaporate to leave a thin film of the polymer adsorbent on the cavity surfaces. The device is then sealed with a Pyrex 7740 wafer using anodic bonding with temperature, pressure, and voltage set to 320 ˚C, 22 kPa, and 1250 V, respectively. Finally, fused silica

capillary tubes (220 μm O.D. and 100 μm I.D.) are inserted and sealed inside the fluidic channels with epoxy to serve as inlet/outlets for the device, as shown in Fig. 3.1 (blue "T" process).

3. Coating SNP

Another alternative adsorbent to Tenax TA which is explored in this study is SNP. Following silicon etching while having photoresist over the un-etched regions, LbL technique [142] was used to coat the interior surfaces of the μTPC with SNPs as shown in Fig. 3.2. The positively-charged long-chain inert PAH acts like a polymeric "glue" to hold the negatively-charged SNP "bricks" together. The pH of the 10 mM PAH solution and SNP colloid were adjusted to 7.0(±0.1) and 9.0 (±0.1), respectively, by adding HCl and NaOH solutions in order to achieve maximum surface charge differences for enhancing the electrostatic bonding between the adjacent layers while maintaining colloidal stability. An automatic dipping system (StratoSequence VI Robot, nanoStrata Inc.) was used to perform the LbL deposition process. Eight beakers were placed in a circle, with one containing PAH solution and another containing SNP colloid. Three beakers were placed between them on each side that could automatically be emptied and refilled with de-ionized (DI) water for rinsing purposes. The μTPC chips, held on glass slides, are first dipped into the PAH solution for 2.5 min, followed by three consecutive one minute rinsing in DI water. They are then dipped into SNP colloid for another 2.5 min followed by another three rinsing steps before the chips go back into PAH solution. The resulting coating covers the entire surface of the μTPCs, including the internal etched 3D structures and the photoresist left on the top of the chip from the chip fabrication process.

A lift-off procedure via sonication in acetone for 5 min is then used to remove the photoresist along with the SNP coating on top of the unetched areas, leaving SNP only on the sidewalls and bottom of the

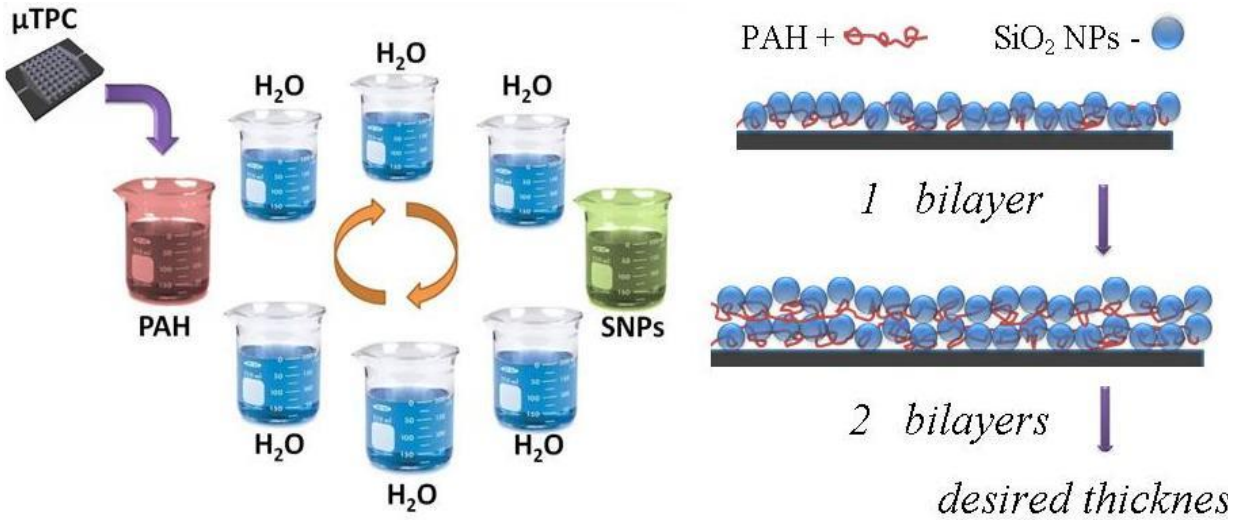

Figure 3.2 *Schematic procedure of layer-by-layer assembly of SNP coating on μTPC.*

etched features. This process guarantees a smooth clean top surface which is crucial for anodic bonding while in the meantime keeps the SNP coating elsewhere intact. Prior to anodic bonding, the chips were placed in an oven at 500 ˚C for 4 h. This calcination step removes the PAH and slightly fuses the SNPs together, resulting in a firm SNP coating as the only adsorbent material for the µTPCs. The devices were then sealed by anodic bonding and inlets/outlets installed as previously described in Section 2.

4. Coating SNP-Tenax TA

After the SNP calcination step, some of the coated µTPCs were further coated with Tenax TA using the same method previously described. The devices were then sealed by anodic bonding and inlets/outlets installed as previously described in Section 2. The process is shown in Fig. 3.1 (orange "S" process).

C. Adsorption Procedures

All the various chip configurations (SNP, Tenax TA thin film and SNP-Tenax TA) were tested under the same flow conditions (typically 1 ml/min). The sample volumes and injection split ratios were varied to determine the adsorption capacity over a range of polarities using hexane, toluene, 1,2-dichloroethane, and isopropanol as test compounds. Flasks were prepared with septum caps containing each compound and the headspace allowed to become saturated with vapor. For example, assuming ideal gas law behavior, a 1 µl injection of hexane vapor at 1 atm and 25 ˚C with a 50:1 split injection (1% reaching the µTPC) would be 70 ng. Samples were drawn from the headspace using gas tight syringes and injected immediately into the heated GC injection port. The GC oven was maintained under isothermal conditions at 30 ˚C. Helium was used as the carrier gas supplied via the GC split/splitless inlet and controlled by the electronic flow controller. The chips were connected directly between the injection port and the flame ionization detector (FID) maintained at 250 ˚C. The µTPC was mounted on a high performance ceramic heater which was rapidly heated to 250 ˚C at a ramp rate of ~100 ˚C s^{-1}. A K-type thermocouple coupled to a digital voltmeter was used for manual temperature monitoring and control. After the sample vapor injection, the breakthrough signal (analyte not retained by the pre-concentrator) was allowed to return to a baseline level prior to heating for analyte desorption. The ratio of the retained area to total area (unretained plus retained) relative to the total mass injected provides the mass adsorption capacity.

II. Results and Discussion

A. Theoretical Background

The adsorption process of a particular compound on the adsorbent bed depends upon several factors, including the mass of the adsorption bed, the number of available adsorption sites, the flowrate of the carrier gas, the vapor pressures and boiling points of the VOCs, surface area of the adsorbent, and the

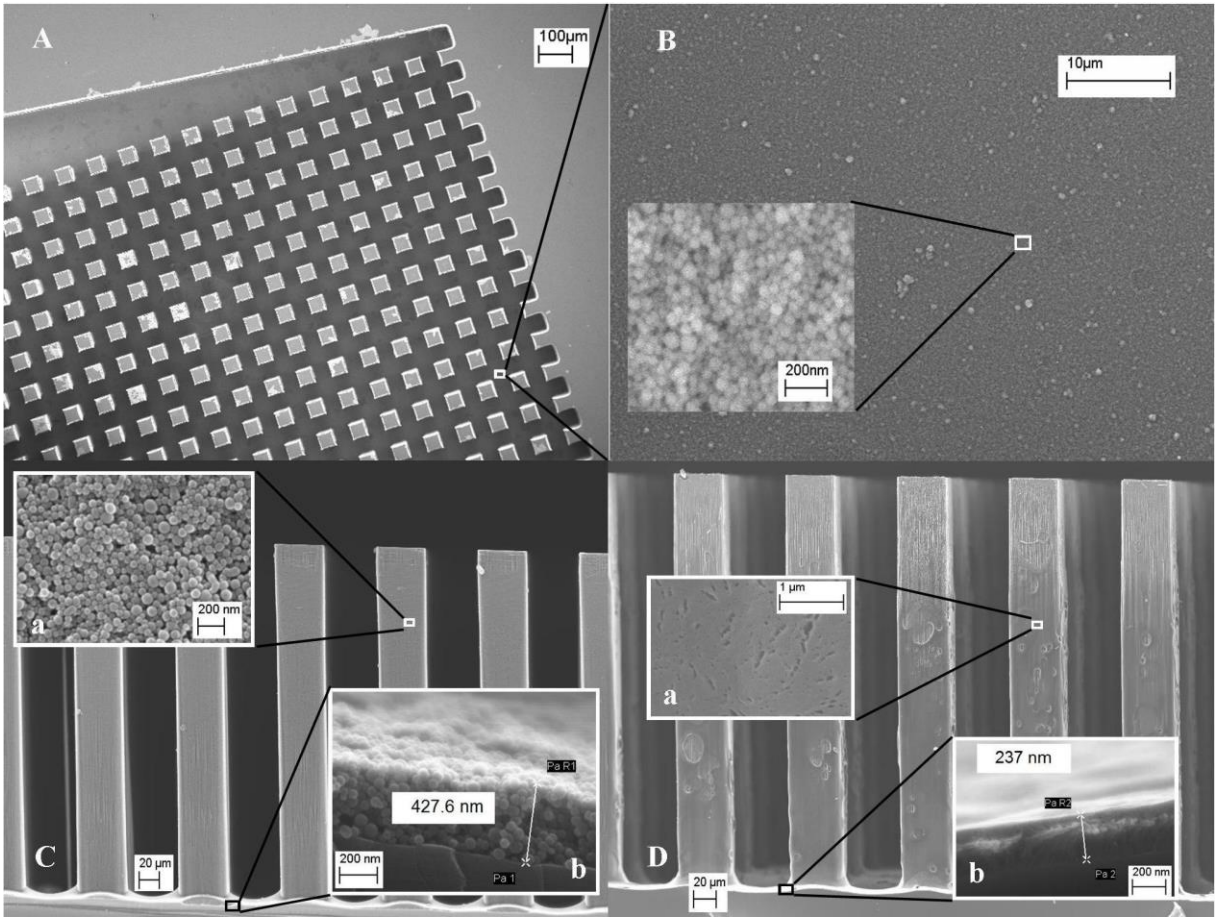

Figure 3.3 *SEM images of (A) the µTPC coated with 10 BLs SNP (B) top view of the SNP coating on the bottom of the µTPC (C) cross-section view of SNP coating on the sidewall of the micro posts, inset C(a) shows the high magnification view and inset C(b) shows the thickness of SNP coating on the bottom (D) cross-section view of Tenax TA thin film on micro posts, inset D(a) is the closer view of Tenax TA coating on the sidewall of the pillars, inset D(b) shows the thickness of the Tenax TA coating on the bottom of µTPC.*

adsorption temperature. Different ways of enhancing the surface area have been reported in the literature [126, 143-145]. For example, our group has reported [126] the role of different shapes and arrangements of microposts in increasing the surface area. Similarly, another strategy to increase the surface area is to increase the porosity [143] or the surface roughness [125, 127-142, 145]. The current method uses both methods for increasing the surface area by employing an innovative technique of nanoparticle deposition. The µTPC was evaluated in terms of the adsorption capacity and flow rate (resident time) through the chip.

B. Surface Characterization of the µTPC Chip

FESEM images of the µTPCs with the three different adsorbents (SNP, thin film Tenax TA and SNP-Tenax TA) are shown in Figs. 3.3 and 3.4. Fig. 3.3A–C shows the FESEM images of the µTPC with only

SNP as the adsorbent. Fig. 3.3A shows the top view of the μTPC after the lift-off procedure. A clean top surface is achieved and is beneficial for the anodic bonding process. Meanwhile, the bottom(Fig. 3.3B) and the sidewall of the microposts (Fig. 3.3C) are covered with a homogeneous, porous SNP coating (insets of Fig. 3.3B and C).The FESEM image of the surface profile of thin film Tenax TA coating in the μTPC is shown in Fig. 3.3D. Thin film Tenax TA coating on the sidewalls of the microposts experiences low density pores (inset a). From the cross-sectional view of the thin film Tenax TA coating on the bottom, it can be seen the coating has a micro-fiber like structure underneath a dense, relatively smooth surface. Thus, the total available surface area is somewhat limited. In comparison, the morphology of the Tenax TA coating inside the μTPC was significantly modified by the underlying SNP coating. The FESEM images illustrating this change are shown in Fig. 3.4.The nanoscaled structure of Tenax TA was developed on the SNP coating present at the sidewall of the microposts. With the help of the SNP coating underneath, the nano "drips" and "strips" Tenax TA fine structure are developed in three dimensions, which significantly increases the surface area of Tenax TA. A different surface morphology of Tenax TA on SNP is achieved on the bottom of the μTPC, where Tenax TA is conformably coated on the rough surface of the SNP, as shown in Fig. 3.4B. This may be caused by the different amount of Tenax TA attached to the sidewall of the microposts and the bottom, due to gravitational effects during the Tenax TA deposition and solvent evaporation. This conformal coating could also largely increase the surface area of the Tenax TA by inheriting the large surface area and porosity from SNP coating. The three dimensional surface profiles of the bare silicon wafer and the 10 bilayers SNP coating on silicon wafer were compared using Atomic Force Microscope (AFM) in Fig. 3.5. It is quite clear that the roughness, and thus the surface area, is substantially increased by the SNP coating. The measured roughness for a 1 μm × 1 μm area of these two surfaces was around 0.4 nm and 13 nm, respectively, which implies that

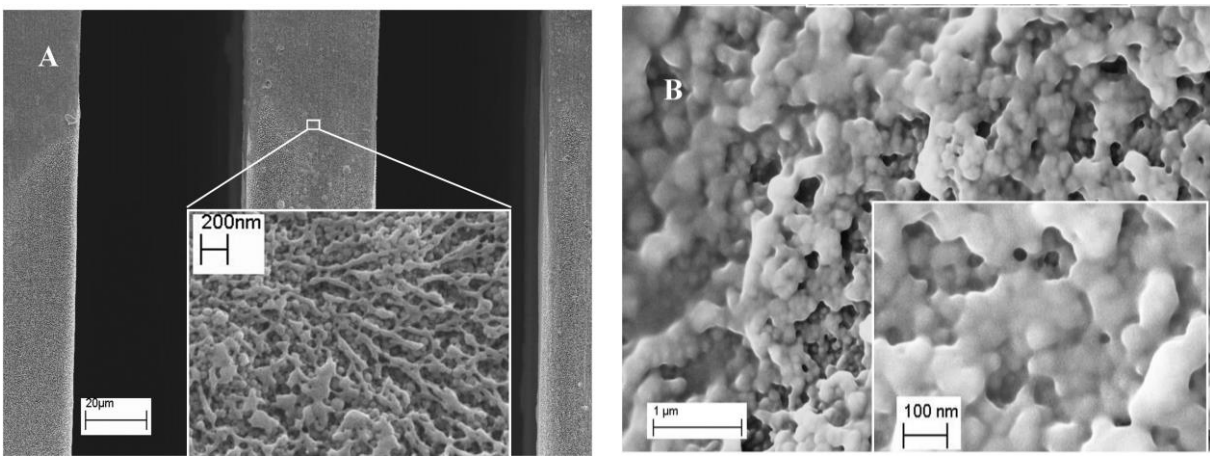

Figure 3.4 *(A) cross-section view of Tenax TA coated SNPs on the sidewall of the micro posts, the inset shows the nano-scale structure of Tenax TA brought in by the SNP coating underneath (B) Tenax TA conformably deposited on the SNP template on the bottom.*

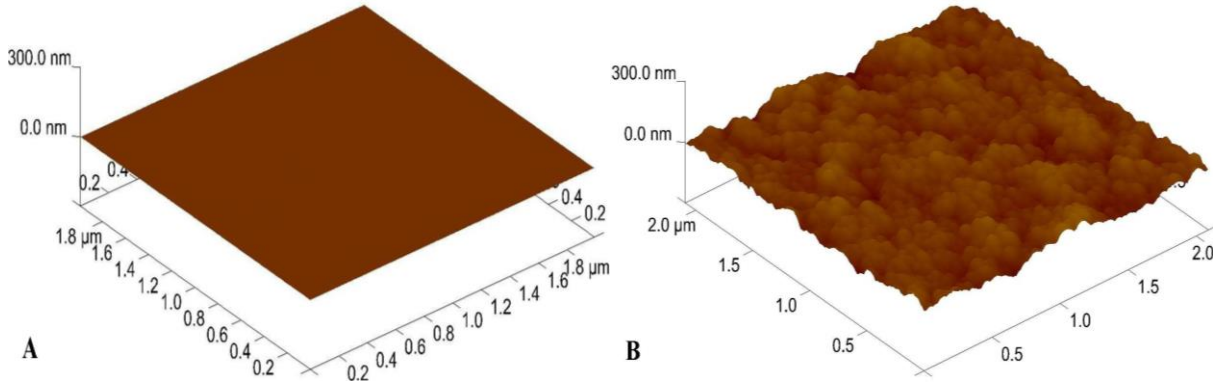

Figure 3.5 *3-D AFM image of the surface of (A) silicon wafer surface and (B) 10 bilayers SNP coating on the silicon surface. The analysis was performed on 1 µm×1 µm chip area.*

the surface roughness is increased by a factor of 30. In the case of the Tenax TA coating, the large scale structures limited the use of AFM for measuring the surface roughness. Since the AFM could not probe the real chip due to the fabricated microstructures, the surface measurements were all performed on a planar surface prepared using the same procedure.

C. Adsorption Capacities

Assuming ideal gas law behavior, the mass amount of analyte injected from a saturated vapor above the pure liquid can be calculated from the injection volume and the split ratio used for the injection. The mass retention of the chips can then be determined from the fraction of the total area retained relative to the total area (breakthrough peak plus retained peak). In this study, the capacity of the devices was initially characterized with µl volumes of analyte sampled from a saturated headspace using gas tight syringes. An example of a typical retention profile for toluene using an SNP-Tenax TA chip is shown in Fig. 3.6 for three replicate runs. Tailing from the excess hexane in the breakthrough peak is expected due

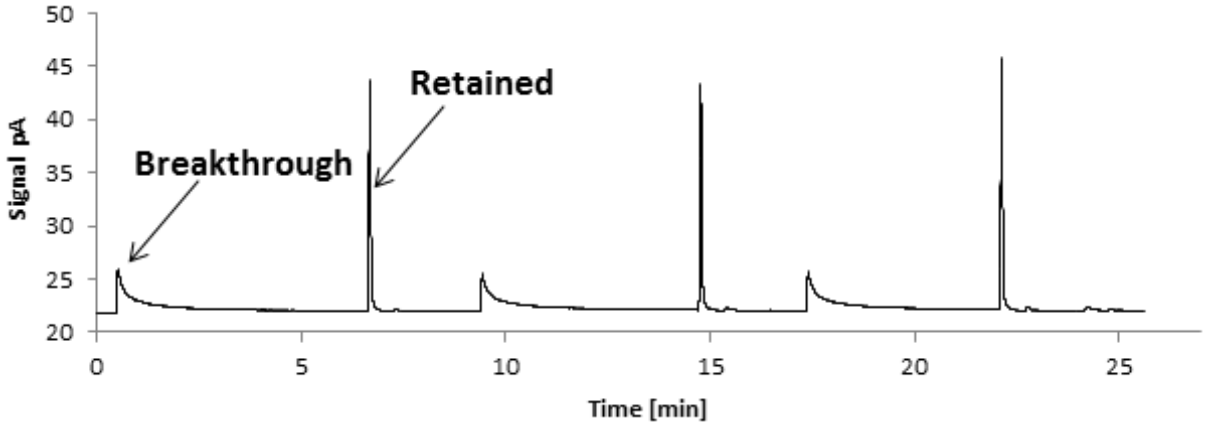

Figure 3.6 *Triplicate desorption profiles for hexane from an SNP-Tenax TA µTPC.*

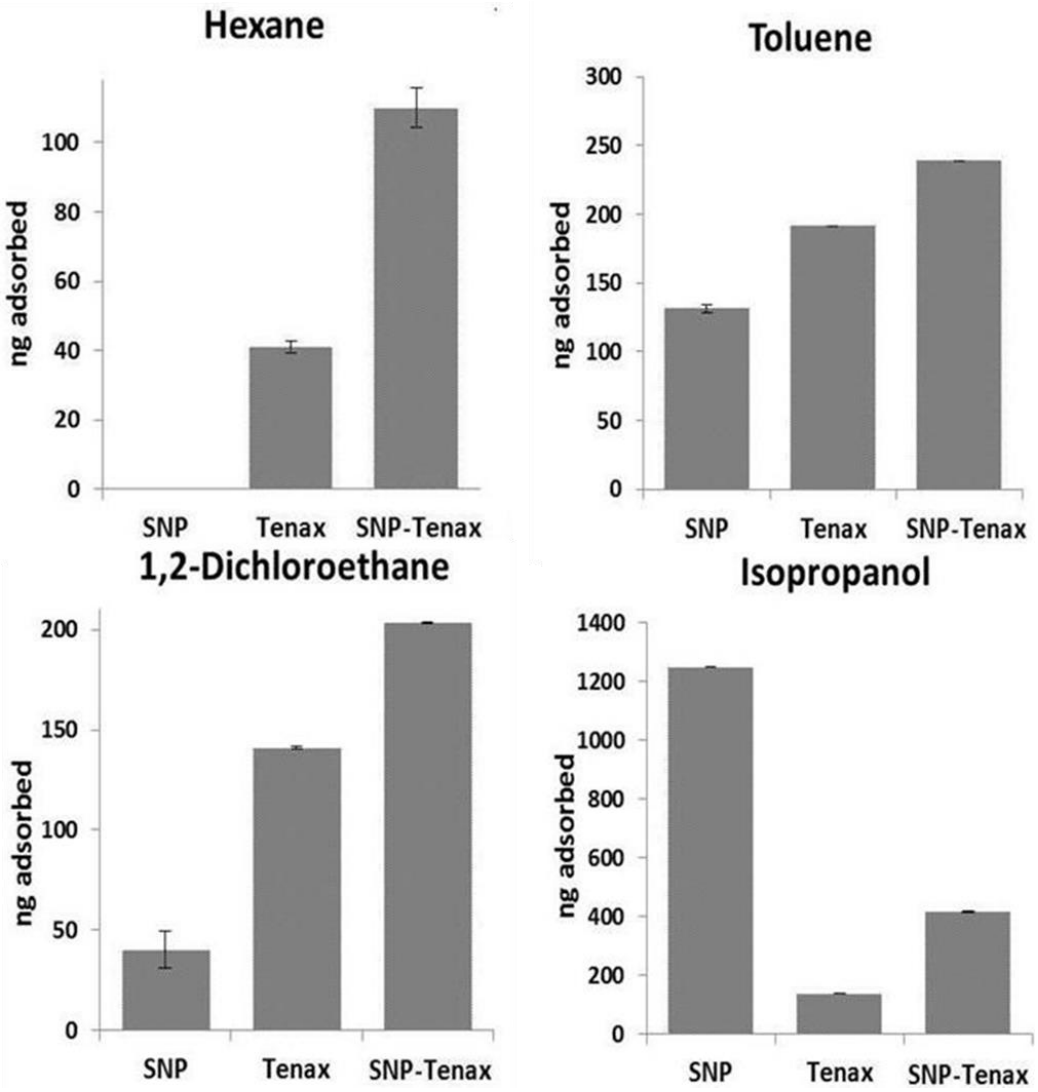

Figure 3.7 *Adsorption capacities of SNP, Tenax TA, and SNP-Tenax TA μTPCs for hexane, toluene, 1,2-dichloroethane, and isopropanol.*

to the porous nature of the SNP layers coupled with weak intermolecular adsorption of multiple analyte layers from oversaturation of the chip; however, the thermal desorption of the trapped hexane at ca. 250 ˚C was very sharp (w_b < 6–8 s; where w_b represents width of the peak at the base) as well as reproducible over multiple firings. This is a very desirable attribute and necessary for efficient transfer of analytes as a narrow band to a chromatographic column for separations. Comparisons of the adsorption capacities for the three types of μTPC chips used are graphically depicted in Fig. 3.7. All the chips were tested under identical conditions with respect to adsorption temperature (30 ˚C), flow rate (1 ml/min), and desorption temperature (~250 ˚C). The adsorption capacity of the SNP-Tenax TA relative to the Tenax TA chip improved by factors of 2.7, 1.3, 1.4, and 3.0 for hexane, toluene, 1,2-dichloroethane, and isopropanol

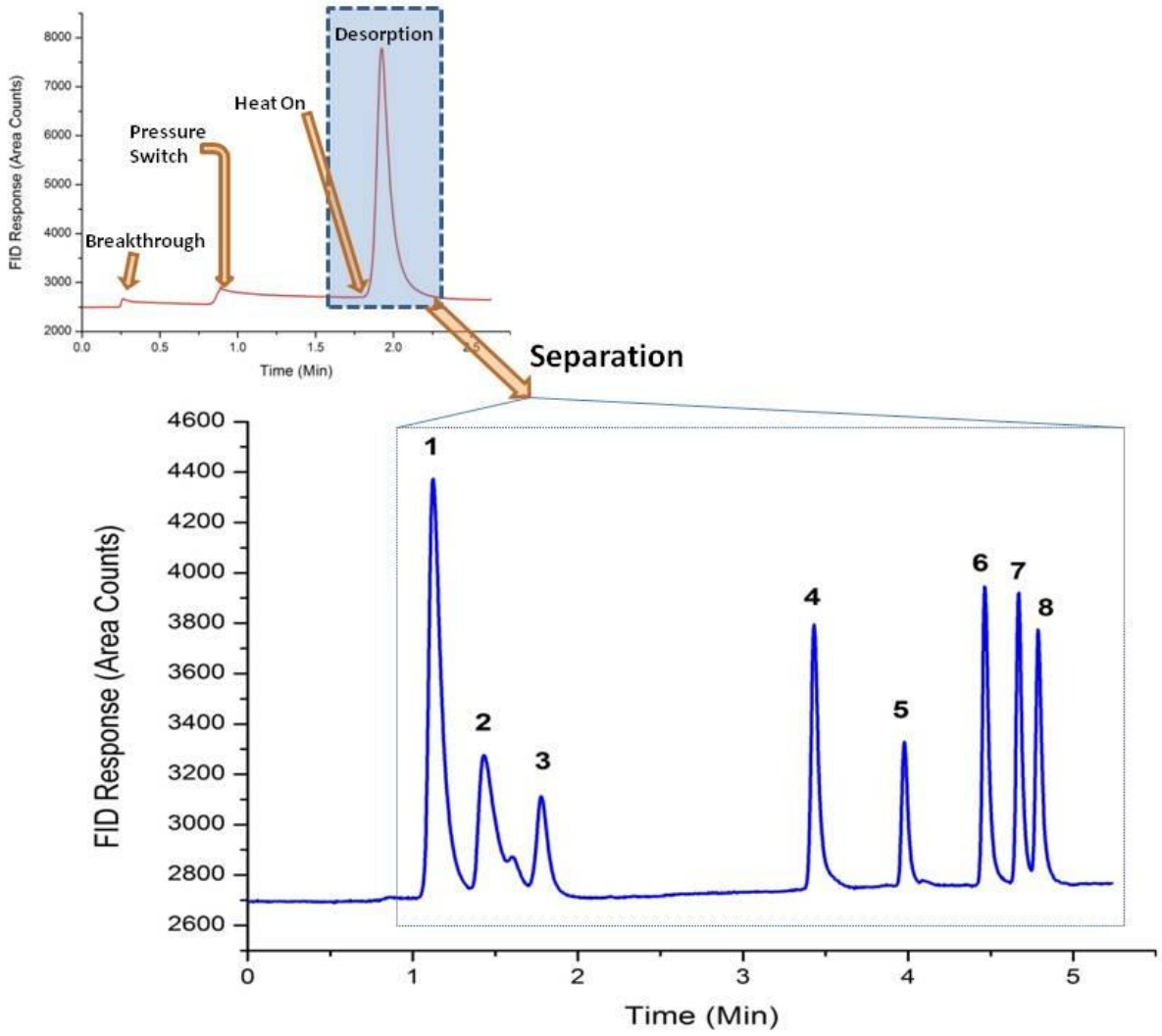

Figure 3.8 *The performance of the μTPC with SNP-Tenax TA chip for eight VOCs. Adsorption conditions: 5 psi and 10:1 split injection ratio. Desorption conditions: 20 psi and temperature programming (30°C-15°C/min-90°C). Compound identification: 1. chloroform, 2. isopropanol, 3. 1-propanol, 4. toluene, 5. tetrachloroethylene, 6. chlorobenzene, 7. ethylbenzene and 8. p-xylene.*

respectively, which represents a range of polarities. The enhanced surface area and morphology of Tenax TA most likely result in these enhancements for low to medium polarity compounds.

The most striking impact from polarity was observed for the SNP chip. Virtually no hexane (a very non-polar compound) was retained by the SNP chips; however, substantially more isopropanol was retained than for either the Tenax TA and SNP-Tenax TA chips (by factors of 9.0 and 3.0 respectively). This is due to the large number of active hydroxyl sites present on the silica surface that will have very strong intermolecular attractions via hydrogen bonding to very polar compounds such as alcohols. The reduced capacity for isopropanol in the presence of Tenax TA is most likely the result of a significant number of these sites being covered by the Tenax TA film. This type of interaction could be advantageous

for producing pseudo-selective chips for retention of polar compounds; however additional studies must be performed to ascertain whether irreversible adsorption could occur with more active polar compounds such as phenols or amines.

The capturing ability of the SNP-Tenax TA chip coupled with a chromatographic separation was successfully demonstrated by testing a mixture of eight commonly found VOCs. The liquid volumes of the VOCs used to produce the mixture were based on the relative vapor pressures of each VOC such that the vapor state mix contained comparable mole amounts of each VOC, assuming ideal gas law conditions. The mixture was contained within a septum sealed bottle. During the adsorption phase, the chip was loaded with a 10 µl headspace volume of the mixture using a gas tight syringe. The pressure was maintained at 5 psi (0.5 ml/min flow rate) to allow sufficient interaction between the analytes and the adsorbent. Before the thermal desorption, the pressure was increased to 20 psi (1.5 ml/min flow rate) and the signal was allowed to return to original level. The increased pressure was necessary to produce an adequate flow rate in the 30-m GC column. In addition, this assists in producing a narrower plug during the thermal desorption process for subsequent separation by increasing the volumetric flow rate. The GC column was then coupled to µTPC and the chip was quickly heated to 250 ˚C to desorb the compounds. The chromatogram in Fig. 3.8 is the result of coupling the µTPC to the GC column. It is evident from the chromatogram that the last few peaks widths (compounds 4–8) are significantly narrower than the preceding ones (compounds 1–3). This is due to the condensation of less volatile compounds onto the beginning of the cold GC column after thermal desorption resulting in a narrower sample plug. On the other hand, the more volatile compounds may tend to remain in the vapor phase and continue through the column, resulting in a broader peak width that is based on the desorption characteristics of the µTPC. The results shown in the top inset of Fig. 3.8 indicate that the chip successfully captured/concentrated all of the injected analytes from the mixture with a desorption peak width of ~10 s and a negligible breakthrough peak, which was expected since the volume injected and split ratio used were comparable to the conditions used for testing the adsorption capacities of the individual compounds previously described. Chromatograms obtained from multiple injections were highly reproducible.

III. Conclusion

A novel approach for enhancing the adsorption capacity of Tenax TA-coated µTPCs using nanoparticle deposition as a surface template has been demonstrated. A promising improvement was attained under similar conditions over ones coated only with thin film Tenax TA. The better capturing ability is attributed to the larger surface area provided by the SNP coating, thus increasing the interaction of gas molecules with the adsorbent surface. The exception to these observations was with a very polar compound, which was pseudo-selectively adsorbed with much higher retention on the SNP chip.

Chapter 4: A Purge and Trap Integrated MicroGC Platform for Chemical Identification in Aqueous Samples

(Part of this chapter reproduced from [193] with permission from Analyst)
M. Akbar, S. Narayanan, M. Restaino, and M. Agah, "A purge and trap integrated microGC platform for chemical identification in aqueous samples," Analyst, vol. 139, pp. 3384-3392, 2014.

Volatile organic compounds (VOCs) are emitted by a wide variety of products including solid and liquids [146]. Prolonged exposure to VOCs can cause serious health effects including liver, kidney, and nervous system diseases and can even cause cancer [147-152]. Similar effects have been reported for various aquatic organisms [153-155]. Different analytical techniques for their detection have been reported in the literature [156-158]. Microscale gas chromatography (μGC) provides a better solution with reduced size, low power consumption, and can lead to perform a handheld analysis of complex VOCs [64, 159]. μGC systems usually consist of an injector/pre-concentrator, a separation column and a detector all developed using micro electromechanical systems (MEMS) technology [26, 61, 141, 158, 160-163]. μTPC is one of the important components which allow the trace level detection of VOCs by accumulating them over a period of time. The trapped VOCs are then released in the form of a concentrated plug through thermal desorption process. The separation column is coated with a stationary phase to separate the VOCs into individual components for final detection by the detector. Several reports have been published for applications of μGC system related to homeland security, biomedical diagnostic and real-time environmental analysis [110-112]. On the other hand, the detection of VOCs in aqueous matrix has not received adequate attention among μGC community due to incompatibility of the system with aqueous matrix [164]. Water is found to saturate adsorbent in μTPC by capturing available adsorption sites and also damage most common polymer based stationary phases resulting in changes in retention time, selectivity and column bleeding. Extinguishing the most widely used flame ionization detector (FID) and a decrease in the sensitivity of electron capture detectors (ECD) has also been reported [165, 166]. The United States Environmental Protection Agency (EPA) has specified a list of water organic compounds (WOCs) with their maximum contamination level (MCL). At levels above the specified MCL (usually in ppb), WOC presence in aqueous media poses serious threat to human and aquatic life as shown in Table 4.1. Current methods for the identification of WOCs rely on removing them from aqueous sample prior to analysis using bench-top GC system. These methods include solid-phase micro-extraction (SPME), purge and trap, and hollow fiber membranes. They cannot be used for on-site monitoring of aqueous sample and rely on transporting the sample to the laboratories. Currently, commercially available FROG-4000TM from Defiant Technologies and Water Analysis Surety Prototype (WASP) from Sandia National Laboratories are capable of performing field analysis of water contamination. Nevertheless, the systems are large, expensive, require a trained technician and rely on conventional purge and trap mechanism. Thus, there still remains a demand for the development of a light

weight, less power hungry, inexpensive independent system capable of extracting and detecting WOCs from aqueous media.

Previously, our group has followed the direct injection method for monitoring water contamination. This approach requires additional time for removing the trapped water contents from µTPC adsorbent (dry purge time) [167]. Additionally, we have also reported microscale headspace sampling as a possible technique to extract WOCs [168], however, better sensitivity can be achieved through purge and trap method [169]. This paper describes fluidic integration of µGC components with our newly developed µPE chip for analyzing WOCs. The results indicate that this hybrid integrated system successfully extracted and separated four WOCs at 500 ppb concentration. This is the first realization of an easily deployable microsystem for on-site water monitoring.

I. Method Description

A. General Operation

Fig. 4.1 shows a block diagram explaining the proposed µGC experimental setup including the µPE for extraction of WOCs from the aqueous sample. The µPE device contains two inlets, one for aqueous sample to be analyzed and one for a pure inert gas to purge the WOCs. The distribution network for aqueous sample entrance provided at the top of the chip is used to uniformly spread the sample inside the

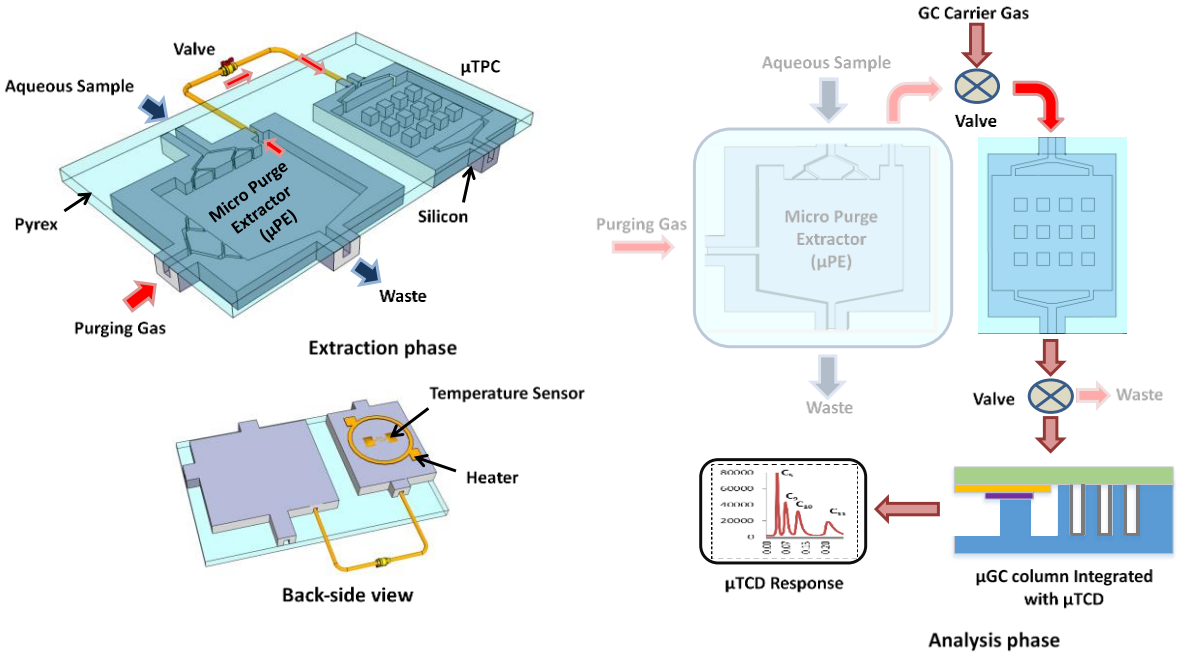

Figure 4.1 *Conceptual diagram showing the topology for the extraction and analysis of water organic compounds. Back-side heater is utilized for thermal desorption of analytes from the µTPC for chromatographic analysis.*

chip. Similarly, the multiple inlets for purging gas are intended to enhance the interaction between two phases (air and water) inside the chip and to facilitate the removal of WOCs from the streaming water. The chip also contains two outlets; one is used as water waste and one for directing the purged WOCs to the trap (µTPC). The outlet for directing WOCs to the µTPC is provided at the top corner of µPE chip. The setup is operated in two phases namely; 1) extraction phase and 2) analysis phase. During the extraction phase, two microfabricated chips (µPE and µTPC) are connected in a tandem configuration using a valve while the µPE chip is maintained vertically (see the supplementary video) to prevent water from entering into the µTPC chip via air outlet. With the vial connected to sample inlet, aqueous solution is introduced into the µPE chip using purified nitrogen. High purity nitrogen gas is supplied through the air inlet of the µPE chip trapping WOCs on the adsorbent surface in the µTPC chip. The analyzed mass is calculated from the sample concentration and the volume of water collected during the purged time. During analysis phase, the µPE is taken offline and µTPC connected in series with the µGC column with embedded µTCD detector using a six port switching valve. Helium is used as a carrier gas while the outlet of the column is connected to the FID of a commercial Agilent HP7890 GC system- for verification purposes. The sensor on the backside of the µTPC is used to monitor the temperature profile of the chip when heated. A voltage applied to the heater on the backside of the µTPC heats it up from room temperature to 150 °C. The desorbed WOCs are separated by the µGC column. A 40 mA current is sourced into a Wheatstone bridge with two resistors of µTCD in each of its arms. The differential voltage measured across the two resistors enables the detection of WOCs which is fed into a Keithley 2700 and recorded on a LabVIEW program.

B. µTPC On-Chip Sensor Calibration

For accurately measuring the temperature reached during desorption process, the on-chip heater was calibrated by placing the µTPC in a commercial GC oven and measuring the resistance for different temperatures.

C. µGC Column Validation

The efficiency of the coated column was evaluated with µTCD switched to ON condition by applying an 8.3 V DC voltage. This voltage corresponds to a temperature of 95 °C. This was measured with helium flowing at the operating pressure of 12 psi, similar to the method we have previously reported [170]. The metric commonly used for column performance is height equivalent to a theoretical plate (HETP),

$$\mathrm{HETP} = \frac{\mathrm{L}}{\mathrm{N}}$$

where L is the length of column and N is the number of theoretical plates in the column. N is calculated experimentally from peak retention time (t_r) and peak width at half height ($w_{1/2}$).

$$N = 5.54 \left[\frac{t_r}{w_{1/2}}\right]^2$$

The plate number was calculated was calculated over a range of column pressures with constant split injection ratio of 150:1 using chlorobenzene diluted to 2% (v/v) in hexane.

D. µTCD Characterization

The separation and identification of the four WOCs using only the column and its µTCD (without the µPE and µTPC) was performed by installing the chip inside the GC oven with its inlet and outlet connected to the injector and the GC FID, respectively. A 0.1 µl volume of sample containing the WOCs diluted to 2% (v/v) in hexane was injected into the µGC column for separation and identification of the four WOCs by the chip.

Similarly, for µTCD response calibration, five samples (0.5%, 10%, 20%, 30%, and 40% (v/v) in hexane) for each WOC were prepared and tested. A 0.1 µl of each sample was injected three times in succession using the GC autosampler module with the split ratio maintained at 150:1. By using the density, mass for each WOC was calculated taking split injection ratio into account.

II. Materials and Instruments

Reagent grade WOCs listed in Table 4.1, solvents, and Tenax TA (80/100 mesh) used in this work were purchased from Sigma Aldrich (St. Louis, MO) in >99% purity. AZ 9260 photoresist and OV-1 were purchased from MicroChemicals (Germany) and Ohio Valley (Marietta, OH), respectively. Silicon wafers (4 in. dia., 500 µm thick, n-type, single side polished) and Borofloat wafers (4 in. dia., 700 µm thick, double side polished) were purchased from University wafers and Coresix Precision Glass (Williamsburg, VA), respectively. Fused capillary tubes (200 µm outer dia., 100 µm inner dia.,) were purchased from Polymicro Technologies (Phoenix, AZ).

A. Fabrication Process

Fig. 4.2 summarizes the fabrication process for all the three MEMS components. We have previously reported the fabrication, characterization, and operation of the µTPC and the column integrated with µTCD [26, 141, 156, 160-163]. Herein, we briefly discuss the fabrication of these two components in addition to the fabrication of our newly developed microfabricated purge extractor.

1. µTPC and µPE Chip

The fabrication of µTPC was performed on a standard 4” wafer using MEMS processing technology. First, photolithography was performed to pattern micro-posts/fluidic ports. The wafer was then subjected to deep reactive ion etching (DRIE, Alcatel) to achieve a depth of ~250 µm. After stripping the

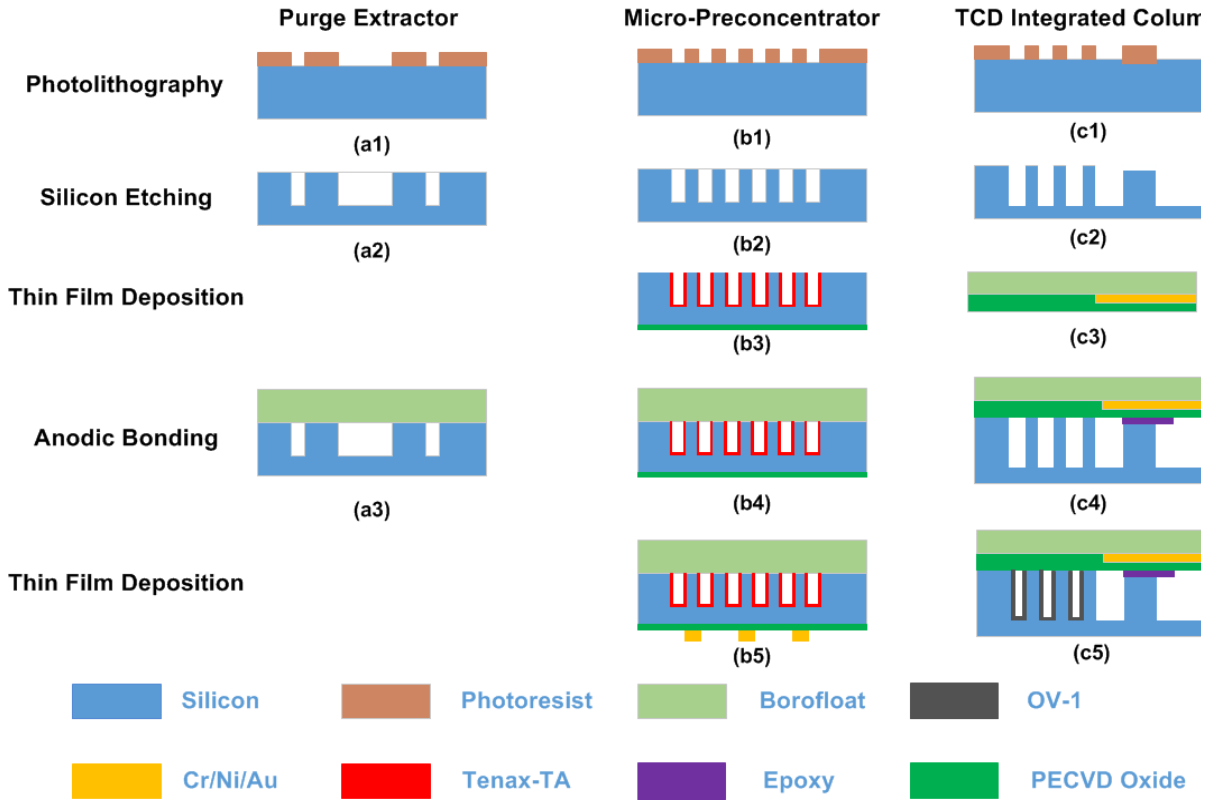

Figure 4.2 *Fabrication procedure for µPE, µTPC and µGC column with µTCD detector. The left column shows MEMS processes performed for fabricating these chips.*

photoresist off the front-side, a 500nm thick oxide layer was deposited on the backside and the wafer diced into individual chips. The chip was then filled with Tenax TA solution (10 mg/ml in dichloromethane) and allowed to evaporate to deposit a thin film (~200 nm) of the polymer adsorbent on the cavity surfaces. The chip was then capped with a Borofloat wafer by anodic bonding. Following bonding, the chips were loaded onto the platen of an e-beam evaporator (PVD-250, Kurt Lesker) with the backside facing the crucible. The chips were masked by a stainless steel shadow mask patterned with the features defining the heater and sensor. Following this, 40nm/100nm/25nm of Cr/Ni/Au was deposited to get nominal resistances of 15 ohm and 250 ohm for the heater and sensor, respectively. Finally, the devices were unloaded; the shadow masks removed off and fused capillary tubes epoxied into the inlet/outlet ports. The fabrication process of the µPE chip followed that of our µTPC but without the adsorbent coating and backside oxide/metal deposition.

2. µGC Column with Embedded TCD

A two-step anisotropic etching of silicon was performed for hosting the feedthroughs and microfluidic channel by spin coating the wafer with S1813. A shallow depth of 2–3µm was achieved which prevented

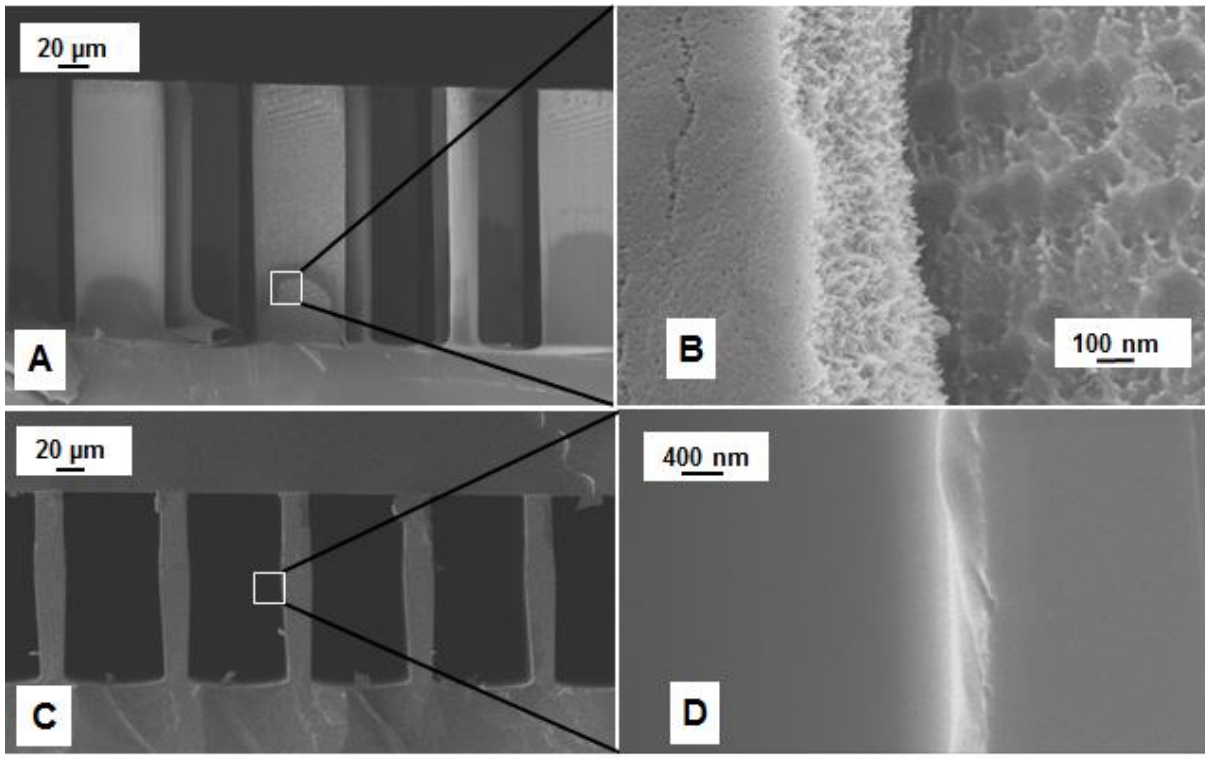

Figure 4.3 *(A and B) SEM images showing Tenax TA coating on sidewall of micro-posts inside µTPC chip, (C and D) polydimethylsiloxane coating on the interior wall of the column channel.*

a contact between the metal interconnects on the Borofloat wafer and the walls of the separation column in silicon upon bonding. A 12-µm-thick AZ9260 photoresist was patterned with a mask for subsequent deep etching of the channels resulting in 250-µm-deep channels for the separation. Then, TCD resistors were fabricated on a glass substrate by utilizing a lift-off process of a 40nm/100nm/25nm Cr/Ni/Au stack in the e-beam evaporator. After aligned anodic bonding of the diced detector on glass and the diced separation column on silicon, capillary tubes were epoxied into the inlet/outlet ports. The chip was static coated with polydimethylsiloxane by filling it with a solution of 10mg/ml OV-1 in pentane, followed by carefully sealing one end with wax and pulling a vacuum at the open end. This procedure left a thin layer of OV-1 coating (~250 nm) on the walls of the column channel. An SEM image of the Tenax TA and OV-1 coating is shown in Fig. 4.3. The optical image of all fabricated chips is shown in Fig. 4.4.

B. Aqueous Sample Preparation

To avoid changing the concentration of WOCs, a 24 ml cylindrical vial was filled completely with deionized (DI) water leaving no headspace. Both 1 ppm and 500 ppb solutions (v/v) were prepared in two steps. First, 1000 ppm (v/v) solution was made by adding 24 µL of each WOC to 24 ml of DI water. Second, the solution was further diluted 1:24 and 1:12 with DI water to achieve concentrations of 1 ppm

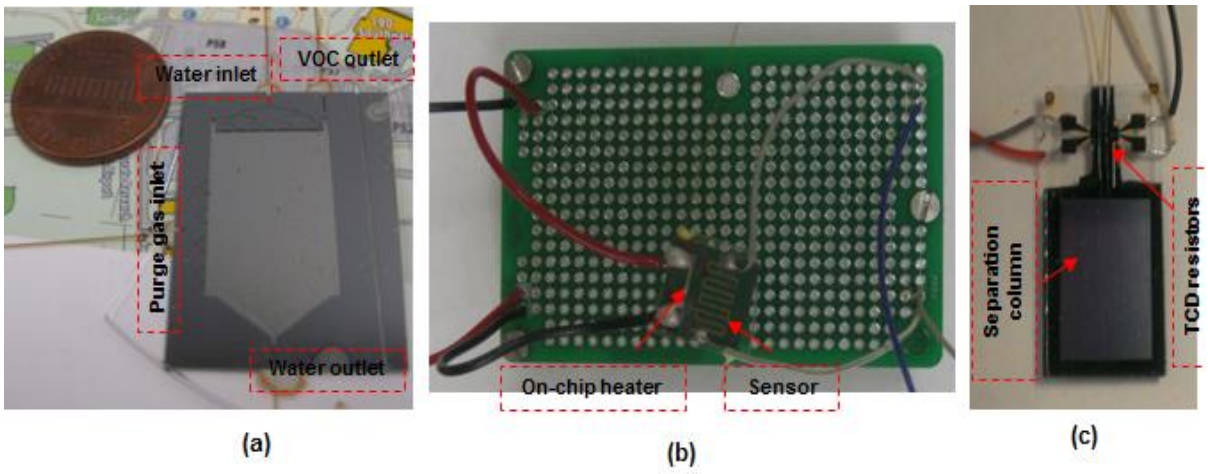

Figure 4.4 *Optical image of fabricated (a) µPE (b) µTPC and (c) µGC chip with embedded resistors utilized as thermal conductivity detector for aqueous analysis.*

and 500 ppb, respectively. The solution was analyzed immediately to avoid compromising the sample integrity. Before processing any sample, all parts of the equipment in contact with the sample were demonstrated to be interference free. This was accomplished through a blank run.

III. Results and Discussion

Before evaluating the performance of the whole integrated purge and trap µGC system, the heating and sensing elements of the microfabricated pre-concentrator, separation column, and the detector were calibrated and the separation performance of the column was evaluated.

A. µTPC On-Chip Heater

A 12 V DC voltage was applied to the heater and the sensor resistance was measured until the resistance representing the desired temperature value was reached. The sensor resistance varied with applied voltage due to ohmic heating. The final temperature of 150 °C was attained within 7 s representing a ramp rate of 20 °C /s. This condition maintained constant during the desorption process of the WOCs trapped on the Tenax TA polymer coating of the µTPC.

B. µGC Column and µTCD Performance

The maximum plate number (optimum condition) observed for the 2-m long column was about 6,200 at 12 psi (flow rate 0.62 ml/min). The column was operating at this optimum flow condition for further investigations.

The separation and identification of the four WOCs was performed by the method described previously. FID was used to verify the chromatogram generated by the µTCD. WOCs were successfully

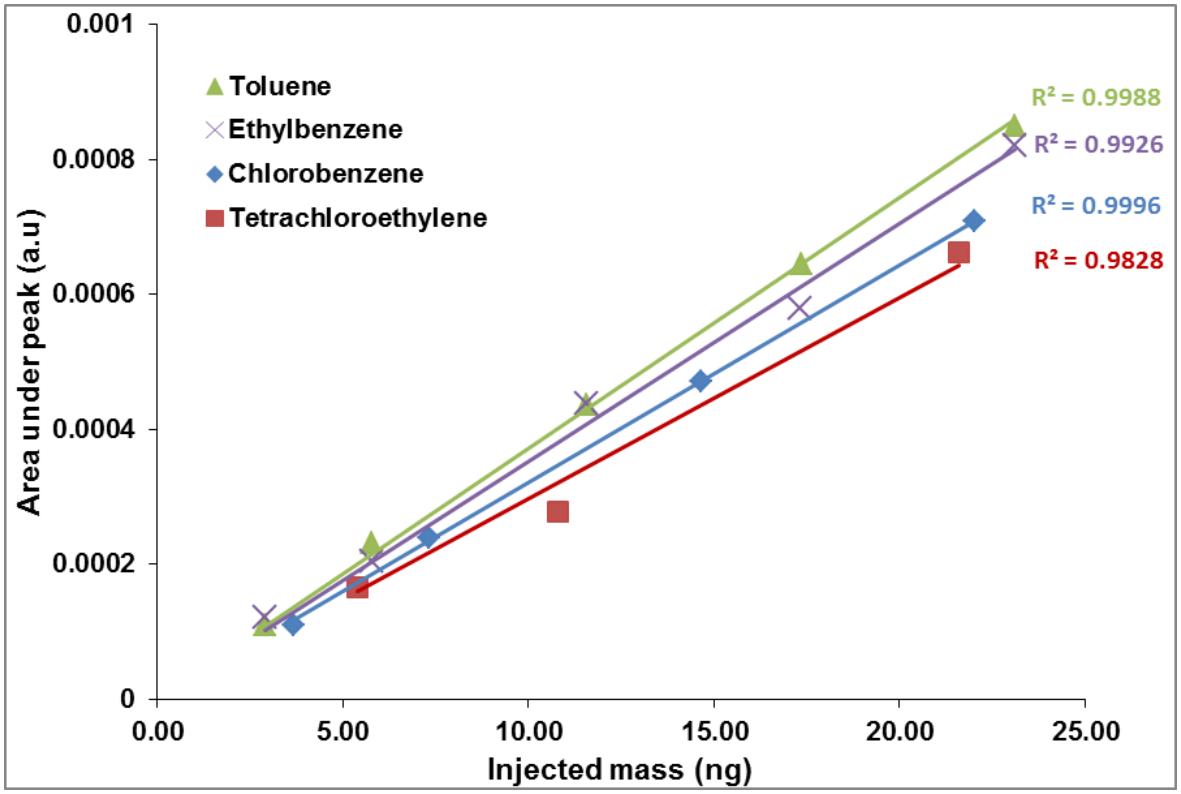

Figure 4.5 *Calibration curve showing response of µTCD for five different concentrations of WOCs in this study. The relative standard deviation is < 10% for all cases.*

separated and detected by the chip within 1.5 min. Next, a calibration curve showing the output of the µTCD as a function of the injected WOC concentration was obtained by the method described previously. The injected mass varied from about 3 ng to 23 ng for toluene, 5.4 ng to 43 ng for PCE, 3.7 ng to 29.3 ng for chlorobenzene and 3 ng to 23 ng for ethylbenzene. A calibration curve showing the average peak area under the µTCD signal obtained for three injections is shown in Fig. 4.5. It is worth-mentioning that the conventional TCD has a minimum detection limit of 1 ng.[171] Results obtained indicate a unique response of the µTCD for each WOC with relative standard deviation (RSD) less than 10% for all cases. The coefficient of determination (R^2) was greater than 0.99 in all cases.

C. Microsystem Evaluation

Following calibration and performance evaluation of each µGC unit, the µPE was put in place. The ability of the complete system comprising µPE and µTPC chip, separation column, and the thermal conductivity gas detector (µTCD) to continuously monitor WOCs in aqueous sample was realized experimentally by the method explained earlier. The aqueous solution was introduced into the µPE chip using purified nitrogen at 10 psi. High purity nitrogen gas was supplied through the air inlet of the µPE chip trapping WOCs on the adsorbent surface with a flow rate maintained at 0.4 ml/min (5psi) through

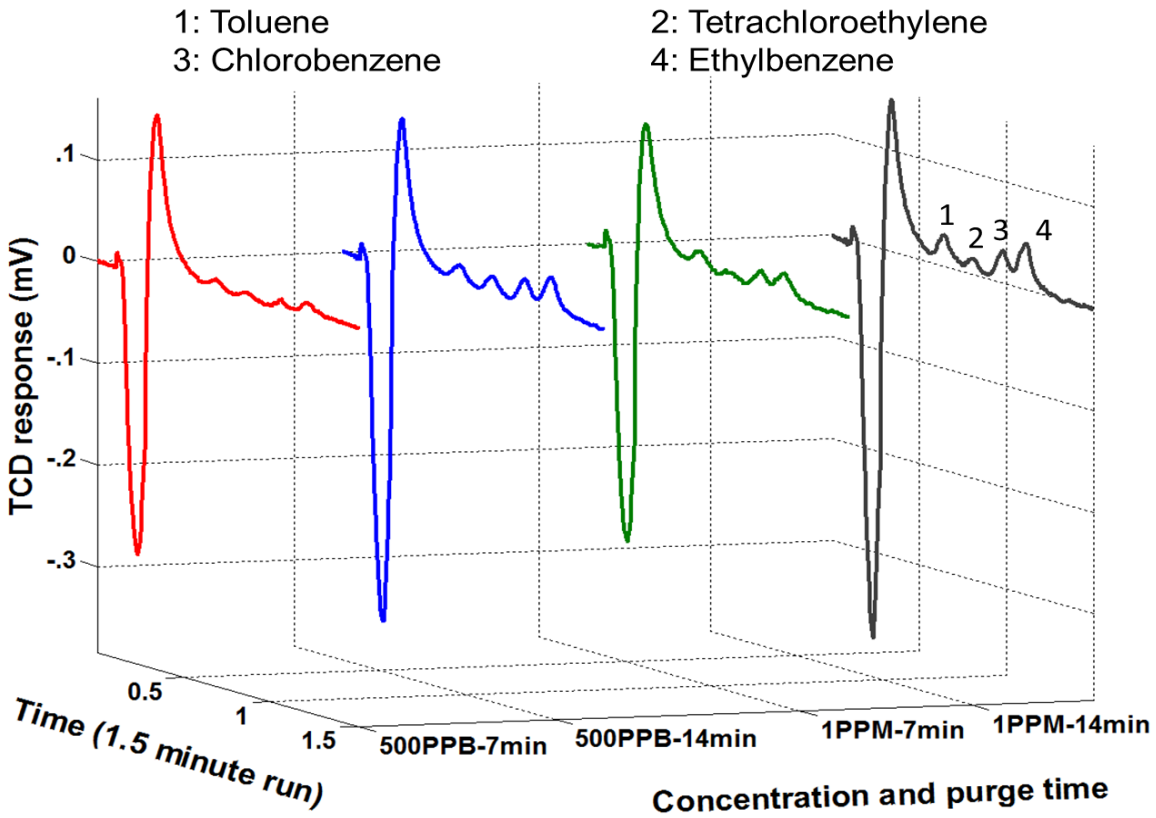

Figure 4.6 *Set of chromatogram indicating increase in µTCD response with increase in purge time and concentration of WOCs. Peak assignments: 1. toluene, 2. tetrachloroetylene, 3. chlorobenzene, 4. ethylbenzene.*

µTPC chip. The extraction period was varied for three discrete periods of 7, 14 and 21 min. The set of chromatograms in Fig. 4.6 was generated using 500 ppb and 1 ppm aqueous samples for two different extraction periods. The initial negative dip is due to the sample mixture passing under the reference detector. At this stage, the signal detector experiences carrier gas and hence is constant. This results in a negative voltage output as explained before [163]. As the sample mixture moves through the column, it is separated over time. When the individual components pass under the sample detector, the reference detector experiences the carrier gas and hence results in positive peaks corresponding to each eluted compound. The second peak is due to trace moisture extracted from the purge chip and is not seen on the FID signal which is insensitive to trace water content. The increase in peak heights for all WOCs with the increase in extraction time was observed which clearly indicated the validation of the proposed approach. It is also evident that rapid chromatographic separation and detection of all four WOCs within 1.5 min is achieved at room temperature.

The method precision was evaluated by three repetitive analyses for each test. After each analysis, the µTCP was heated to 150 °C (conditioning step) to prevent carry-over from the previous runs, following which a blank run was performed to confirm the same. The change in detector response (area under the

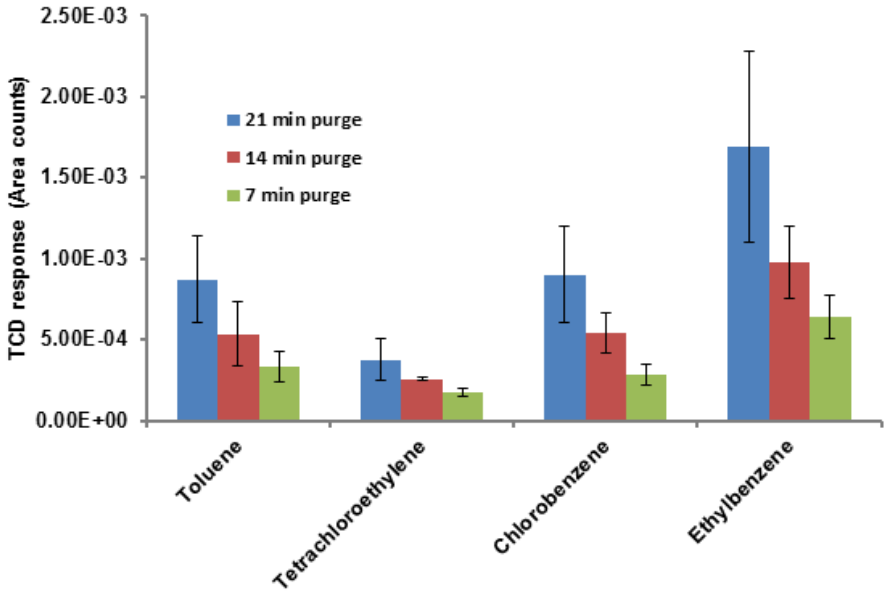

Figure 4.7 *Graph showing the μTCD response variation with increasing purge time for a sample containing four WOCs at 1 ppm concentration.*

peak) with purge time was then monitored for a sample containing four WOCs at 1 ppm concentration. The experiment was repeated thrice for three different purging times and the average value was plotted for each WOC. Fig. 4.7 shows that the peak area increases with purging time. The increase in peak area was attributed to the increase in the quantity of nitrogen (inert gas used) that bubbled through the aqueous sample, and consequently, more quantity of WOC moved from the liquid to the vapor phase. Additionally, in streaming mode more fresh sample entered the μPE chip replacing the old one, thereby increasing the amount of WOC purged over time.

The results in Fig. 4.7 indicate that ethylbenzene and chlorobenzene are purged easily from the aqueous sample as compared to PCE and toluene. This is due to their relatively high partition coefficient (K_{ow}) value which is defined as the ratio of concentration of a compound in a hydrophobic solvent (usually octanol) to its concentration in water at equilibrium. In other words, it is a measure of hydrophobicity and depends on size, polarity and hydrogen bond strength of a compound. Hydrophilic compounds (with low partition coefficient) are held by very strong dipole-dipole interaction and hydrogen bond in water and thus could not be easily purged from the sample. Increasing the temperature of the sample should increase the purged amount by supplying enough thermal energy to the molecule to break the dipole-dipole interaction [172]. The sample analyzed during the purge time was collected to determine the percent recovery of each compound. Assuming that the trap is able to capture the entire purged amount, percent recovery is defined as the ratio of the amount that is collected for chromatographic analysis relative to the amount that was originally present in the aqueous sample. Table 4.1 summarizes

Contaminants	Potential Health Effect	Contamination Sources	Amount Recovered (ng)	Recovery	Log (K_{ow})	MCL (mg l^{-1})
Toluene	Nervous System Liver Problems	Petroleum Factories	5.70	23%	2.75	1
Perchloroethylene	Liver Problems Risk of Cancer	Discharge from Factories and Dry Cleaners	5.40	18%	2.57	5
Chlorobenzene	Liver and kidney problems	Discharge from Chemical Factories	9.00	25%	2.86	0.1
Ethylbenzene	Liver and kidney problems	Petroleum Refineries	18.7	38%	3.14	0.7

Table 4.1 *List of water organic compounds with their originating sources and potential health risks.*

the percent recovery for each compound at 1 ppm concentration. The percent recoveries are lower than those reported in literature [173, 174]. This can be attributed to the fact that commercial purge and trap systems use high purging gas flow rates (normally 40 ml/min) and also use traps consisting of a short length micro-bore tubing packed with granular form of adsorbent material. Such traps at the cost of high pressure drops and high power consumptions can provide higher adsorption capacity. It is notable that low recoveries have also been reported previously by Sandia National Laboratories in their bench-top (WASP) system described earlier due to the flow limitations in their setup [175]. In addition, we have achieved the detection limit of 500 ppb which is comparatively higher than the commercial purge and trap systems. Part of this is attributed to small sample volumes (in µl) analyzed by the µPE chip when compared to the commercial purge and trap systems. Efforts are underway to improve the extraction efficiency and bring it up to par with the commercial systems. Nevertheless, the purpose of this article is to integrate all µGC components to automate the sampling of water and extract and identify WOCs in real world situation. Modification in design parameters and thermal manipulation for optimization of µPE chip performance will be described in a separate report.

IV.Conclusion

First micro-scale version of purging device for the extraction of WOCs from aqueous sample has been described. The potential application of the chip for on-site monitoring of aqueous sample when equipped with all necessary µGC components has also been discussed. We have first characterized the performance of the µGC column with µTCD turned ON and explored the optimum conditions for the µGC column. Next, we have obtained a calibration curve indicating the change in µTCD response to different amount of individual WOCs (in the absence of the µPE and µTPC). We have shown that fixed volume samples of water spiked with known concentrations of the WOCs can be extracted using the µPE chip and subsequently trapped on the µTPC. We have finally determined the percentage recovery of each compound thereby successfully demonstrating the ability of the complete system in analyzing WOCs in an aqueous sample.

Chapter 5: Zebra GC-A Mini Gas Chromatography System for Trace-Level Determination of Hazardous Air Pollutants

(Part of this chapter reproduced from [207] with permission from Sensors and Actuator B: Chemical)
A. Garg, M. Akbar, E. Vejerano, S. Narayanan, L. Nazhandali, L. C. Marr, et al., "Zebra GC: A mini gas chromatography system for trace-level determination of hazardous air pollutants," Sensors and Actuators B: Chemical, vol. 212, pp. 145-154, 2015.

Hazardous air pollutants, such as aromatic compounds and polycyclic aromatic hydrocarbons have serious environmental and health effects that are implicated in a variety of diseases in humans ranging from birth defects to cancer [176]. Toxic volatile organic compounds (VOCs) such as benzene and toluene found in gasoline, and xylene used in ink, rubber, and leather industries are of concern as they are present at elevated concentration due to their high vapor pressure. Exposure to these toxicants may cause adverse health effects. Most of these pollutants emerge from man-made sources and activities including emissions from automobile, refineries, factories, and power plants. To safeguard the health of exposed individuals and to ensure that the concentrations of these VOCs do not exceed the permissible exposure levels set through federal regulations, it is critical to monitor exposure to these compounds.

Among various analytical methods, gas chromatography (GC) has been the established method for assessing the presence and concentration of VOCs in the environment, and GC coupled to mass spectrometry (GC-MS) is one of the most accurate and widely used tools. In this technique, samples are first collected from the field through trap based systems such as sorbent tubes or canister and then are analyzed in a laboratory by trained technicians. This technique requires manual intervention and multiple steps including sampling, storage, and shipping before analysis, and therefore is susceptible to higher losses and has longer measurement cycles. Most of these drawbacks can be overcome by using portable, field-deployable, and real-time detection systems. There have been attempts at miniaturizing GC-MS systems [177, 178], but such systems are still bulky, expensive, and consume high amount of power. Other real-time detection techniques involve using a sensitive photo-ionization detector (PID)[179] to realize a total VOC analyzer. PID-based systems suffer from selectivity issues and require filtering at the source which renders them ineffective and expensive for multi-compound analysis. Colorimetric tubes are another inexpensive and popular technique for VOC analysis which rely on a color change induced by the irreversible reaction between the sensing material and the analyte [180]. However, this technique requires human intervention, and its use is limited by slow response and large uncertainty. A more comprehensive solution for detection of VOCs is based on portable gas chromatography systems leveraging micro-fabricated components to achieve a small form factor, low power consumption, selectivity, and high sensitivity. Several commercial high performance portable gas chromatography systems [181, 182] have been reported, but they are still bulky, energy inefficient, and expensive for real-time environmental

monitoring applications. Such system limitations can be addressed to a reasonable extent by making them more application specific and using lower cost, batch-fabricated micro components.

Currently, considerable research efforts in the development of micro gas chromatography (μGC) systems are directed towards developing and optimizing high-performance microfabricated components such as pre-concentrators (μPC) [60, 74, 183], separation columns (μSC) [24, 29, 57], and gas detectors [184-187]. However, integration of the various components is a critical yet underexplored aspect.

In this work, we present an innovative μGC architecture, which leverages monolithic integration of a separation column with micro-thermal conductivity detectors (μSC-TCD) [47] to minimize band broadening and chip-to-chip fluidic interfaces. The integration eliminates the need for a reference line and requires fewer external components. Another innovative aspect of this architecture is a method to perform very sharp injections from the μPC even in the presence of flow-sensitive gas detectors like TCD. This innovative system design relaxes constraints on the design of the μPCs by mitigating the effect of vapor desorption rate on the injection-plug width. The design enables us to achieve low detection limits suitable for environmental monitoring applications. We report in this current work the detailed system design, prototypal implementation, operation, and laboratory characterization of the proposed μGC system, dubbed Zebra GC. Table 5.1 provides a detailed comparison of four μGC systems, including Zebra GC, and highlights the features, advantages, and disadvantages of different system components. As seen, other reported μGC systems [34, 67, 188-190], while producing promising results, use individually fabricated chips which require extra effort to avoid compound condensation in cold spots. Also, some of these systems still use conventional components to achieve high performance which can lead to increased energy consumption or increased analysis time.

I. Zebra GC System Architecture, Fabrication and Operation

The Zebra GC has two major units: 1) sampling and pre-concentration, and 2) separation and detection. The μPC and μSC-TCD chips used in this work have integrated thin film heaters and sensors which are used for temperature control during desorption and separation. These microfabricated components are integrated with off-the-shelf flow controllers to implement GC flow cycles – loading, injection, analysis, and cleaning. An embedded platform, based on an 8-bit microcontroller (ATmega640, Atmel Corporation), is responsible for fluidic and thermal control. It also implements the user interface, signal processing, and data acquisition circuitry. The system is highly portable, battery powered, and easy to operate. It can be paired with a laptop for device control and data visualization through a LABVIEW application.

A. Materials

Features	INTREPID system, University of Michigan, Ann Arbor [64]	µGC system, Arizona State University [188]	µGC system, CNR-IMM Institute for Microelectronics and Microsystems [67]	Zebra GC system, Virginia Tech
Sampling and Injection	Hybrid 2-stage (sorbent tube + micro trap, Carbopack) **Pros**: Short sampling time and sharp injections **Cons**: Power consumption and trap cleaning time increases.	Sorbent tube packed with Carbopack **Pros**: High volume sampled **Cons**: High power consumption, long cleaning times and wide injection plug	Microfabricated cavity packed with adsorbent. **Pros**: Low power consumption **Cons**: Medium sample volume and wide injection plug	Microfabricated cavity with embedded pillars and TenaxTA coating **Pros**: Low power consumption, High surface area, very sharp injections **Cons**: Low sample volume
Separation	1-m, spiral channel (150 µm × 240 µm) PDMS coated micro-column, temperature controlled Separation Time: 1 min	Multiple configurations. 2-m & 19-m carbowax coated capillary columns Separation Time: 3 min	0.5-m, spiral channel (800 µm deep) carbograph packed micro-column, temperature controlled Separation Time: 10 min	2-m, rectangular channel (70 µm × 240 µm) PDMS coated micro-column, temperature controlled Separation Time: 1 min
Detection	Chemi-resistor array. LODs – 0.48 to 2.2 ng. **Pros**: Identification of co-eluted compounds **Cons**: Sensor response varies with flow rate and temperature, and optimal operating point changes according to analyte	Tuning-fork. Sensitivity ~ 100 ppbv. **Pros**: Low power consumption and high selectivity **Cons**: Long response time	Metal-oxide semiconductor. Sensitivity ~ 5 ppbv **Pros**: High sensitivity **Cons**: Long-term drift, Long response time	µTCD embedded in separation column. LOD – 1 ng **Pros**: High reliability, Integrated, Low cost **Cons**: Low selectivity
Integrated System	Carrier gas: Ambient-air **Pros**: High performance, selective, fast analysis **Cons**: High system power consumption expected due to conventional trap	Carrier gas: Ambient-air **Pros**: High selectivity **Cons**: Only one microfabricated component, high system power consumption expected	Carrier gas: Ambient-air **Pros**: All microfabricated components, Highly-sensitive **Cons**: Detector drifts over time – calibration(weekly) and replacement (few months) required	Carrier gas: Helium **Pros**: All microfabricated components, monolithic integration, good performance, low cost, high reliability **Cons**: Low selectivity detector, low sample volumes

Table 5.1 *Summary and comparison of µGC systems*

Silicon wafers (4 inch dia., 500 µm thick, n-type, double side polished) and Borofloat wafers (4 inch dia., 700 µm thick, double side polished) were purchased from University wafers and Coresix Precision Glass (Williamsburg, VA), respectively. Tenax TA (80/100 mesh) and all other chemicals used for chromatographic testing were of analytical standard (>99% purity) and purchased from Sigma-Aldrich (St. Louis, MO). AZ 9260 photoresist and polydimethylsiloxane (PDMS or OV-1) were purchased from MicroChemicals (Germany) and Ohio Valley (Marietta, OH), respectively. Fused capillary tubes (200 µm outer dia., 100 µm inner dia.) were purchased from Polymicro Technologies (Phoenix, AZ).

B. Microfabricated Components

The fabrication process of the µPC and µSC-TCD has been depicted in Fig. 5.1 and described in our previous publications [47, 125, 141, 156, 161, 191] in detail. The µPC is a 13 mm×13 mm silicon-glass chip and consists of an array of high aspect ratio micro-posts inside its 1 cm square cavity. The micro-posts are realized by bulk micromachining of a 4 inch silicon wafer utilizing a deep reactive ion etching process to achieve a depth of 240 µm. A 1-µm thick plasma enhanced chemical vapor deposition (PECVD) oxide layer that acts as an insulator is deposited on the backside (Fig. 5.1-a2). The wafer is then diced into individual chips. The micro-posts are then coated with a thin film (~200 nm) layer of Tenax TA adsorbent (Fig. 5.1-a3) followed by capping with a Borofloat wafer via anodic bonding (Fig. 5.1-a4). A 40 nm/230 nm of Cr/Ni stack is deposited which serves as a heater and temperature sensor on the

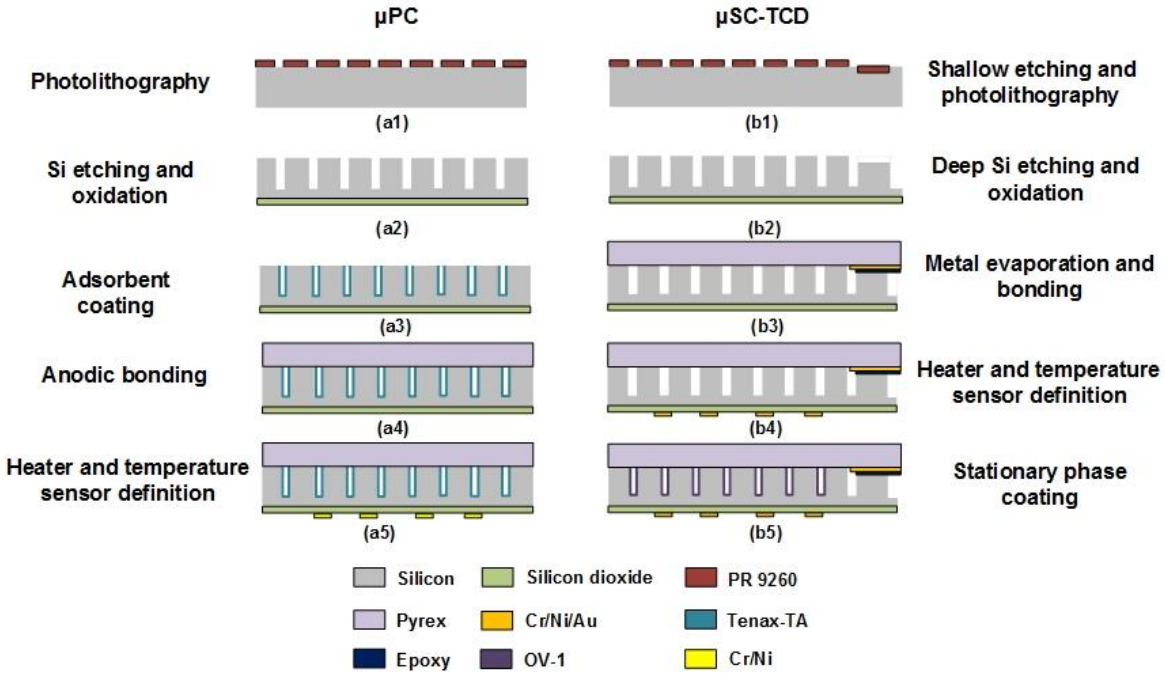

Figure 5.1 *Process flow for the fabrication of µPC and µSC-TCD with embedded temperature programming capability.*

backside of the chip using an e-beam evaporator (PVD-250, Kurt Lesker) (Fig. 5.1-a5). The nominal resistance of the heater and sensor is around 15 Ω and 250 Ω, respectively. Finally, fused capillary tubes are inserted and epoxied to the inlet/outlet ports.

For the μSC-TCD, two-step anisotropic etching of silicon is performed. First, a shallow depth of 2–3 μm (Fig. 5.1-b1) is achieved which prevents the contact between the metal interconnects on the Borofloat wafer and the walls of the separation column in silicon upon bonding. Second, a 2 m long, 70 μm wide and 240 μm deep channel is etched into silicon wafer (Fig. 1-b2). TCD resistors are fabricated on a glass substrate using a lift-off process for a 40 nm/100 nm/25 nm Cr/Ni/Au stack deposited employing the e-beam evaporator. The glass and silicon substrates are then aligned and bonded together (Fig. 5.1-b3). The heaters and temperature sensors are fabricated on the backside of the chip using stainless steel shadow mask (Fig. 5.1-b4). Afterwards, the capillary tubes are epoxied into the inlet/outlet ports. The chip is finally coated with a thin layer (~250 nm) of OV-1 on the walls of the column channel (Fig. 5.1-b5). An SEM image of the Tenax TA and OV-1 coating is shown in Fig. 5.2. The optical image of all fabricated chips is shown in Fig. 5.2-A.

C. Integrated Electronic Module

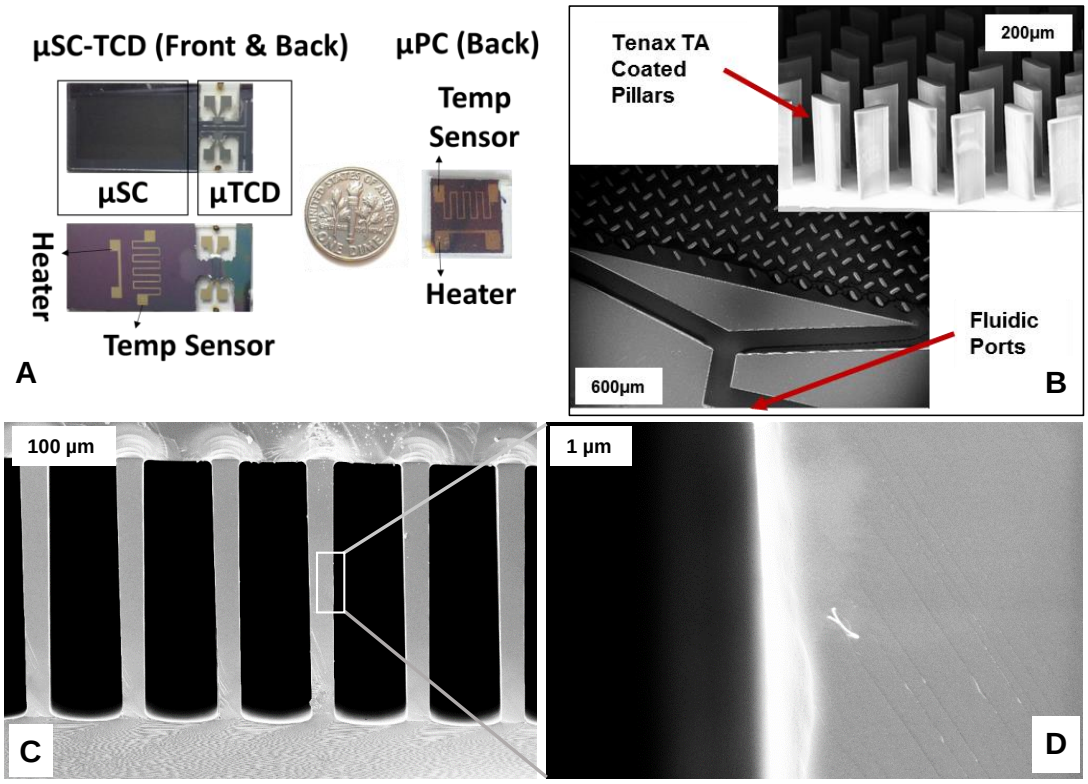

Figure 5.2 *(A) Micro-devices (B) SEM images showing micro-posts in μPC (C, D) polydimethylsiloxane coating on the interior wall of the column channel.*

The microfabricated components, integrated with the pump (Parker Hannifin Co.), multi-way valves (The Lee Co.), and a portable helium cylinder, are controlled through an integrated electronic module managed by an 8-bit micro-controller, as shown in Fig. 5.4-a. Latching valves are selected to optimize power consumption and controlled by applying a 100 ms 5 V DC pulse through an H-Bridge. The pump flow rate is adjusted by varying the pulse-width modulation (PWM) duty cycle, which is an important parameter during sample collection. The on-chip temperature sensors are connected in a 3-wire resistance temperature detector (RTD) configuration by using two well-matched current sources with a high precision 24-bit ADC. The reference voltage for the ADC is also generated using these matched current sources, through a precision resistor and applied to the differential reference pins of the ADC. This scheme ensures that the span of the analog input voltage remains ratio-metric to the reference voltage and any error in the former due to temperature drift of the excitation current is compensated by the variation of the latter. On-chip heaters are controlled through PWM channels and a digital proportional control system is implemented as part of the embedded firmware, which generates different profiles for temperature reference signal based on the user input (initial temperature, step, ramp, final temperature).

The µTCD is connected in a Wheatstone bridge, driven by 7.5 V DC, with low noise thin film resistors (PF1260 series, Riedon Inc). The differential signal is conditioned and filtered prior to feeding into an ultra-low noise 24bit ADC (AD7793, Analog Devices). The signal is further filtered digitally, using an on-chip low pass modified Sinc3 filter that also provides 60 Hz rejection. The TCD, along with the entire system, is operated at a data rate of 10 Hz, which provides substantial resolution for the peaks.

D. System Integration, Interface, and Operation

Microfabricated components along with the flow controllers, integrated electronic module, and user

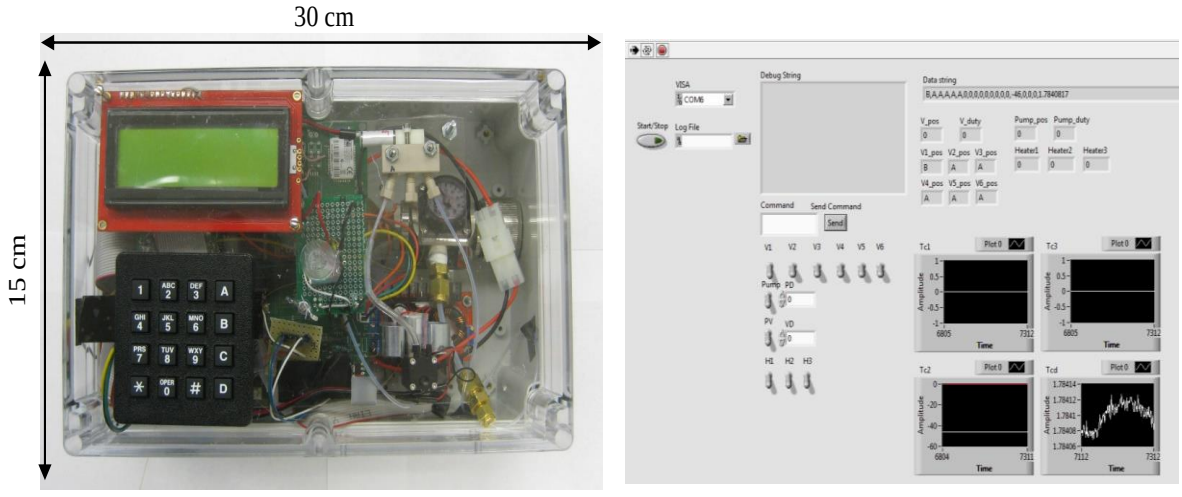

Figure 5.3 *(left) Zebra GC prototype implementation, (right) LABVIEW application interface.*

interface circuitry are assembled in a 30 cm (l) × 15 cm (w) × 10 cm (h) box, schematically shown in Fig. 5.4-b. The box also houses a lithium ion battery (2200 mAh) pack and a small helium cylinder (95 mL, 2700 psi) to make the Zebra GC, shown in Fig. 5.3, highly portable (~ 1.8 kg). The system can be operated in a manual or automatic mode using the LCD/Keypad based human-machine interface, which has a menu driven system. Once the mode is selected, the screen shows the state of the system in terms of valve positions, temperature readings, pump duty cycle, and sensor value. Sensor data can be visualized and recorded in the LABVIEW application, which receives data packets through USB or Bluetooth interface.

Fig. 5.4-c shows the timing diagram for the following automated stages: loading, injection, analysis, and cleaning. In loading stage, the pump applies negative pressure at the µPC outlet to load it with VOCs present in the air sample. Once sufficient sample is loaded in the µPC, the valves are switched to flow helium through the bypass path into the µSC-TCD. In order to ensure a sharp injection plug, the µPC is heated first at a rate of 25 °C/s to 200 °C without flow, and then the valve is switched to inject analytes into the µSC-TCD. The valve is switched back to the bypass path after injection and this stage typically lasts 10-12 s. Once the analytes are injected, they get separated and simultaneously identified in the µSC-TCD. This separation for the analytes of interest (BTEX) takes ~1-2 min; the µSC can be operated at higher temperatures to reduce the analysis time or to resolve higher boiling compounds. Once the analysis phase is complete, the valves are switched back to flow helium at a rate of 3 mL/min through the µPC. The µPC is heated several times if necessary, to minimize residual analytes from the previous run. Typically, one temperature cycle (10-12 s) is sufficient to desorb the remaining analytes because of the high desorption efficiency of our silicon-based µPC.

II. Results and Discussion

Individual components were tested and characterized before integrating them into the portable Zebra GC.

A. Integrated Electronic Module Testing

The integrated electronic module primarily consists of temperature controllers, TCD interface, flow controllers, user interface, and data acquisition circuitry. Each module was tested and optimized separately before integration. For accurate temperature measurement, on-chip sensors were calibrated by placing the MEMS devices in a conventional GC (7890, Agilent, Palo Alto, CA) oven to characterize sensor resistance that responded linearly with respect to temperature with correlation coefficient of (R2) >0.99. The calibration was completed by updating the firmware with calibration slope and offset, which were computed from the resistance vs temperature data. The temperature profile required for the µPC is very different from that required for the µSC; the former requires heating at a high ramp rate (20-100

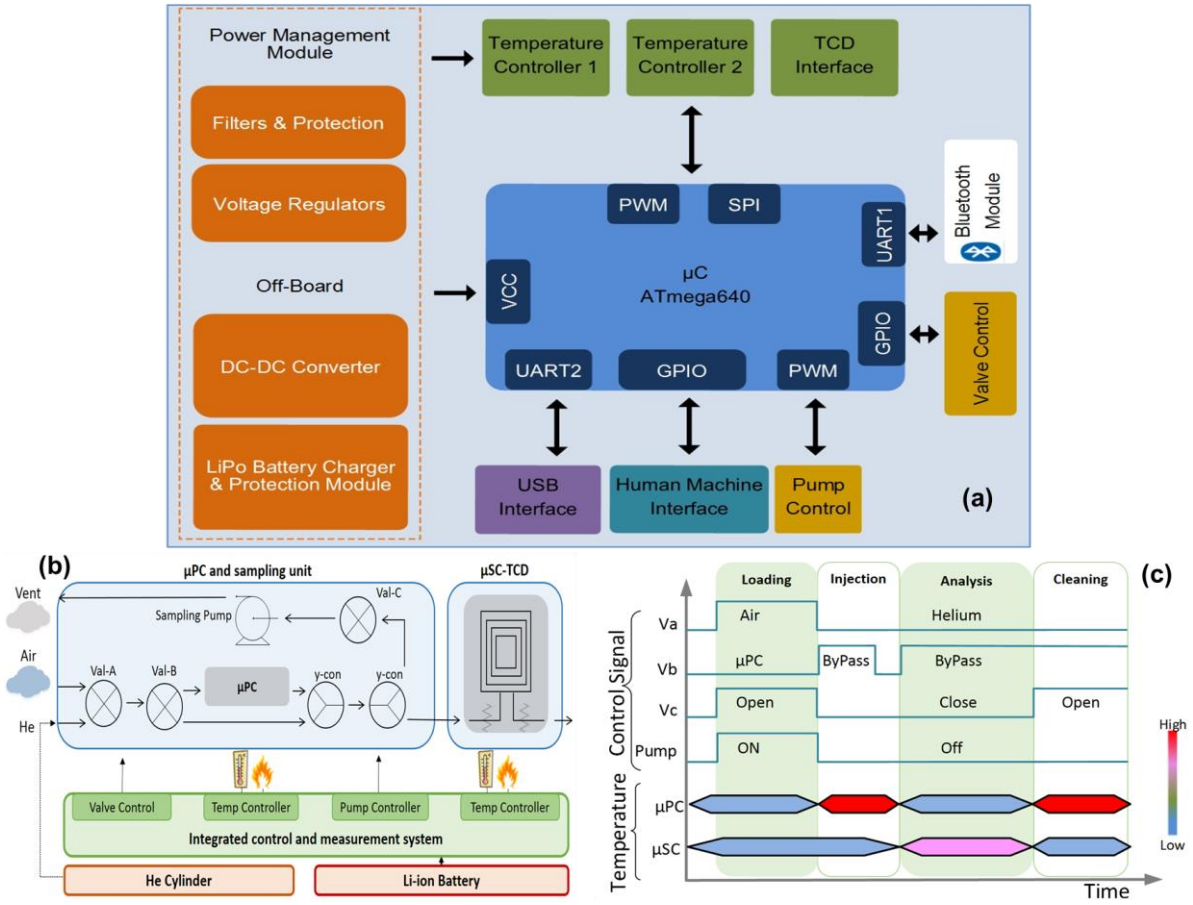

Figure 5.4 *(a) Integrated electronic module block diagram, (b) Zebra GC system block diagram and (c) Operation cycles and timing diagram.*

˚C/s) to quickly desorb the analytes and generate a sharp injection plug, whereas the µSC requires heating at much lower ramp rates (0.2 – 1 ˚C/s) during the analysis phase to accelerate elution of high-molecular weight analytes. The µPC temperature reference was generated through the firmware, and a step input was given to heat the µPC to 200 ºC, which was sufficient to completely desorb (~ 99%) the analytes of interest. The heating ramp rate depends on the thermal mass, power dissipated, and heat losses. As shown in Fig. 5.5-a, the maximum heating ramp rate of 25 °C/s was achieved for the µPC, by applying an 18 V DC across the heater resistance (15 Ω). Further increase in the voltage resulted in deterioration of the thin film heater due to high current density. As shown in Fig. 5.5-b, the µSC was temperature programmed for ramp rates of 20 ºC/min and 30 ºC/min. The power consumptions were determined to be 0.5 W and 1.2 W for isothermal operation of the µSC at 45 ºC and 65 ºC, respectively.

The sensitivity of the µTCD detector was improved by increasing the signal-to-noise (S/N) ratio. The signal was amplified (Gain 32x), and the noise was reduced by filtering the signal and packaging the detector in a small aluminum box to mitigate the effects of ambient fluctuations. Once the measurement circuitry was tuned, noise measurements were made under normal operating conditions with the carrier

gas flowing and the µTCD turned ON. The average peak-to-peak detector noise was 8.08 µV, measured using the technique reported in [192], for baseline signal captured for 10 s. The power consumption for the µTCD and pump operation was 280 mW and 165 mW, respectively. As shown in Table 5.2, the full measurement cycle of the Zebra GC consumes an average power of 2.75 W meaning that the battery can last up to 8 hours (~110 full cycles). It is notable that in our current system, each helium refill (95 mL, 2700 psi) will last around 10,000 full cycles, meaning that the size of the helium cylinder and subsequently the Zebra GC can be considerably reduced.

B. µPC Testing

For optimum operation, the µPC was characterized in terms of four important parameters: adsorption capacity, breakthrough volume, desorption peak width, and desorption efficiency. While evaluating the maximum adsorption capacity of the µPC, the effect of flow rate on the adsorption process was minimized by keeping it to a low value of 1 mL/min. Analytes were injected into the µPC from headspace in sealed 1 mL vials using a conventional GC autosampler module. The split ratio and the injection volume were changed to vary the amount of analyte introduced into the µPC. Analytes not retained by the adsorbent bed appeared as breakthrough peak which was allowed to return to the baseline prior to heating the µPC. The maximum adsorption capacity was defined as the mass retained in the µPC when the injection led to ~10% immediate breakthrough. Fig. 5.6-A illustrates that the µPC can adsorb ~30-400 ng of analytes depending on their affinity to Tenax TA. The masses retained were ~ 30 ng, 130 ng, 240 ng, and 350 ng for benzene, toluene, chlorobenzene, and ethylbenzene, respectively. These results indicate that the µPC can retain a sufficient amount of compound well above the detection limit of our µTCD (~1 ng) and that it has higher affinity to high boilers as expected [140, 156].

For breakthrough volume (BV) identification, about 4 ng of each analyte was loaded separately on the

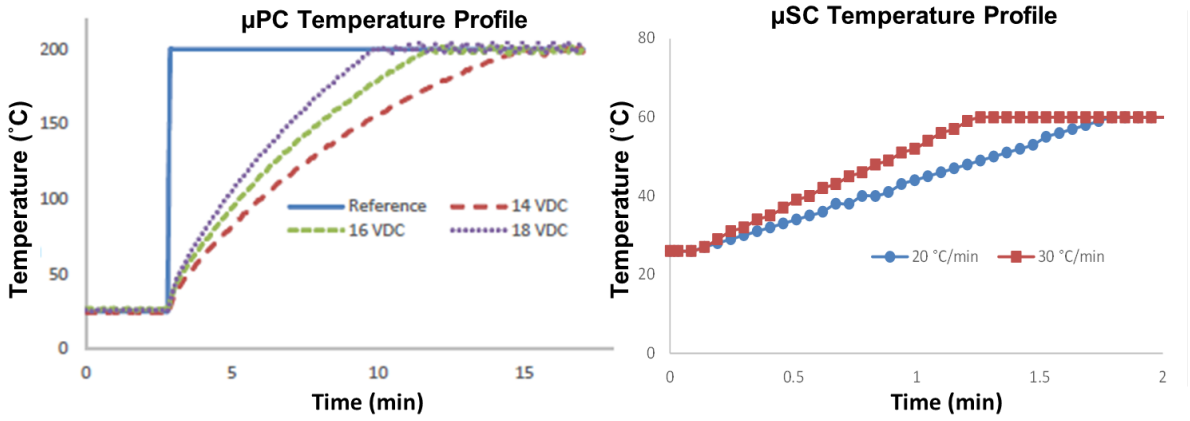

Figure 5.5 *a) µPC temperature profile and effect of heater voltage on µPC heating. Average ramp rate – 25 ºC/s, 20 ºC/s and 15 ºC/s; Average power consumption – 16 W, 13 W and 10.8 W; for heater voltage 18 V, 16 V and 14 V respectively b) µSC temperature profile for ramp rate 20 ºC/min and 30 ºC/min.*

µPC at a flow rate of 1 mL/min and then 5, 10, 15, 25, and 30 mL of the carrier gas was passed through the µPC at the same flow rate. The µPC was subsequently heated and the volume of carrier gas which resulted in a 10% reduction in the total mass retained was noted. Fig. 5.6-B illustrates that only benzene has a BV less than 1 mL; toluene has BV of 13 mL, while chlorobenzene and ethylbenzene have BVs above the typical volume sampled in our experiments (15 mL).

Another important parameter is the width of the desorption peak that can directly influence the chromatographic resolution achieved by the separation column. The initial desorption peak width attained on the µPC at a ramp rate of 25 °C/s and flow rate of 1 mL/min, was ~4 s. This was reduced by first heating the µPC without the carrier gas flowing and next, passing the carrier gas through when the chip temperature reaches 200 ˚C. As shown in Fig. 5.7, this flow-manipulation technique resulted in a reduction of the peak width at half height (PWHH) from 4 s to ~0.8 s. A minimum PWHH of ~ 350 ms was achieved when the desorption flow rate was increased to 2.5 mL/min. It is notable that 99% desorption efficiency for the analyte of interest was achieved by heating the µPC to 200 °C. The remaining amount was removed by subsequent heating of the µPC prior to another run to minimize carry over from the previous adsorption run.

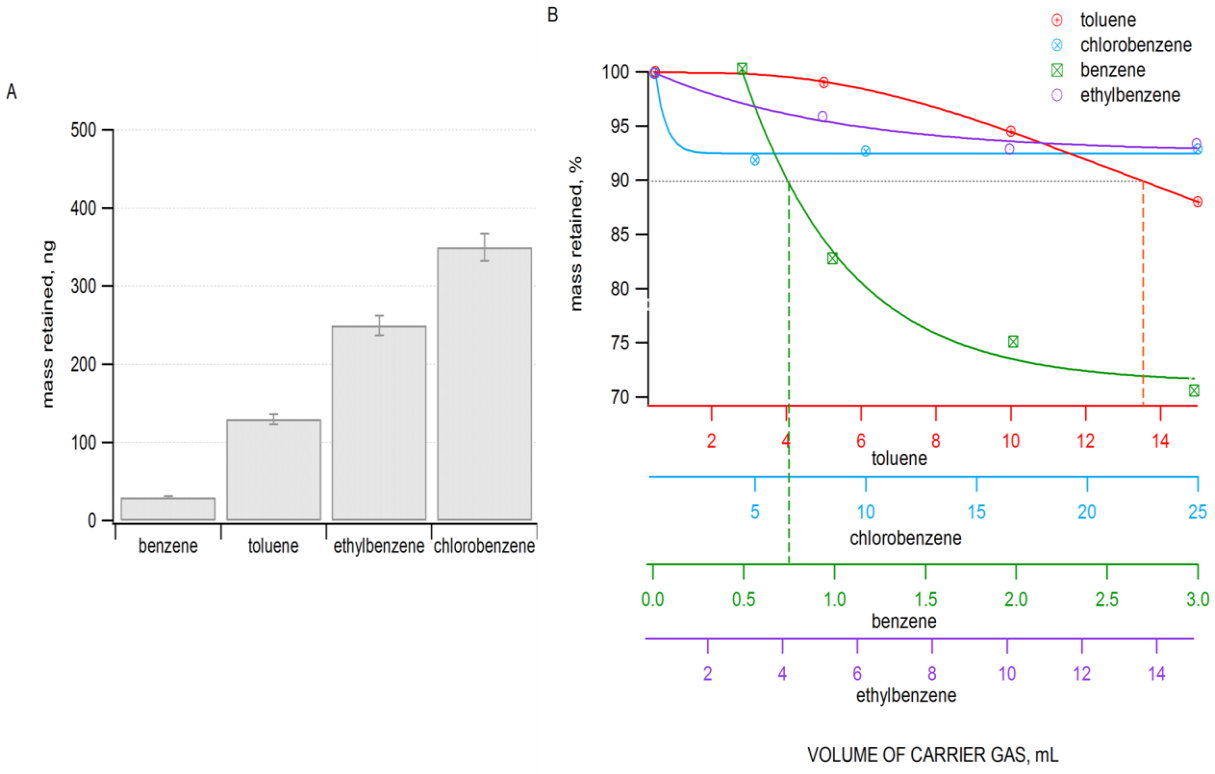

Figure 5.6 *(A) Maximum amount of test components retained in the µPC. (B) BV_{10} curves for benzene, toluene, chlorobenzene, and ethylbenzene. The x-axes are the volume of carrier gas needed to desorb the retained analyte. Dash lines represent breakthrough volumes, Ethylbenzene and chlorobenzene have breakthrough volumes greater than the typical volume sampled (15 mL).*

C. µSC-TCD Testing

The efficiency of the coated column was evaluated with the µTCD switched ON by applying a 7.5 V DC to the Wheatstone bridge. This voltage corresponds to a temperature of 80 °C for the µTCD and was measured with helium flowing, using the method reported previously [46]. The heated µTCD elevated the temperature of the column to 32 °C. The metric commonly used for the column performance is the height-equivalent-to-a-theoretical-plate (HETP),

$$\mathrm{HETP} = \frac{\mathrm{L}}{\mathrm{N}}$$

where L is the column length and N is the number of theoretical plates in the column. N is calculated experimentally from peak retention time (t_r) and peak width at half height ($w_{1/2}$).

$$\mathrm{N} = 5.54 \left[\frac{t_r}{w_{1/2}}\right]^2$$

The plate number was calculated over a range of column pressures using the method reported in our previous work [193]. The maximum plate number (optimum condition) observed was ~6200 for 2-m long

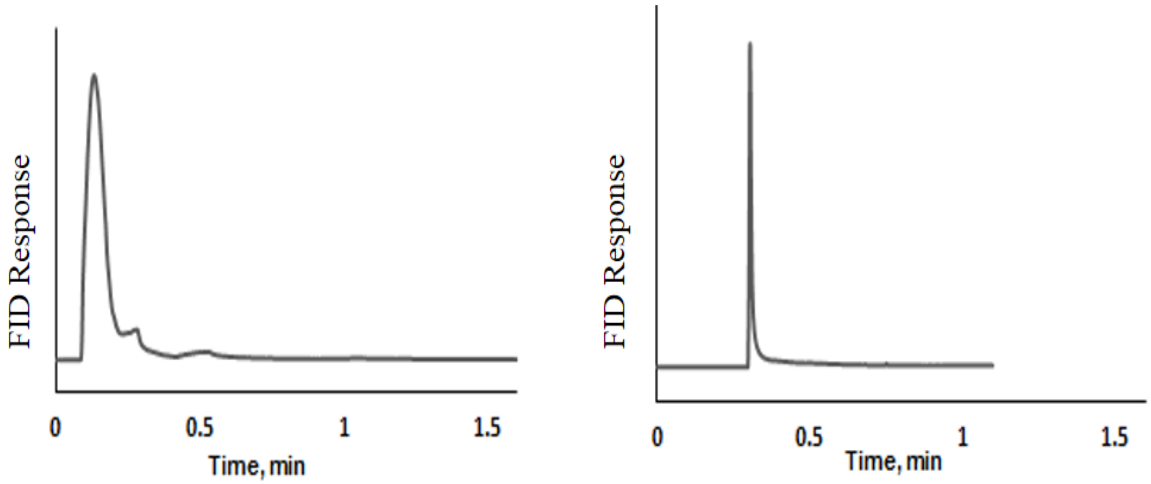

Operation Stage	Average Power (W)	Average Time (min)	Major Load
Loading	2.53	2	Pump, Interface Circuitry
Injection	16.5	0.2	µPC Heating
Analysis	2.22	2	µTCD, Interface Circuitry
Cleaning	16.5	0.2	µPC Heating
Full cycle	2.75	4.4	

Figure 5.7 *(left) Desorption peak profile (PWHH ~ 4s) generated from µPC by heating to 200 °C (ramp rate 25 °C/s) with flow rate 1 mL/min, (right) Desorption peak profile (PWHH ~ 350 ms) generated from µPC by heating to 200 °C (ramp rate 25 °C/s) with flow rate 2.5 mL/min, using flow manipulation technique.*

Table 5.2 *System power consumption.*

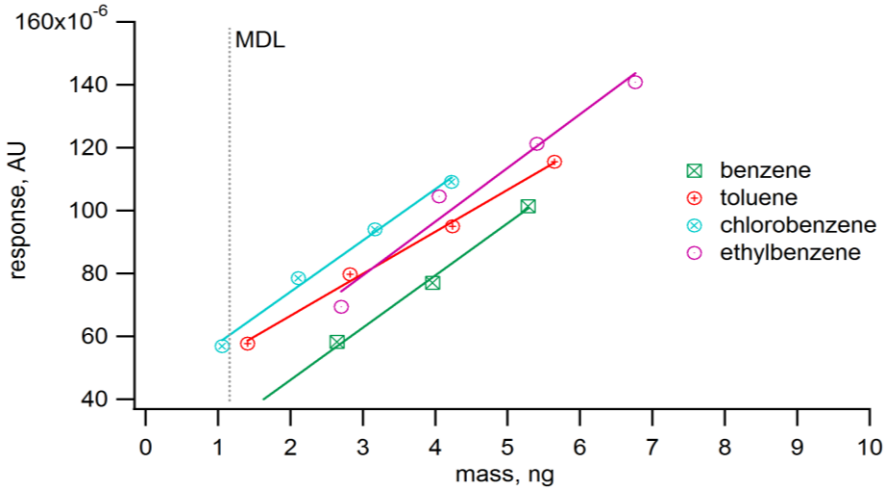

Figure 5.8 *Minimum detectable limit (MDL) for test compounds by µTCD.*

column at 12 psi (flow rate of 0.7 mL/min).

Further, we tested the separation and identification of six VOCs using the column and its µTCD. The µSC along with the interface circuitry was installed inside the conventional GC and connected to the injection port and FID with fused-silica capillaries. A mixture of 6 compounds (headspace), containing benzene, toluene, tetrachloroethylene, chlorobenzene, ethylbenzene, and p-xylene, was injected by autosampler through the heated injection port (1 µl, 50:1 split ratio). The peaks were found to be well resolved and the separation required less than 2 minutes. Next, a calibration curve showing the output (peak area) of the µTCD as a function of the VOC injected mass was obtained. For that purpose, a headspace sample for each VOC was prepared and tested. The split ratio was varied from 120:1 to 50:1 based on the vapor pressure of the VOC. Injected volumes were varied from 0.5 µL to 4 µL, to achieve the mass injected in the range of 1 to 7 ng. Calibration curves showing the average peak area vs injected mass for three injections are shown in Fig. 5.8. Results indicate a linear response of the µTCD for each VOC with a relative standard deviation (RSD) less than 10% for all cases. The R^2 was greater than 0.99 in all cases.

D. Integration of µPC and µSC-TCD

Once individual chips were tested and characterized, the µPC was connected upstream of the µSC-TCD to test the hybrid integration. The integration was expected to both improve and compromise the system performance of different aspects of the µGC. The compact design reduced the transfer lines, thereby reducing the formation of a cold spot that decreases efficiency. On the other hand, the optimal flow rate for operating the µPC and µSC was different; therefore, there was a trade-off in establishing the flow rate for the integrated system. The inlet port of the µPC was connected to the GC injector (280 °C,

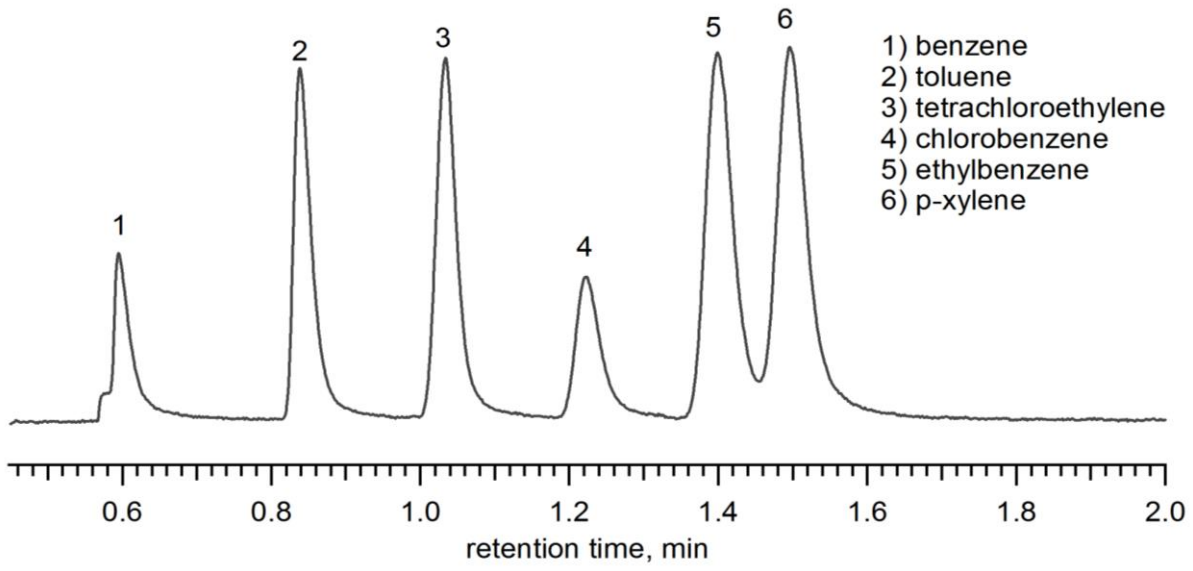

Figure 5.9 *FID response for separation of test compounds with integrated µPC and µSC. Injection performed using flow manipulation technique with µPC heated to 200 °C and desorption flow rate set to 1 mL/min.*

split ratio 50:1) and it was loaded with a mixture containing six compounds (headspace, 1 µL). For initial testing, the outlet port of µSC was connected to the FID detector of a conventional GC. The flow rate was set to 1 mL/min, for which the PWHH was measured to be 0.8 s from the µPC and the µSC exhibited well resolved peaks for the analytes of interest. As shown in Fig. 5.9, the six compounds were separated and identified in less than 2 min.

TCD is sensitive to flow perturbation during the switching of carrier gas into the µPC; therefore, the integrated µTCD presented some challenges because of interference stemming from the injection of the analytes by the µPC. The problem was solved by adopting an innovative system architecture. As shown in Fig. 5.4-a, an alternate flow path for the µPC was provided to maintain a steady flow in the µSC-TCD during the injection cycle. The fluidic resistance of the alternate flow path was matched closely with that of the µPC path to minimize flow perturbations while switching between the two paths. The new architecture decreased the µTCD stabilization time by one order of magnitude (from 1-2 min to 10 s) and ensured continuous flow of the carrier gas. As shown in Fig. 5.10-b, 5 out of 6 compounds tested were easily identified.

E. Zebra GC Testing, Calibration and Evaluation

The components of the Zebra GC were assembled as schematically shown in Fig. 5.4-b. In addition to the integration of µPC and µSC-TCD mentioned above, a Y-connector was added between them to connect the small pump through a valve. The connector isolated the loading path of the µPC from the µSC-TCD, which reduced contamination in the µSC-TCD. This also permits loading at higher flow rates to the µPC since the high fluidic resistance in the µSC was avoided.

The Zebra GC was tested by loading the system with a mixture of five compounds (headspace), containing toluene, tetrachloroethylene, chlorobenzene, ethylbenzene, and p-xylene, injected by the GC autosampler through the heated injection port (1 µL, 40:1 split ratio) at 1 mL/min. As shown in Fig. 5.10-b, calibration standards were generated with this method. The injected masses were ~ 2.7 ng, 3.2 ng, 1.8 ng, 1 ng, and 1.3 ng for toluene, tetrachloroethylene, chlorobenzene, ethylbenzene and p-xylene respectively. These masses are equivalent to 10 mL loading of ~100 ppbv gas mixture, approximating a 10-min loading using a pump operated at 1 mL/min. The test was performed three times and retention times were highly repeatable with an RSD less than 1.3% for all analytes. The peak areas and peak heights had average RSDs less than 4.7% and 8%, respectively.

Finally, the fully-assembled Zebra GC was evaluated in a simulated environment using gasoline as the source of exposure. The test atmosphere was generated by placing 50 mL of gasoline in a 100 mL beaker which was placed inside a large glass chamber (~4 L). Air was circulated inside the chamber but outside the gasoline beaker at 500 mL/min to simulate a car refueling scenario in which gasoline vapors displaced from the tank disperse in the atmosphere, where they may be inhaled [194]. The top of the chamber was kept open to the atmosphere and the chamber was allowed to be filled with vapors for 10 minutes. The vapors were sampled through the µGC, by keeping the system inlet close to the top of the chamber.

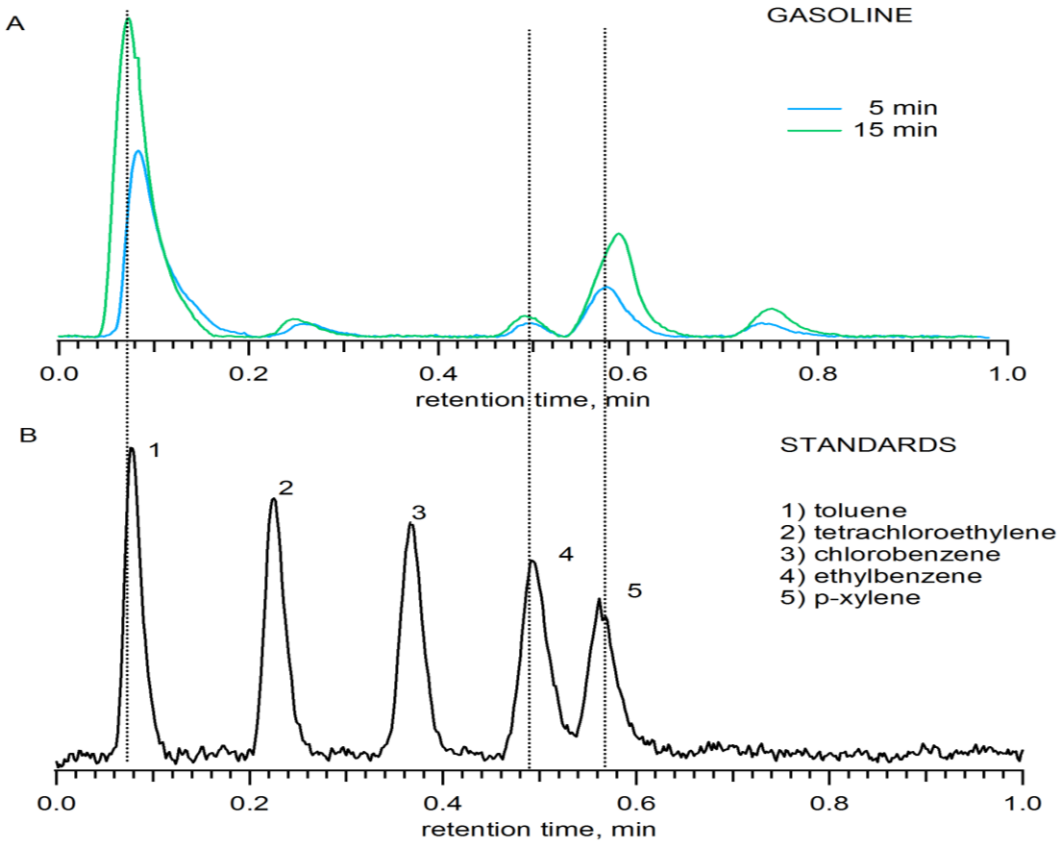

Figure 5.10 *Chromatogram of (A) gasoline vapor and (B) standards using Zebra GC.*

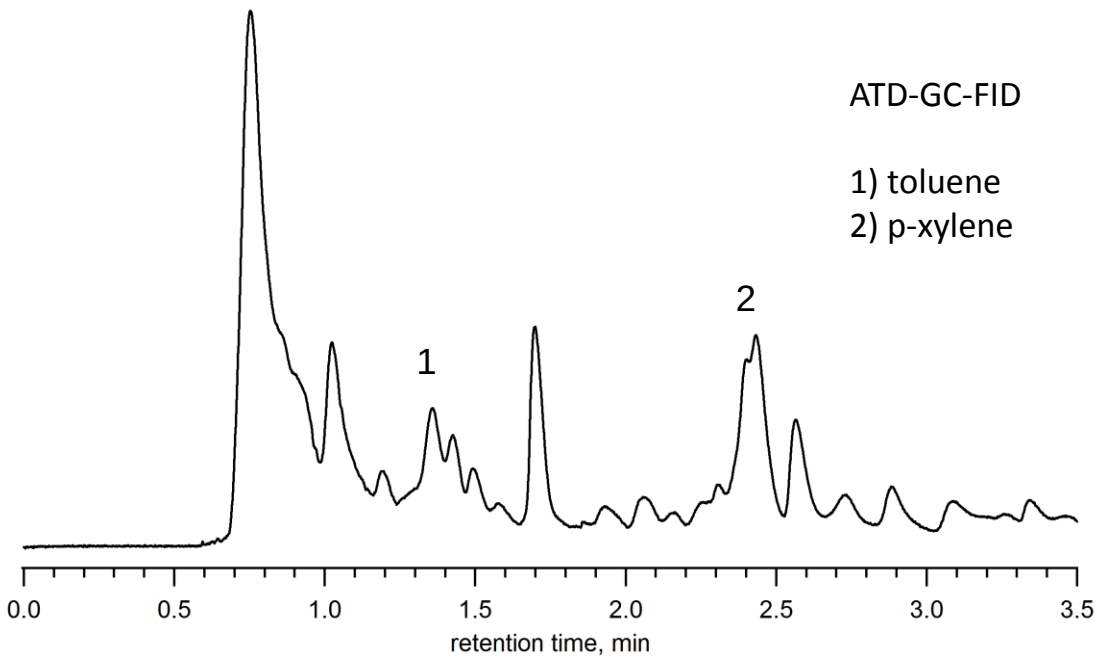

Figure 5.11 *Chromatogram of gasoline vapor sampled at ambient pressure and temperature using sorbent tubes containing ~200 mg of Tenax TA. Gasoline vapor was analyzed by thermal desorption coupled to GC-FID using conventional column containing (5% phenyl-, 95% dimethyl-polysiloxane). Desorption temperature and time were 300 °C and 25 min respectively. Toluene peak at ~1.4 min (16 ppmv) and p-xylene (14 ppmv) peak at ~2.4 min. Benzene and ethylbenzene not detected. Temperature programming: 35 ^{o}C, hold for 10 min, 5 ^{o}C/min to 150 ^{o}C, final hold time 1 min.*

Vapors were sampled under ambient temperature and pressure for two different sampling times, 5 and 15 minutes.

To compare results with a conventional sampling system, gasoline vapors were also sampled using sorbent tubes packed with Tenax TA at a sampling flow rate of 69 mL/min for 3 hours. Sorbent tubes were desorbed using a thermal desorption system coupled to a GC-FID (TD-GC-FID, Perkin-Elmer ATD 400). Toluene and p-xylene were identified at a concentration of 16 and 14 ppmv, respectively (Fig. 5.11). In both systems (Zebra GC and TD-GC-FID), benzene was not identified because it co-elutes with the other low-boiling point components in gasoline. Fig. 5.10-a illustrates that the Zebra GC detected five peaks, three of which were identified as toluene, ethylbenzene, and p-xylene based on retention times. Also, because Tenax TA has low affinity to benzene, the µGC system retained lesser mass of it compared to the other analytes. The sample volume collected and analyzed in the µGC was ~3 orders of magnitude lower than those collected on sorbent tubes. These results illustrate that the Zebra GC is capable of detecting and separating compounds with a much shorter sampling time and lower sample volume compared to conventional systems to complete one full cycle of analysis.

III. Conclusion

This study shows prototypal implementation of a μGC system suitable for environmental monitoring applications. The system leverages micro-machined components to achieve low power consumption (2.75 W) and fast analysis time (4.4 min). A Limit of Detection (LOD) of ~1 ng was achieved, which enables monitoring of HAPs at sub-100ppbv concentrations. The fabricated prototype was functionally characterized and compared with a conventional ATD-GC-FID system for real gasoline samples. Future work will focus on: (i) comparing the accuracy and robustness of system through extended field tests in indoor and outdoor environments against conventional systems; (ii) design modification such as integrating a deep-etched μPC, enabling high sample volume, and utilizing semi-packed/multi-capillary columns for increased separation efficiency.

Chapter 6: GC-on-Chip: Integrated Column and Photo Ionization Detector

(Part of this chapter reproduced from [229] with permission from RSC, Lab on a Chip)
M. Akbar, H. Shakeel, and M. Agah, "GC-on-chip: integrated column and photoionization detector," Lab on a Chip, vol. 15, pp. 1748-1758, 2015.

The analysis of volatile organic compounds (VOCs) using gas chromatography (GC) is required for applications in environmental monitoring, homeland security, biomedical diagnostics, and food processing [195-198]. The increasing demand for on-site monitoring of VOCs has led to the development of micro gas chromatography (μGC) systems providing the desirable features of smaller size and higher portability, lower power consumption, and minimal production and maintenance costs. μGCs are realized by employing the microelectromechanical systems (MEMS) technology which enables the miniaturization of key GC components namely pre-concentrators [125, 161, 199, 200], separation columns [25, 31, 57, 201-204], and detectors [48, 50, 205].

Since its first conceptual demonstration by Terry et al. [44], the trend followed by the research community to realize a complete μGC has been the fabrication of individual μGC components and their hybrid integration [64, 67, 193, 206-208]. This implies that the μGC components are assembled manually using fluidic interconnection which is labor intensive, time consuming, prone to error and incompatible with future mass production. Furthermore, each MEMS component in the hybrid approach is designed and developed separately, thereby significantly increasing the fabrication costs. In addition, the presence of cold spots in the fluidic connection between the μGC components mainly μSC and the detector can adversely affect the column performance. The VOCs after eluting from the μSC may experience extensive band broadening or sample condensation when passing through these cold spots. Thus, there is a critical demand for the development of a monolithic integrated module which includes separation and detection stages on a single chip. Few research milestones accomplished in this regard have been summarized in Table 6.1 [41, 43, 46, 47, 209]. The table also describes the features, pros and cons of the monolithic integrated modules. As seen, our group has implemented the monolithic integration of polymer-coated open rectangular micro-columns with μTCDs in silicon-glass architectures [46, 47]. While being universal and simple to operate, μTCD could not provide very sensitive detections and were sensitive to flow and temperature variations [210]. This restricted the integrated module to operate under the flow and temperature programming conditions and therefore the rapid screening of complex mixtures spanning over a wide range of boiling points was not possible. Meanwhile, our group invented the first generation of μDPID in all-glass format [50]. In this paper the fabrication of μDPID in silicon-glass format has been demonstrated which led to the development of a new GC-on-chip module addressing the deficiencies listed in Table 6.1. The chip comprises of a high performance semi-packed μSC with novel stationary phases based on atomic layer deposition and a μDPID. The chip requires only two masks for

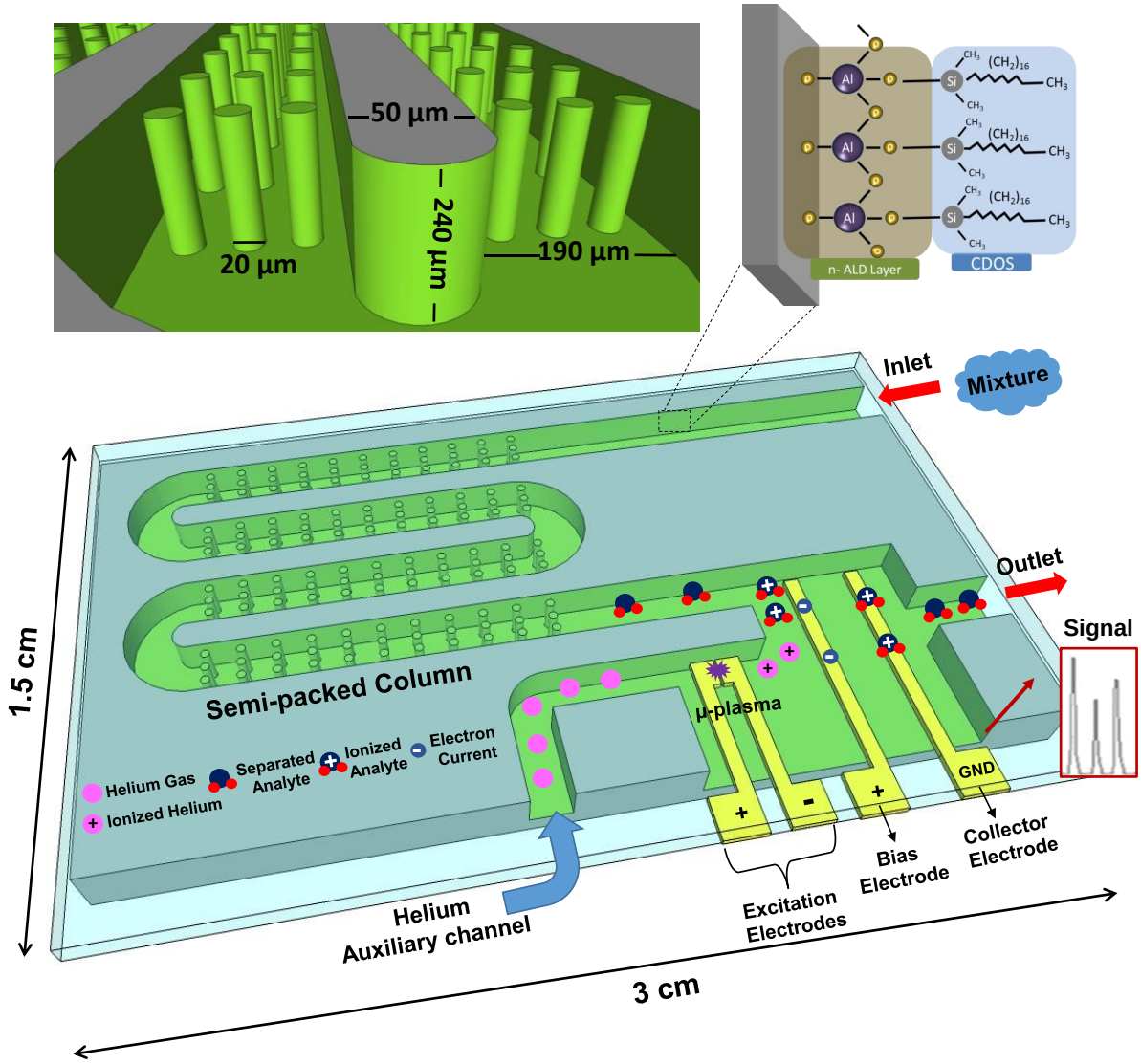

Figure 6.1 *Conceptual image showing the operation of the monolithic integrated chip (GC-on-Chip). The top right image shows the stationary phase coating procedure while the top left image shows the channel dimensions of the micro separation column.*

fabrication. Our comprehensive characterization of the integrated chip indicates that it provides highly efficient separations, reduced analysis times using temperature and flow programming, very sensitive detection equivalent to the current state-of-the-art commercial FIDs, and fast detector response times suitable for high speed gas chromatography.

I. Chip Operation

Fig. 6.1 shows the conceptual image elaborating the working principle of the chip. The dimensions chosen for the µSC and µDPID in the module are based on our previous work [202, 210]. A mixture of VOCs is introduced through the inlet port of the chip which travels through the semi-packed µSC by an inert carrier gas called the mobile phase. The inner surface of the µSC is covered with a finely

Reference	µSC geometry	Detector type	Pros	Cons
Kaanta (2010) [209]	Microfabricated columns packed with Carbopack/Hayesep A	Thermal conductivity detector	Simple to fabricate Universal	Poor separation efficiency Poor detection limit Sensitive to flow and temperature
Reddy (2012) [43]	Multiple stage microfabricated columns coated with PDMS, Carbowax	Fabry-Perot (FP) cavity sensor	Sub-ng detection limit	Selective Requires laser, photodetector and collimator Bulky and power hungry
Yuz Sun (2010) [41]	1.8 m long regular GC column followed by 10 cm long capillary column	Optofluidic ring resonator (OFRR)	Sub-ng detection limit	Selective Fragile, difficult to operate for field-application
Narayanan (2012) [47]	Microfabricated columns coated with PDMS	Thermal conductivity detector (anchored to the substrate)	Simple to fabricate Universal	Poor detection limit (1 ng) High power consumption (50 mW) Sensitive to flow and temperature
Narayanan (2013) [46]	Microfabricated columns coated with PDMS	Thermal conductivity detector (released in the fluidic channel)	Good detection limit (100 pg)	Complex fabrication procedure Sensitive to flow and temperature

Table 6.1 *Summary and comparison of the efforts for the monolithic integration of µSC and detector.*

controllable stationary phase which is a silane-treated alumina layer as established in our previous work [202]. The compounds spend different amount of time in the stationary phase coating depending on their relative solubility and vapor pressure in the stationary phase, and hence, they emerge from the µSC at different times. This results in their separation into the individual compounds. The operation of the new silicon-glass µDPID is similar to that implemented in glass-glass architecture as described previously [50]. Briefly, a high voltage DC discharge in helium is generated across a pair of excitation electrodes separated by a 20 µm gap. The discharge is sustained by the continuous supply of helium from the auxiliary channel. The discharge is a complex mix of positive and negatively charged ions, metastable He atoms, electrons, and photons (ionizing flux). The photons (energy>10eV) and metastable He atoms (energy>19.8eV) are responsible for the ionization of VOCs emerging from the outlet of µSC. The distance of micro plasma from the µSC outlet is 1 mm. The outlet of the µSC bypasses the micro-plasma for two purposes: 1) it enables non-destructive analysis and 2) it allows the flow programming of the µSC

without significant noise generation in the detector baseline as seen later. In addition to the pair of excitation electrodes, the detector is also equipped with a bias and a collector electrode. The bias and the collector electrodes are 1.5 mm apart. The space between the μSC outlet and the collector is called the collector volume. The ionized compound induces a current in the collector electrode. This current is measured by a picoammeter connected to the collector electrode. The purpose of bias electrode is to collect the negatively charged species from the ionizing flux. This reduces the possibility of their recombination with the ionized compound inside the collector volume which can lead to the reduction in the collector current.

II. Experimental Section

A. Materials

All test compounds used in this work were purchased from Sigma-Aldrich (St. Louis, MO) in >99% purity. AZ9260 photoresist was purchased from MicroChemicals (Germany) while titanium and gold were purchased from Kurt J. Lesker. Silicon wafers (4 in. dia., 500 μm thick, n-type, single side polished) and Borosilicate glass wafers (Borofloat, 4 in. dia., 700 μm thick, double side polished) were purchased from University Wafers and Coresix Precision Glass (Williamsburg, VA), respectively. Fused capillary tubes (200 μm outer dia., 100 μm inner dia.,) and Epoxy 907 were purchased from Polymicro Technologies (Phoenix, AZ) and Miller Stephenson (Danbury, CT) respectively. Ultra high purity helium (UHP 300) and industrial grade air (AIB 300) were purchased from Airgas (Christiansburg, VA).

A multicomponent mixture including eight compounds (n-heptane, toluene, tetrachloroethylene, chlorobenzene, ethylbenzene, p-xylene, n-nonane and n-decane) was prepared. Equal volumes of 200 μl were pipetted into an autosampler vial for each compound except for n-heptane and toluene. Based on the response of both FID and μDPID, a 20 μl volume of each of n-heptane and toluene was deemed sufficient to produce peak heights comparable to the other compounds. Another mixture of high-boiling hydrocarbons including n-nonane, n-decane, n-undecane and n-dodecane was prepared by pipetting 50 μL, 100 μL, 300 μL and 500 μL volume of each compound, respectively.

A 5 parts-per-million (ppm) solution of n-octane was prepared by pipetting 5 μl of n-octane in a custom-made 1L volumetric flask. The mouth of the flask was sealed with a 24/40 septa and left overnight to allow n-octane to volatilize. To prepare a fresh sample again, the n-octane in the flask was cleared by heating the flask in an oven set to 80 ˚C for approx. half an hour followed by purging with nitrogen.

B. Chip Fabrication

The fabrication process for the monolithic chip required two masks: one for the bulk micro-machining of silicon wafer to create the separation stage, fluidic interconnects and cavities for the detector and the other for the metallization of the Borofloat substrate which served as the detection stage. The silicon wafer processing started with spin coating of AZ9260 photoresist at 2000 rpm to achieve ~8 µm thick photoresist layer (Fig. 6.2a). The wafer was then patterned using mask aligner (Karl Suss) and developed in AZ400K. The wafer was subjected to deep reactive ion etcher (DRIE, Alcatel) which resulted in the creation of 190 µm-wide and 240 µm-deep channels with 20 µm-embedded circular micropillars and a cavity (Fig. 6.2b). The photoresist was then stripped off using acetone. Finally, the chip was coated with a thin layer (~10 nm) of alumina deposited at 250 ˚C using the atomic layer deposition (ALD) technique (Fig. 6.2c). Trimethylaluminum (TMA) and water are used as precursors in the process.

$$-Si-OHAl(CH_3)_3 \rightarrow -Si-O-Al(CH_3)_2 + CH_4$$

$$-Si-Al(CH_3)_2 + 2H_2O \rightarrow -Si-O-AlO * (OH) + 2CH_4$$

The lithography step for the fabrication of the detector electrodes on the Borofloat wafer followed the same procedure as described earlier. However, after the development of photoresist the hard-bake time was reduced to 1 min at 110 ˚C to facilitate the subsequent lift-off process. A 700 nm/40 nm thick Ti/Au metal stack was evaporated using e-beam evaporator (PVD-250, Kurt J. Lesker) to serve as the detector electrodes. The wafer was left in acetone for 10 min and then placed in a sonic bath for 15 s to ensure

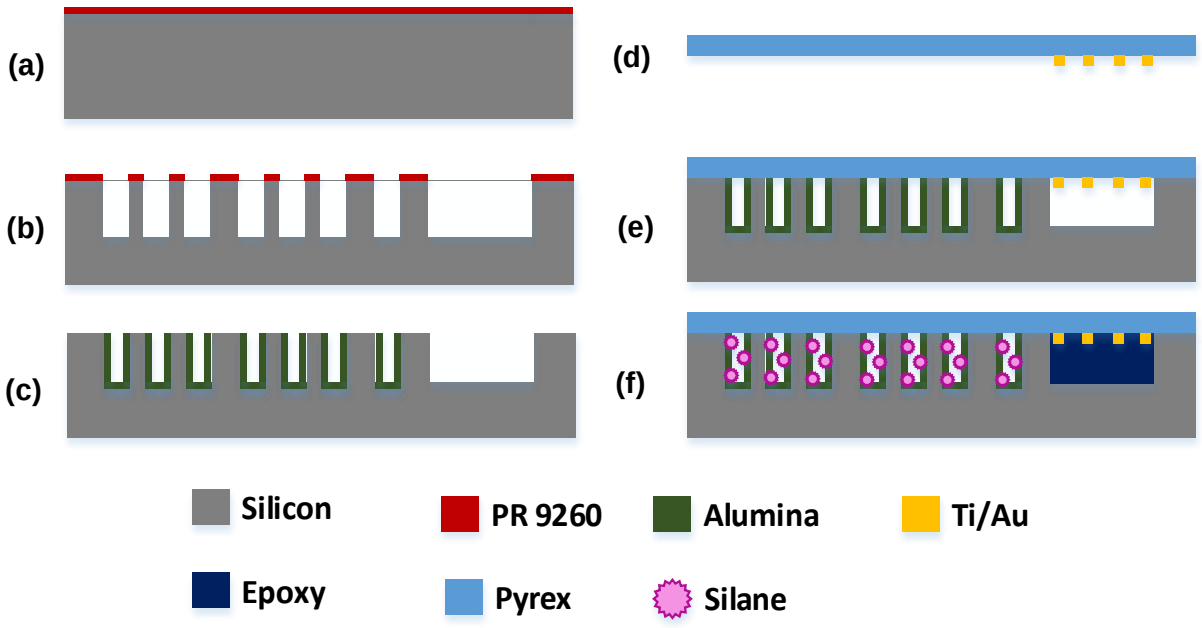

Figure 6.2 *Standard MEMS processes for the fabrication of integrated chip (a) photolithography (b) deep reactive ion etching (c) atomic layer deposition (d) physical vapor deposition (e) anodic bonding and (f) surface functionalization.*

complete lift-off (Fig. 6.2d). Before anodic bonding, both silicon and Borofloat wafers were diced into individual devices. The substrates were aligned and bonded at 1000 V and 370 ˚C for 45 min (Fig. 6.2e). After bonding, the edge of the detector cavity was sealed with the epoxy and the electrical wires were soldered to the bond pads. Next, the capillary tubes were inserted into the three ports of the chip. Finally, the functionalization of alumina film and Borofloat cover was accomplished by filling the µSC with 10 mM chlorodimethyloctadecylsilane (CDOS) in toluene for 24h at room temperature (Fig. 6.2f). The inlet and outlet of the chip was attached to the injector and the FID of a conventional GC system. The µSC temperature conditioning was performed in the GC oven for approximately 1 h (35 ˚C ramped at 2 ˚C/min to 150 ˚C) at a constant inlet pressure of 10 psi.

C. Testing Setup

The testing setup for the chromatographic evaluation of the fabricated chip is shown in Fig. 6.3. A bench-top 7890 series Agilent GC system equipped with two electronic pressure control (ECP) inlets, an FID and an autosampler (7359A) module was used for this purpose. Helium was used as the carrier gas while the injectors and the FID were maintained at 280 ˚C. The inlet of the chip was connected to injector A while the outlet was fed to the FID for cross-examination purposes. The auxiliary channel of the chip was connected to injector B to provide helium for the micro-plasma generation. The micro plasma was initiated across 20 µm gap by applying a 550 V DC voltage using high voltage power supply (PS-310, Stanford Research Systems) to the excitation electrode pair establishing the baseline current which was recorded on a picoammeter (Model 480, Keithley) connected to the collector electrode. A 100 MΩ resistor (not shown in the Fig. 6.3) was connected in series with the excitation electrodes to avoid excessive amount of current flow which could damage the electrodes. A DC voltage was also applied to the bias electrode while a LABVIEW program recorded the measurement from the rear-terminal output using a Keithley 2700 multimeter.

III. Results and Discussion

The optical image of the semi-packed µSC and the µDPID are shown in Fig. 6.4a and Fig. 6.4b, respectively. Fig. 6.4c shows the photograph of the entire chip with the external capillaries attached and the electrical connections affixed to the bond-pads. The inset shows the close-up of micro plasma across the 20 µm gap. Here we discuss the results from characterizing the µDPID first and then demonstrate the chromatographic analysis performed with the GC-on-chip.

A. Performance Evaluation of µDPID

1. Plasma Characteristics

The circuit used for studying the electrical characteristics of plasma is shown in the inset in Fig. 6.5. A 100 MΩ resistor and a 3.3 MΩ resistor were connected in series with the excitation electrodes of the packaged device. The helium flow of 1 mL/min was maintained through the device. The current through the plasma was calculated by measuring the voltage across the 3.3 MΩ resistor using a Keithley 2700 DMM. Fig. 6.5 shows the current-voltage plot of the plasma. For the discharge voltage less than 480 V, the current measured was on the order of tens of nanoamperes. At 500 V an unstable plasma was observed with the current changing anywhere between tens of nanoamperes and a few microamperes. A stable plasma was initiated when the discharge voltage was raised to 550 V with the current value measured around 2.5 µA. After 550 V, the plasma current was observed to increase linearly with the discharge voltage. The discharge voltage of 550 V was selected due to two reasons: 1) the photon energy from the plasma generated at 550 V was sufficient to ionize the compounds eluting from the µSC and 2) the operation of the detector under the stable plasma can be ensured with minimum power consumption. The power consumption at 550 V was determined to be 1.4 mW.

2. Mass Flow Rate Sensitivity of the Detector

In addition, the classification of µDPID as a mass flow rate sensitive detector (MSD) was demonstrated. The detectors typically employed for µGC can be categorized either as a concentration sensitive detectors (CSD) or MSD. The CSD measures the concentration of the compound in the carrier gas compared to MSD which measures the absolute amount of compound regardless of the volume of carrier gas. The effect of flow rate on the peak parameters for the same amount of sample can be used to distinguish between the two types of detectors [211]. For CSD with increasing flow rate, the peak area decreases and the height is unchanged whereas for the MSD the peak height is increased and the area is unchanged. The classification of µDPID either as CSD or MSD was determined by injecting the same amount of n-octane under different flow rates (by maintaining constant split ratio of 100:1) and measuring effect on the peak properties of the compound. For that purpose, five runs were performed with injector A pressure set to the discrete values of 10, 12, 15, 20 and 25 psi. The pressure at the auxiliary channel was kept constant at 10 psi for each injection. The flow rate measured at the chip outlet corresponding to each pressure value was 0.9, 1.1, 1.4, 1.9 and 2.5 mL/min, respectively. Triplicate runs were performed for each value and the standard deviation was calculated. A 2 µl headspace volume of n-octane contained in a vial was sampled using an autosampler module to ensure repeatable injections. The peak width, height and area of the detector response was calculated and plotted as shown in Fig. 6.6. The graph shows that by increasing the flow rate the peak width decreases. It is important to recognize that the increased pressure (flow rate) forces the molecules to exit the volume of the detector cell faster resulting in a narrower peak width. However, the peak area remained unchanged (~160 pA.s) which is reflected by the

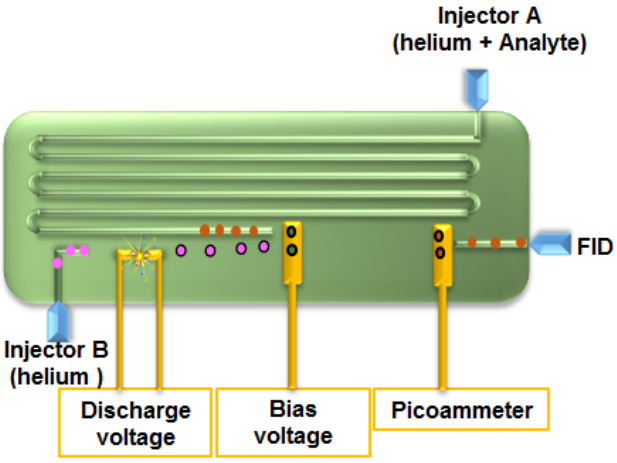

Figure 6.3 Testing setup of the integrated chip inside HP7890 bench-top GC system.

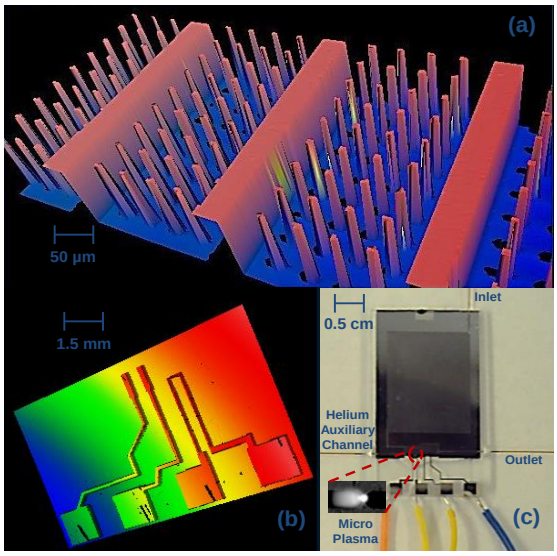

Figure 6.6 Optical images of the actual fabricated devices (a) µSC with the embedded pillars to serve as the separation stage (b) metal electrodes on the Borofloat to serve as the detection stage and (c) complete chip after packaging.

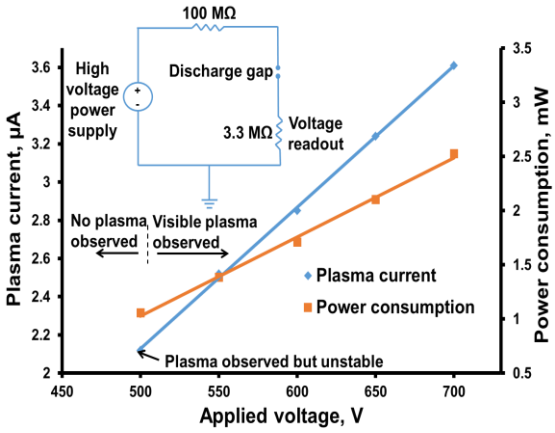

Figure 6.4 Graph showing the current through the micro plasma and power consumption of the µDPID as a function of the applied voltage. The electrical circuit used for measurement is shown in the inset.

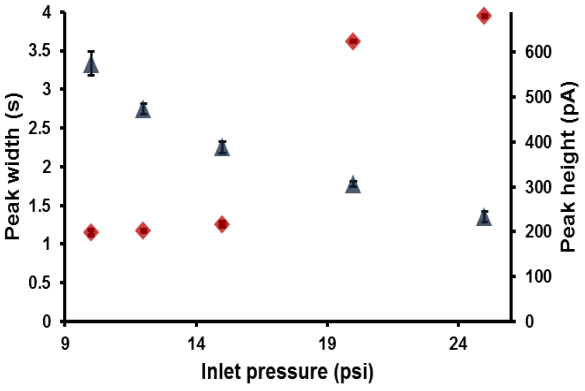

Figure 6.5 Graph showing the effect of the flow rate on the peak shape (width and height) for a 2 µL headspace volume injection of n-octane. The triangle represents the peak width whereas the diamond corresponds to the peak height. The peak area remained constant confirming the mass flow rate sensitivity

increase in the peak height. Similar relationship between the peak width and height vs. inlet pressure has been reported for FID [211]. These results signify that the µDPID measures the absolute mass of the compound and is therefore classified as a mass flow rate sensitive detector. Furthermore, the rise and fall time of the µDPID response was calculated. It is an important parameter which indicates the speed with which the detector can respond to the instantaneous changes of the input signal. Increasingly longer rise or fall time can vary the retention time of the compound, distort its peak shapes, and result in wider peak width affecting the chromatographic resolution. The rise and fall time of the µDPID response for n-octane were calculated at the flow rate of 0.9 and 2.5 mL/min were remarkably short. For 0.9 mL/min the rise time was ~370 ms and fall time was ~ 3 s whereas for 2.5 mL/min it was noted to be ~200 ms (Fig. 6.7) and 1 s respectively. Both these values indicate that the µDPID can respond effectively to the rapid changes of the input signal (~1 s wide peak).

3. Reliability Assessment of the Detector

The reliability of µDPID was investigated by examining the influence of its continuous operation on

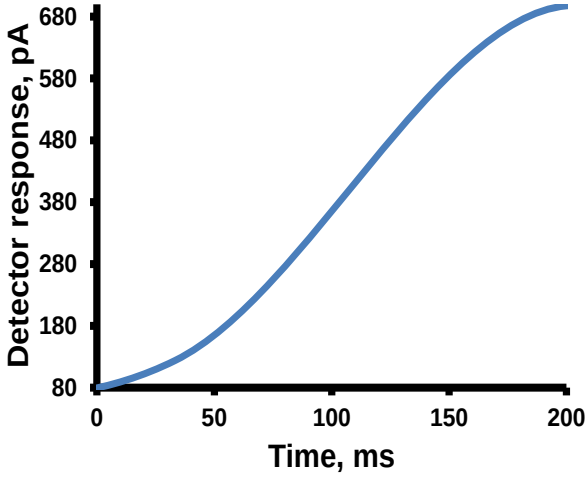

Figure 6.7 *Graph showing the rise time of µDPID response for a 2 µL headspace volume of n-octane. The time required to rise from the baseline current of 80 pA to a peak value of 680 pA was ~200 ms.*

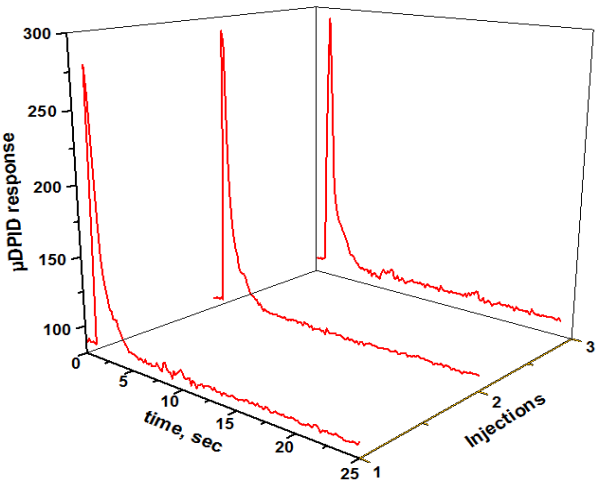

	Mean	Standard Deviation
Peak Height (pA)	199.3	8.22
Peak Width (s)	3.2	0.22
Peak Area (pA.s)	153.2	8.43

Figure 6.8 *Chromatogram showing the repeatability of µDPID response for three injections performed every hour. Table shows the means and standard deviation of the peak parameters (height, width and area) for the injections of n-octane performed every hour over a continuous operation of 12 hours.*

the response of the detector. The detector was challenged with 2 µl headspace volume of n-octane with the pressure maintained at 10 psi at the inlet and auxiliary channel of the device. The flow rate measured at the outlet was 0.9 mL/min. The mean and the standard deviation of the peak area, width and height were calculated for the injections performed every hour over a time span of 12 hours. The experimental findings shown in Fig. 6.8 indicate that the µDPID produces highly repeatable results with less than 10% variations in the response. Moreover, no deterioration of the excitation electrodes was observed after the continuous operation for 12 hours.

4. Effect of Bias Voltage

The effect of bias voltage on the response of the detector was also examined. The bias voltage was increased from 0 to 60 V in increments of 10 V. The detector response was measured for a 7 µL headspace volume of n-octane injected with the split ratio of 100:1. The pressure at the injector A and B were maintained at 15 psi and 10 psi, respectively. Fig. 6.9 shows the effect of the bias electrode voltage

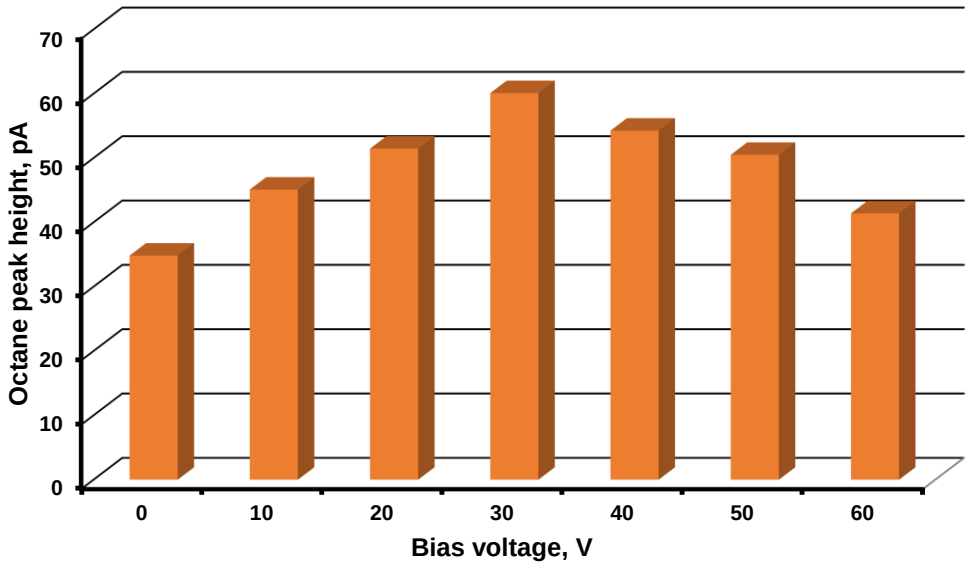

Bias Voltage, V	Peak Height, pA	S/N
0	1.8	3.6
10	3	6
20	3.1	6.2
30	3	6

Figure 6.9 *Response of the µDPID for a 7 µL headspace volume of n-octane versus bias voltage. Each data point is the average of three replicates.* ***Table 6.2*** *The effect of bias voltage on the peak height of n-octane for ~10 pg injection. The signal to noise ratio (S/N) was doubled by increasing the bias voltage to 30V.*

on the detector response. Initially, ~10 pA increase in the n-octane peak height was observed for every 10 V rise in the bias voltage. This is attributed to the fact that by increasing the bias voltage, the negatively charged species from the ionizing flux are collected more effectively at the bias electrode. This reduces the probability of their recombination inside the collector volume with the positive ions produced by the ionization of the compound. The recombination process can cause a portion of the generated ions to be neutralized and hence not detected. Thus, by increasing the bias voltage, an increase in the collector current is observed. However, beyond 30 V, the bias voltage is strong enough to repel the positively charged species in the ionizing flux; as a result a decrease in the detector response with increasing the bias voltage beyond 30 V is observed.

5. Limit of Detection

Generally, the smallest signal that can be safely attributed to the compound is the one with a signal to noise ratio (S/N) of three or more. Therefore, S/N=3 was specified as the criteria for measuring the limit of detection (LOD) for a particular compound in the characterization of the µDPID. LOD for n-octane was evaluated by operating the integrated chip under the isothermal condition of 40 ˚C with the pressure at injector A and B set to 15 psi and 10 psi, respectively. A 0.5, 1 and 1.5 µL volume of 5 ppm n-octane sample prepared as explained in the Materials section was injected into the chip. The split ratio was maintained at 150:1 and the bias voltage was set to 0 V during the analysis. These volumes translate to ~10, 20 and 30 pg of n-octane, respectively [50]. The response profile from the µDPID for these three injected mass of n-octane with the corresponding FID results are shown in Fig. 6.10. The retention time

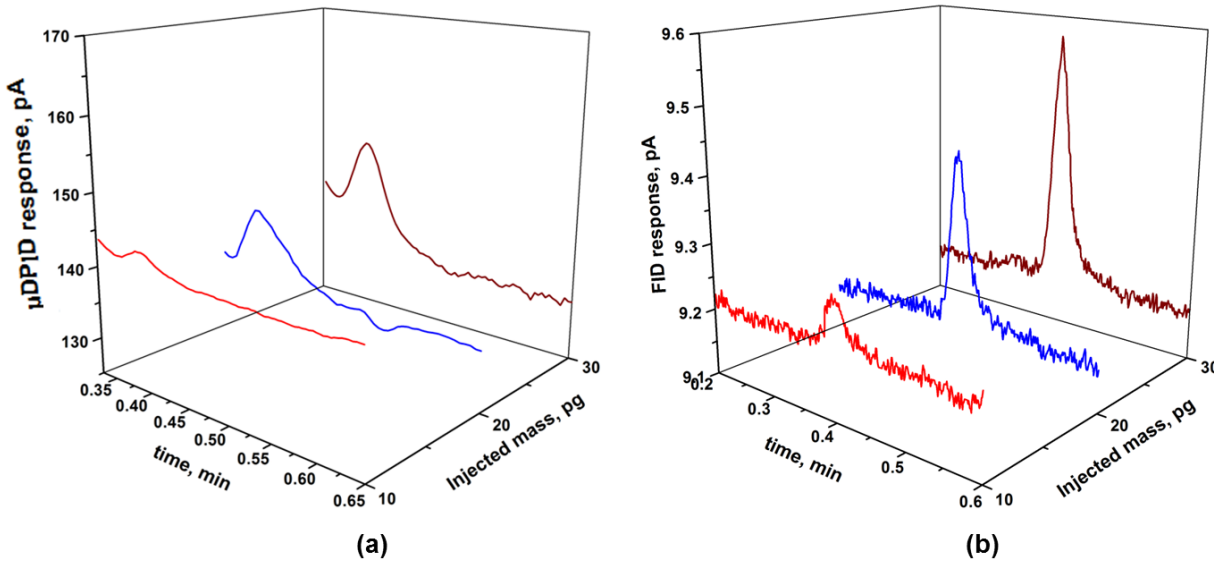

Figure 6.10 *(a) Response profiles from the µDPID for ~10, 20 and 30 pg injection of n-octane. A 10-point moving average filter was used to smooth the high-frequency noise (b) Response from the FID for the corresponding injections.*

for n-octane was around 0.35 min. A 10-point moving average filter was used to smooth the high-frequency noise. The S/N for these three injections was calculated to be 3.6, 16 and 22, respectively for the µDPID. These results clearly indicate that the LOD as low as ~10 pg is possible with the µDPID. The corresponding S/N for the FID was found to be 3, 8 and 10, respectively. Afterwards, the bias voltage was varied to improve the n-octane peak signal. Table 6.2 shows that the peak height of n-octane was doubled by increasing the bias voltage to 30 V signifying opportunity for further improvement in the LOD. It should be noted that the LOD depends upon the testing compound properties in addition to the system operating conditions. For instance, the compound may experience significant band broadening due to the presence of extra-column volume or with increasing retention time which could result in wider peaks and higher LOD. Similarly, the temperature and flow rate play an important role in increasing the peak height especially for the late eluting compounds which can create significant impact on the LOD.

B. Performance Evaluation of GC-on-Chip

Following the performance evaluation of the µDPID, the monolithic integrated chip was tested. It should be noted that ALD-treated/silane-functionalized semi-packed µSCs have yielded ~4,200 plates per meter, using n-decane at 50 °C at the inlet pressure of 7.5 psi (linear velocity 8.5 cm/s) as recently demonstrated by our group [202]. The chromatographic performance of individual µSCs, however, was tested in our previous work only under isothermal conditions [202]. The presented work herein evaluates the separation efficiency of the column under simultaneous flow and temperature programming while using the on-chip detection stage. The GC-on-chip performance was evaluated with eight compound mixture containing alkanes and aromatic hydrocarbons prepared as explained before. The chip was configured inside an HP7890 GC system as shown in Fig. 6.3. The injector A and B were set to 15 psi and 10 psi, respectively. A 550 V DC voltage was applied to create the discharge and the bias voltage was

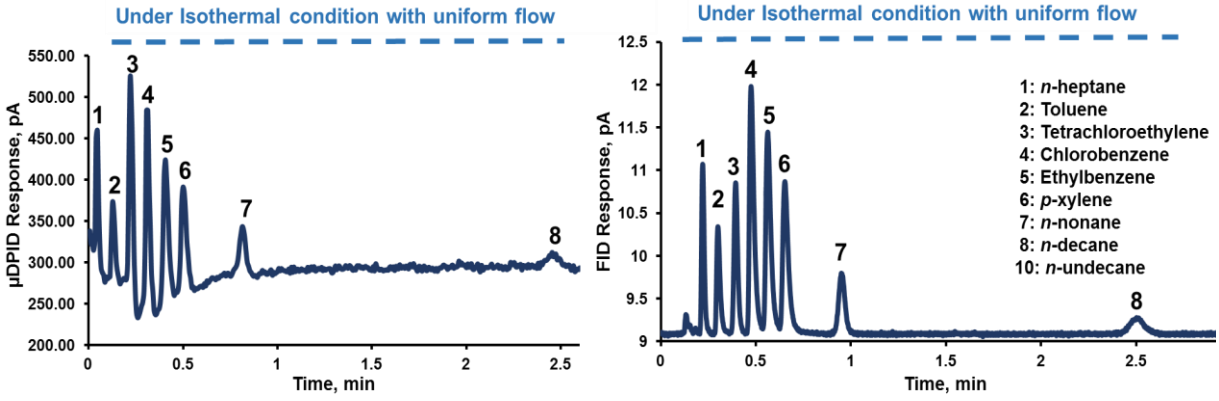

Figure 6.11 *(a) Response of the µDPID to a 10 µL headspace volume of eight compound mixture under the isothermal condition of 40 ˚C and flow rate of 1.33 mL/min. (b) Corresponding chromatogram generated by the FID.*

set to 20 V. The chip was maintained under an isothermal condition at 40 ˚C. The resulting chromatographic separation was achieved in 2.5 min (Fig. 6.11a), providing good resolution and retention of the compounds. The tested compounds were eluted in the order of increasing boiling points with the most volatile compound eluting first. The air peak (not shown here) precedes the n-heptane compound which shows the universality of the µDPID. A similar response was observed on the FID (Fig. 6.11b) except for the air peak which could not be detected due to the selectivity of the detector to only organic compounds. As seen in the chromatogram, the first six compounds were baseline separated from each other; however, p-xylene, C_9 and C_{10} peaks were well separated from each other resulting in an increased analysis time. The resolution (R_s) is defined as

$$R_s = \frac{(t_r)_B - (t_r)_A}{\frac{(w_b)_A + (w_b)_B}{2}} = \frac{2d}{(w_b)_A + (w_b)_B} \qquad (1)$$

where d is the distance between the peak maxima for the two compounds, A and B; w_b is the peak width at the base. The resolution was noted to be 5 between p-xylene and C_9 and 18.6 between C_9 and C_{10}; while their peak width was noted to be 4.2, 3 and 7 s, respectively. Raising the temperature of the chip or increasing the flow rate was considered to reduce the analysis time. However, it resulted in the poor resolution among the early eluting peak. Therefore, flow and temperature programming techniques were utilized in these ALD-coated µSCs for the first time to accelerate the separation of p-xylene, C_9 and C_{10} with an effort to achieve satisfying resolution between all the other compounds. This was achieved by first flow programming the µSC while maintaining the chip under isothermal conditions at 40 ˚C. The injector A pressure was initially maintained at 15 psi (1.3 mL/min) for 0.7 min (holdup time) and then increased to 35 psi (2.7 mL/min) at the rate of 30 psi/min. The hold time of 0.7 min was necessary to

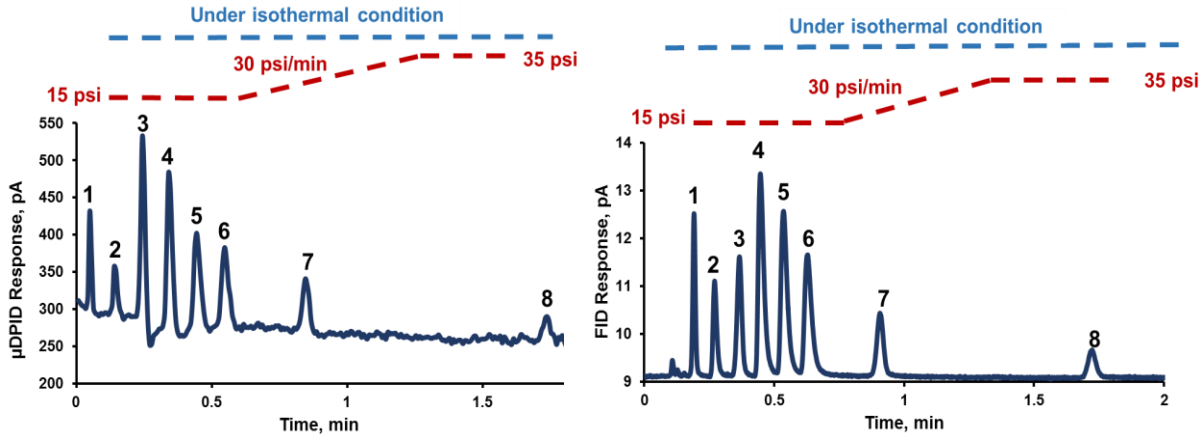

Figure 6.12 *(a) Response of the µDPID to a 10 µL headspace volume of eight compound mixture under the flow programming and isothermal condition of 40 ˚C. The initial and final flow through the column was 1.3 mL/min and 2.7 mL/min respectively (b) Corresponding chromatogram generated by the FID.*

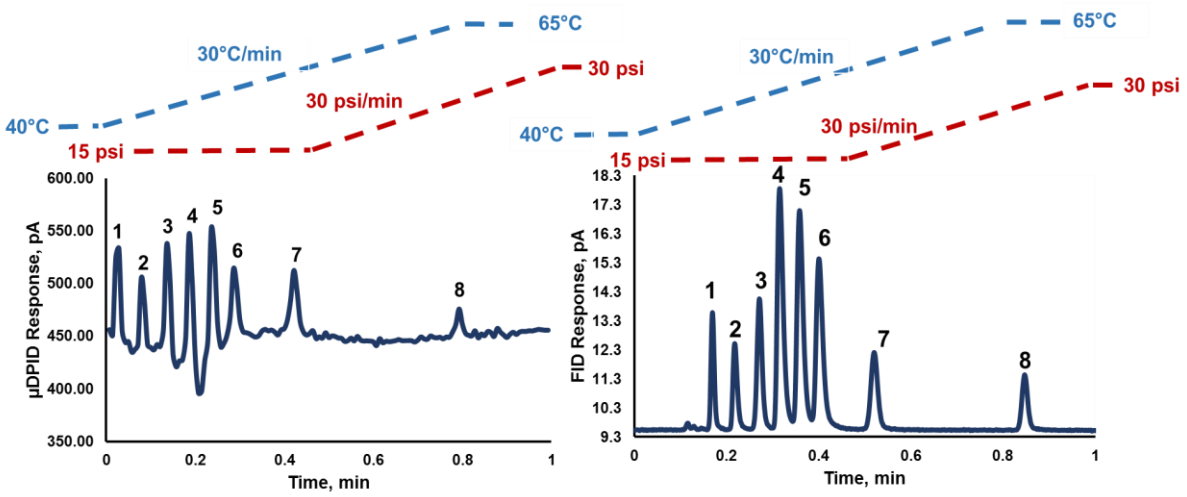

Figure 6.13 *Figure 6.13 (a) Response of the μDPID to a 10 μL headspace volume of eight compound mixture under the flow and temperature programming condition. The initial and final flow through the column was 1.3 mL/min and 2.3 mL/min respectively. (b) Corresponding chromatogram generated by the FID.*

achieve baseline separation between the first six eluting compounds. Reducing the holdup time causes early eluting peaks to merge together degrading the overall separation resolution.

The chromatogram in Fig. 6.12 reveals that the separation was completed in 1.8 min (28% reduction in the analysis time) with the resolution of 5.8 between p-xylene and C_9 and 15 between C_9 and C_{10}. It should be noted from the chromatogram that the peak width of C_9 was reduced to 2.9 s (3% reduction) while that of C_{10} was reduced to 4.5 s (35% reduction). The peak heights of p-xylene, C_9 and C_{10} also increased due to the increased flow rate during the flow programmed run providing better detection of the late eluting compounds.

Another effective method for reducing the analysis time is the temperature programming of the μSC. In this process, the μSC temperature increases which decreases the partition coefficient of the compounds still inside the column so they can move faster yielding a decrease in the retention time. As explained before, temperature programming (Tinitial = 40 ˚C, ramp = 30 ˚C/min, Tfinal = 65 ˚C) in conjunction with flow programming of the chip shortened the analysis time considerably. Fig. 6.13 indicates that the complete separation was achieved in 0.8 min (68% reduction in the analysis time) while the peak width of p-xylene, C_9 and C_{10} were noted to be ~ 1.8, 2.1 and 3 s, respectively. As expected, a further decrease in the resolution also observed. These findings have been compiled and presented in Table 6.3. To further shorten the analysis time for high-boiling hydrocarbons, a series of exploratory trials were performed with four n-alkanes (C_9-C_{12}) to establish the flow and temperature conditions for the best possible separation in the shortest period of time. For that purpose, the chip temperature was raised to 100 ˚C with the injector A pressure maintained at 25 psi (1.9 mL/min). A 50 μL headspace volume of four-compound mixture

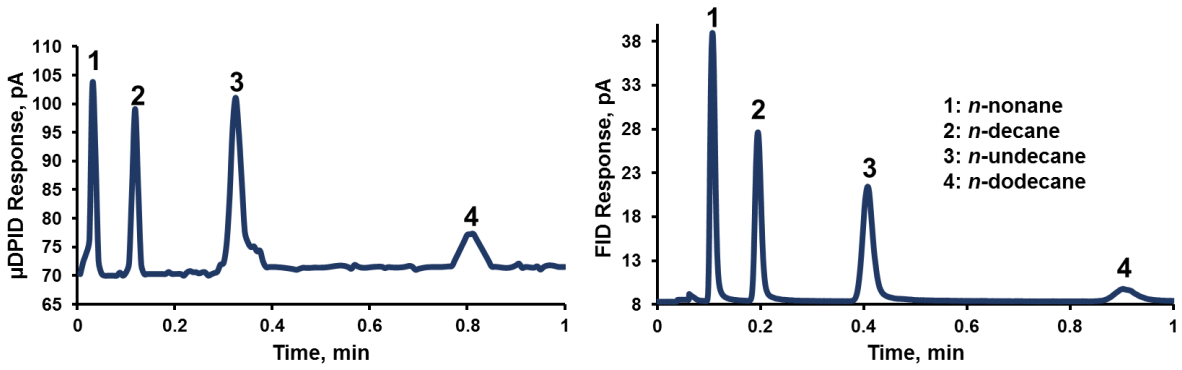

Figure 6.14 *(a) Response of the μDPID to a 50 μL headspace volume of four compound mixture of high boilers under the isothermal condition of 100 ˚C and flow rate of 1.9 mL/min. (b) Corresponding chromatogram generated by the FID.*

Testing conditions	p-xylene		n-nonane (C_9)		n-decane (C_{10})		Resolution $\frac{(t_r)_B - (t_r)_A}{\frac{(w_b)_A + (w_b)_B}{2}}$	
	Retention time (s)	Peak width (s)	Retention time (s)	Peak width (s)	Retention time (s)	Peak width (s)	p-xylene- C_9	C_9-C_{10}
Isothermal 40 ˚C	30	4.2	48	3	141	7	5	18.6
Flow programmed run	30	3.3	48	2.9	104	4.5	5.8	15
Flow and temperature programmed run	17	1.8	25	2.1	47	3	4.3	8.4

Table 6.3 *Summary of the results from Fig. 6.11-6.13 for the late eluting compounds including p-xylene, n-nonane and n-decane. The results are summarized in terms of the peak width, the retention time and the resolution.*

prepared as explained in Materials section was injected into the chip. The resulting chromatogram (Fig. 14) shows the separation and detection of these compounds in less than a minute. The peak width values were 1.3, 1.7, 3 and 5.4 s for C_9, C_{10}, C_{11} and C_{12}, respectively. It can be deduced from the results shown in Fig. 6.11-6.14 that the faster analysis of complex samples with compounds, covering a wide range of boiling point, is possible through the optimization of flow rate and temperature settings of the chip. A baseline signal with <5 pA of noise level in these chromatograms, clearly demonstrate the simultaneous temperature and flow programming capabilities of our newly developed GC-on-chip module. Such a stable response was not possible in our previously published work when the monolithically integrated chip with μTCD was subjected to temperature and flow programming conditions. However, small dips (negative peaks) in the baseline signal in the chromatograms (Fig. 6.11a-6.13a) were observed between few compounds which might be related to the time response of the detector. The exact origin of these dips is unclear at this stage and will be ascertained in the future investigations. It is important to note that such variation in the response has been noted with the chemiresistor (CR) sensors as well [211]. Furthermore,

these results (Fig. 6.11a-6.14a) present a proof-on-principle that rapid chromatographic analysis of a mixture containing low and high-boiling point compounds can be achieved through multiple GC-on-chip modules operated in parallel under different temperature and flow rate conditions.

IV. Conclusion

The µDPID presented in this article has many desired feature that bode well for its use in µGC. The detector is easy to fabricate, requires silicon and glass substrates which are the most commonly used materials for the fabrication of µGC components. This provides the opportunity of its monolithic integration with the other µGC modules such as the µSC reported in this article. This integration reduces the disadvantages of hybrid arrangement of µGC components including the dead-volume along the flow path, overall size and the implementation cost. Furthermore, the detector resistance to temperature and flow rate variations allows the programming of the µSC to achieve faster analysis with better performance. We have demonstrated that through temperature and flow programmed operation of the µSC, 68% reduction in the analysis time compared to the isothermal condition can be achieved. Similarly, operating the chip under an elevated temperature with higher carrier gas flow rate can provide quick separation and detection of high boilers. Furthermore, a network of these chips working in parallel can be envisioned with each row maintained under a different temperature and carrier gas flow rate conditions to enable the rapid separation of low and high-boiling point compounds. Rapid response time of the µDPID enables the detection of sharp peaks (~1 s wide) which can be beneficial in high speed µGCs. The LOD (~10 pg) attained with the µDPID is significantly lower than other detectors typically used within µGC community [40, 209, 211]. Additionally, the fact that the bias voltage can increase the signal level provides excellent opportunity to improve the LOD which can be realized through the modifications in the design and location of the bias electrode. In the future, we will study the influence of the distance between the discharge and the outlet of the µSC and the size of the collector volume on the detector performance. We are pursuing these design alterations along with the electronic board development for the µDPID. The circuit board will generate the high voltage (550 V, 2.5 µA) required for plasma generation. It will also provide the necessary current limiting protection circuitry to eliminate the possibility of electrical hazards as well as the interface for processing pico-ampere level of current signal for µDPID.

Chapter 7: Chip-Scale Gas Chromatography-From Injection through Detection

Over the past several decades, the progress in microfabrication technology has revolutionized the world in the field of computing, signal processing, and automobile industry. Miniaturization of well-established analytical instruments is another paradigm where the use of this technology has produced significant advancements. One such example is a gas chromatography (GC) system used in a number of scientific, medical, and industrial settings to separate and analyse volatile organic compounds (VOCs). Monitoring of VOCs is of interest in several applications including homeland security, space and fossil fuel exploration, worker exposure assessment and biomedical diagnostics [195-198, 212-215]. µGCs are under intense development to perform rapid diagnosis of VOCs in remote locations with low cost and consumable usage. A typical µGC consists of three important components including an injector/pre-concentrator for sample introduction [216, 217], a micro machined column for VOC separation [30, 31] and a single detector or an array of detectors [40, 211] located at the column exit to identify the separated compounds.

Since the first conceptual development of µGC in 1979 by Terry and co-workers [44], µGC research was silent for almost a decade with very little work reported in 1980s. In early nineties, the concept of micro Total Analysis System (µTAS) or Lab-on-a-chip was presented in the groundbreaking work of Manz [218], Harrison [219] and Jacobson [220]. Inspired by this concept, several research groups revisited the µGC research with the hope of developing a chip-scale GC platform. Nevertheless, majority of standalone µGC systems reported so far deal with the manual assembly of separately fabricated µGC components using commercially available off-chip fluidic interconnects [64, 67, 190, 206, 207]. This approach is commonly known as hybrid integration method. The implementation of µGC system in hybrid format is time consuming, cumbersome, expensive and prone to error. In addition, it degrades the overall performance of µGCs due to presence of cold spots between transfer lines. The condensation of compounds in these cold spots can result in extensive peak broadening. In particular, high boilers experience it in a more profound manner which can be deteriorating for their analysis. Alternatively, a chip-scale GC system which has all the three components on a single chip may suffer from thermal crosstalk between the individual µGC components. Thermal crosstalk can happen during two chromatographic events including: 1) desorption process of the pre-concentrator and 2) the temperature programming of the column. Thermal crosstalk could potentially change the retention time of a compound and also produce undesirable drift or noise in the detector signal. Fortunately, these issues can be avoided in chip-scale GC platform by developing an optimal back-end detector technology.

Recently, there has been significant advancements in detector technology and a wide variety of chemical detectors have been developed [40, 211, 221-228]. The micro helium discharge photoionization detector (µDPID) presented by our group has demonstrated a minimum detection limit of ~10 pg which is equivalent to an FID mostly used in bench-top GC systems [229]. Such a high sensitivity of µDPID reduces the reliance on the front-end pre-concentration step which is usually performed to facilitate the detection limit of the detector. In addition, we have previously demonstrated that the µDPID can be easily integrated with the separation column and demonstrated its operation under the temperature and flow rate programming conditions [229]. These two features of µDPID make it a promising candidate for developing chip-scale GC system; thereby addressing the above-mentioned issues and improving the overall cost and performance of this technology.

This paper is intended to demonstrate a truly compact chip-scale GC platform. To the best of our

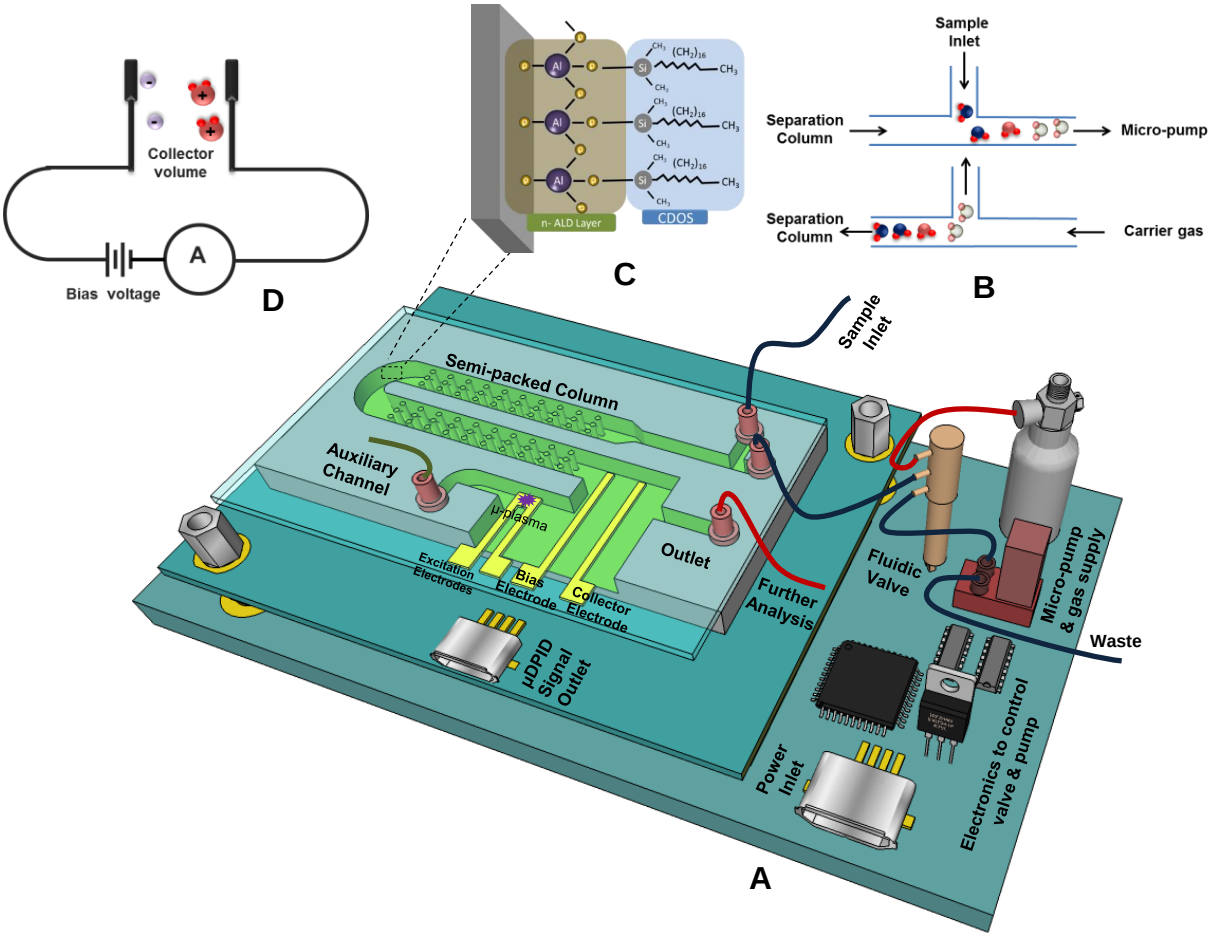

Figure 7.1 *Conceptual image showing the description of major components of chip-scale GC platform: (A) set up showing the configuration of fluidic interconnections between the chip, valve, micro-pump and the carrier gas (B) description of injection mechanism: top image shows the loading phase while the bottom one depicts the injection phase (C) coating mechanism for µSC (D) electrical circuit for measuring the current signal produced by the ionization of volatile organic compounds.*

knowledge this is the first demonstration of a lab-on-a-chip GC which has the following three essential elements, all on the same platform: a sample injector, a separation column and a detector. Our results indicate that the loading time of a few seconds is required to introduce a VOC mixture into the chip with a quick subsequent analysis performed in less than a minute for compounds present over wide boiling point range (110 ˚C-216 ˚C). This development will be especially suitable to produce low cost and efficient µGC system for rapid analysis of compounds in real time situations.

I. System Description

Fig. 7.1A elaborates the configuration of fluidic connections between the chip, valve, miniaturized pump and the helium carrier gas supply. The valve position and the pump are controlled by an 8-bit micro-controller interfaced with a keypad to initiate the command. The operation of the chip-scale GC platform is quite straightforward. In normal operation, the valve is connected to the carrier gas supply. The sample inlet port is manually inserted into a sealed vial containing the unknown mixture of VOCs. To avoid liquid phase injection, the sample inlet port is kept in the headspace volume above the sample. To perform an injection, a single command from the keyboard initiates a sequence of events which is completed within few seconds. First the valve is switched to the pump position and the pump is turned on. The pump applies negative pressure (flow rate 1mL min^{-1}) to load the sample into the fluidic channel

VOC	p_v	B.P	Ionization Potential
Toluene	22.0	110	8.82
Tetrachloroethylene	14.2	121	9.32
Chlorobenzene	11.7	131	9.07
Ethylbenzene	9.9	136	8.76
p-xylene	9.0	138	8.45
n-nonane	4.6	151	9.70
Bromobenzene	4.2	156	8.98
n-decane	1.4	174	9.60
1,2-dichlorobenzene	1.0	180	9.07
n-undecane	0.4	196	9.60
1,2,4-trichlorobenzene	0.3	214	9.04
n-dodecane	0.3	216	—

Table 7.1 *Physical properties of the volatile organic compounds used in this study.*

connecting the valve and the chip. Subsequently, the valve position is turned again to the carrier gas position which injects the sample into the μSC (Fig. 7.1B). The sample moves through the μSC with helium carrier gas and are separated into individual compounds. The separation process is based on the relative solubility of the compounds in the silane-treated alumina stationary phase (Fig. 7.1C) and their relative vapor pressure. As the compounds separated in space and time elute from the μSC, they are ionized with high-energy (>10 eV) photons. These photons are generated through a micro-plasma produced in helium by applying a 550 V DC voltage across a pair of excitation electrode. The gap between the excitation electrodes is ~ 20 μm. The micro-plasma is sustained by a constant supply of helium from the auxiliary channel. A 50 MΩ ballast resistor is connected in series with the excitation electrode to limit the amount of current flow which could potentially damage the electrodes. In addition to the pair of excitation electrodes, the detector has a bias and a collector electrode. The bias and the collector electrodes are 1.5 mm apart and the space between them is called the collector volume. The circuit shown in Fig. 7.1D measures the signal in the form of an electrical current which is produced through the ionization of VOCs. Here, a pico-ammeter and the bias voltage are connected in series to the collector and the bias electrode respectively. The positive voltage applied to the bias electrode assists in capturing the electron inside the collector volume. The recombination of electrons with the ionized species can essentially reduce the measured current. The current measured by the pico-ammeter is fed to the Keithley 2700 multimeter which communicates with the LABVIEW program to plot the output signal.

II. Experimental Methods

A. Materials

All VOCs listed in Table 7.1 were purchased from Sigma Aldrich (St. Louis, MO) in >99% purity. Silicon wafers (n-type, 4 in. diameter, 500 μm thickness, single side polished) and Borofloat wafer (4 in diameter, 700 μm thickness, double side polished) were purchased from University Wafers (Boston, MA) and Coresix Precision Glass (Williamsburg, VA) respectively. Ultra high purity helium (UHP 300) was purchased from Airgas (Christiansburg, VA). Fused silica capillary tubes (100 μm I.D. and 200 μm O.D) were purchased from Polymicro Technologies (Phoenix, AZ). The miniaturized pump (P/N SP 270 EC-LC-L) and 3-way latching solenoid valve (LHLA0521111H) were purchased from Schwarzer Precision (Germany) and Lee Company (Westbrook, CT) respectively.

B. Chip Fabrication

The chip fabrication requires bulk micro-machining of silicon wafer and the metallization of Borofloat substrate. The silicon processing started with spinning of AZ 9260 resist on the substrate at 2000 rpm (Fig. 7.2i). The resist was patterned using mask aligner (Karl Suss) followed by the development in AZ

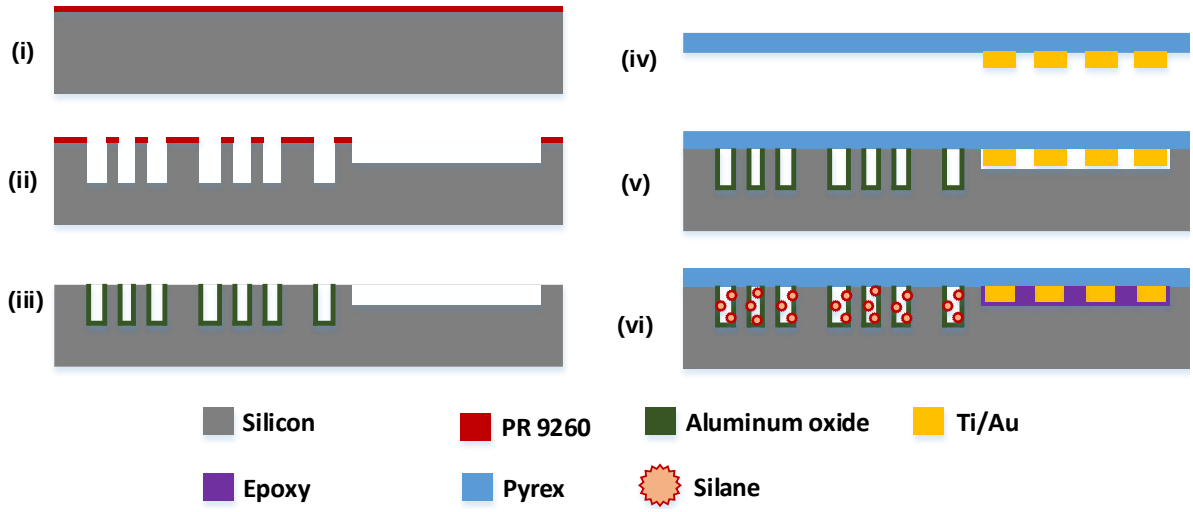

Figure 7.2 *Standard MEMS processes for the fabrication of the integrated chip. (i) Photolithography, (ii) deep reactive ion etching, (iii) atomic layer deposition, (iv) physical vapor deposition, (v) anodic bonding and (vi) surface functionalization.*

400K. Deep reactive ion etcher (DRIE, Alcatel) was utilized to create the separation stage (1 m long, 190 µm wide and 240 µm deep with 20 µm embedded circular pillars), fluidic ports and a cavity for the detector (Fig. 7.2ii). After etching, the photoresist was removed from the substrate using acetone. Atomic layer deposition (ALD) was used to coat a thin layer of alumina (~10 nm) at 250 ˚C (Fig. 7.2iii). Trimethylaluminum (TMA) and water were utilized as precursors in the process. The detector electrodes were fabricated on the Borofloat wafer by evaporating 700 nm/40 nm of Ti/Au on patterned AZ9260 resist and performing lift off using acetone (Fig. 7.2iv). The silicon and Borofloat wafer were diced and the individual devices were bonded at 1000 V and 370 ˚C for 45 min (Fig. 7.2v). Next, the detector cavity was sealed with epoxy, electrical wires were soldered to the bond pads and capillary tubes were inserted into the four ports of the chip. A solution containing 10 mM chlorodimethyloctadecylsilane (CDOS) in toluene was filled in the µSC and left for 24 h at room temperature (Fig. 7.2vi). Finally, the solution was purged using nitrogen and µSC was conditioned inside the conventional GC system for approximately 1 h (35 ˚C-ramped 2 ˚C/min-140 ˚C) at a constant pressure of 10 psi.

III. Results and Discussion

The top and cross-sectional images of the µSC using scanning electron microscopy (SEM) are shown in Fig. 7.3a-b respectively. The optical image of the completely packaged device is shown in Fig. 7.3c with the capillaries attached to four ports of the chip and the electrical connections in place. We will first explain the performance evaluation of sample injection unit and the µDPID. It is important to note that both the components were diced from the integrated chip for that purpose. The chromatographic analysis performed using the integrated chip will be demonstrated afterwards.

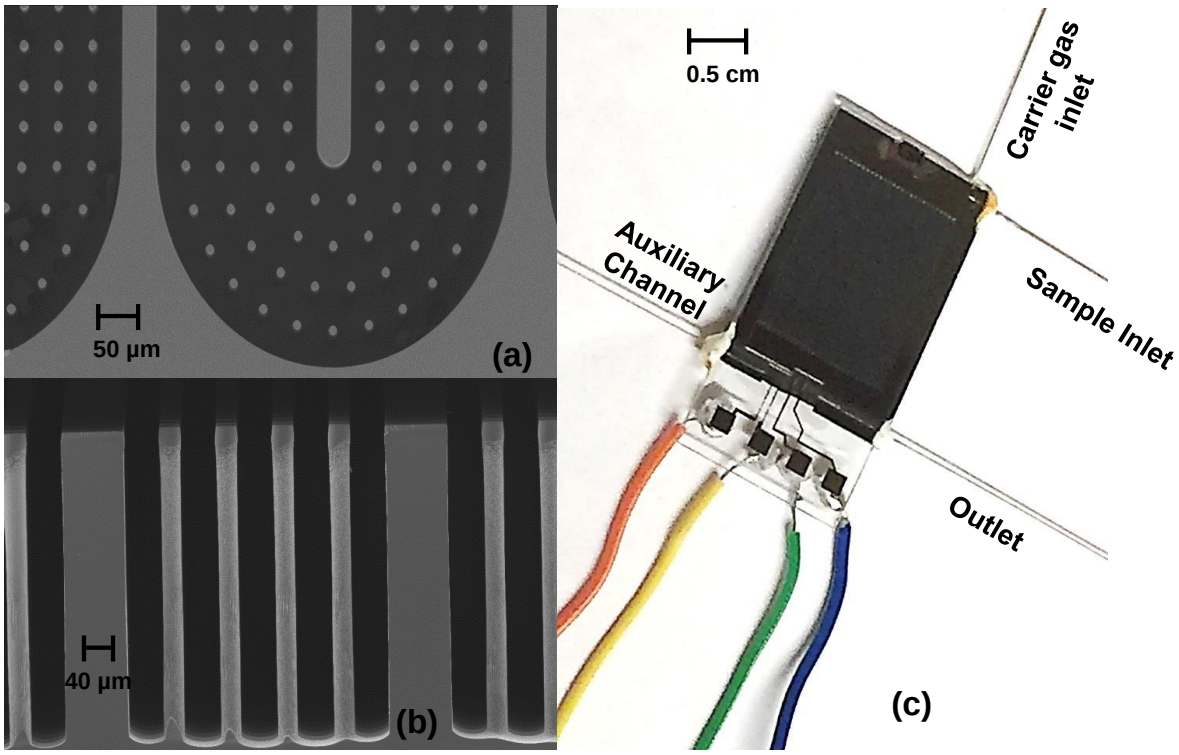

Figure 7.3 *SEM images of the semi-packed µSC column showing (a) top view of the channel with embedded 20 µm circular micro-pillars (b) cross-sectional view showing high aspect ratio pillars (c) Optical image of the packaged chip.*

A. Evaluating Sample Injection Unit

The performance of sample injection unit was characterized in terms of peak parameters (full-width-at-half-maximum [FWHM], peak height and area). Five compounds including heptane, toluene, chlorobenzene, ethylbenzene and p-xylene were used in these tests. Each compound was separately injected at flow rates set to five discrete values of 0.3, 0.45, 0.72, 1 and 1.4 mL min^{-1}. These flow rates correspond to the inlet pressures of 10, 15, 20, 25 and 30 psi. The loading time of 500 ms was used for all VOCs. The outlet of the injector was connected to the FID installed in the conventional GC system (HP 7890). Triplicate runs were performed for each value and the average value of FWHM and peak height was plotted as shown in Fig. 7.4.

It is evident from these results that for all VOCs, the FWHM depends on the injector flow rate condition. All compounds experienced a sharp decrease in FWHM initially between 0.3 and 0.72 mL min^{-1} and then more gradually afterwards. This can be understood by the fact that molecules diffuse in the carrier gas from the region of high concentration to that of lower concentration with the passage of time. Increasing the flow rate decreases the time that molecules spend in the injector and therefore the diffusion

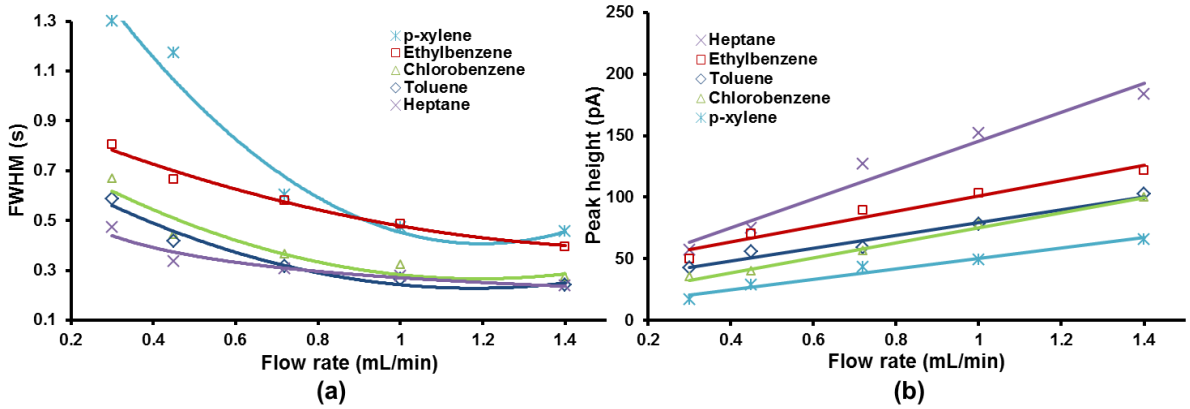

Figure 7.4 *The effect of carrier gas flow rate on full-width-at-half-maximum value of the injection plug. The curves were approximated with an order 2 polynomial trend line. The R-squared value was calculated to be 0.88, 0.96, 0.91, 0.98 and 0.97 for heptane, toluene, chlorobenzene, ethylbenzene and p-xylene respectively. The standard error calculated for each point over triplicate runs were <10% showing that the sample injection unit produces repeatable injections.*

The effect of carrier gas flow rate on peak height of the injection plug. The curves were approximated with linear trend line. The R-squared value was calculated to be 0.96, 0.96, 0.99, 0.96 and 0.97 for heptane, toluene, chlorobenzene, ethylbenzene and p-xylene respectively. The standard error calculated for each point over triplicate runs were <10%. .

of molecules in the carrier gas is decreased which results in lower value of FWHM. However, beyond 0.72 mL min^{-1} there is a slightly less decrease in the FWHM which is due to the dilution of VOCs in the carrier gas at higher flow rates condition. The superposition of both phenomena explains the curves in Fig. 7.4a. In addition, the compound with higher boiling points experience more peak broadening owing to the cold spots present in the injector and the fluidic interconnections. This effect can be seen in case of ethylbenzene and p-xylene especially at lower flow rates. Accordingly, this supports the concept of integrating the individual modules of µGC technology since it become very difficult to produce a narrow peak for high boilers due to the presence of cold spots in fluidic interconnects. Increasing the flow rate has significant impact on reducing the peak broadening for ethylbenzene and p-xylene. Nevertheless, the FWHM for these two compounds are comparatively more than the other compounds at 1.4 mL min^{-1}. Heating the injector and transfer lines could address this issue as will be noticed later in the chromatographic analysis of the chip. The overall decrease in FWHM for heptane, toluene, chlorobenzene, ethylbenzene and p-xylene over the entire flow rate range was noticed to be 40%, 59%, 59%, 50% and 64%, respectively.

Since FID is a mass flow rate sensitive detector, the decrease in FWHM was compensated by a corresponding increase in the peak height to maintain uniform peak area. Fig. 7.4b shows the peak height increases linearly over the entire flow rate range (from 0.3-1.4 mL min^{-1}) for all VOCs. This is attributed to the increase in mass/time as measured by the FID. The peak area for all compounds remained

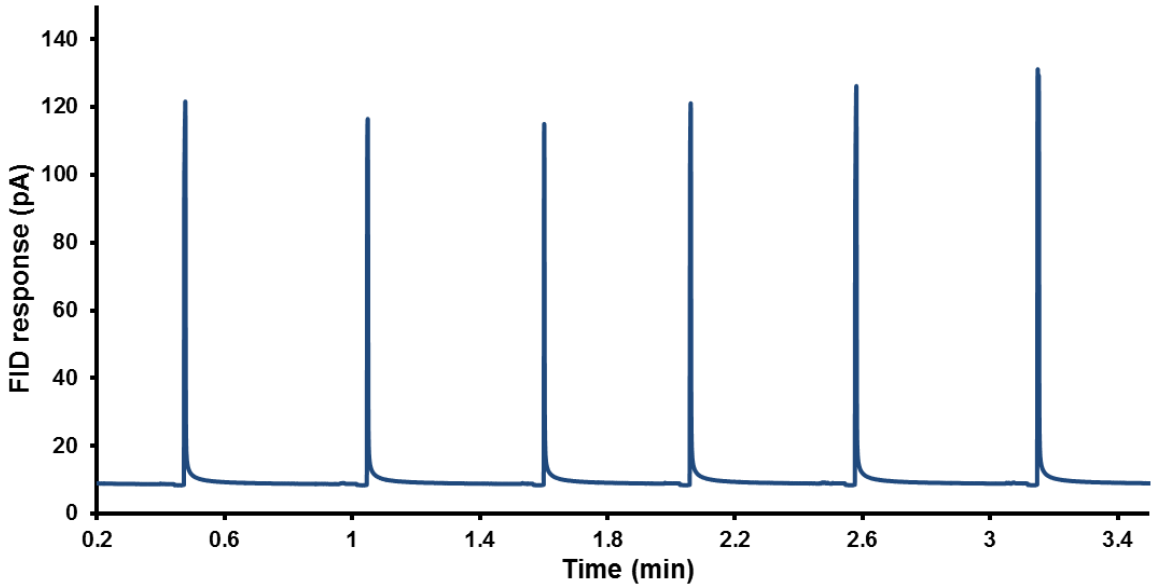

Figure 7.5 *Chromatogram showing the repeatability of sample injection unit over multiple injection of toluene vapor. The FWHM was ~200 ms at the flow rate of 1.4 mL min^{-1}. Less than 5% variation was noticed in the standard error values for peak parameters (FWHM, peak height and area) over six injections.*

approximately constant for all flow rate conditions. Peak areas were calculated to be ~ 20 pA for these compounds except for ethylbenzene which was ~35 pA measured by the FID.

Furthermore, the repeatability of the sample injection unit was investigated by monitoring change in peak parameter (FWHM, peak height and area) over multiple headspace injections. For that purpose, toluene was chosen as a test compound and multiple injections were performed in succession approximately every half a minute. The flow rate in this experiment was set to 1.4 mL min^{-1}. Fig. 7.5 shows that sample injection unit produces highly repeatable results. Less than 5% variation in the standard error values for peak parameters over six injections was noted. The FWHM for these injections were found to be ~200ms.

B. Linearity of µDPID

The previous characterization of µDPID has demonstrated encouraging results indicating the minimum detection limit of ~10 pg, the response time of ~200 ms and the stability of excitation electrodes over a long period of time.[229] Here we have experimentally analyzed the linear detection range of the detector.

To evaluate the linear range of µDPID, the inlets of the detector were connected to the injector A and B of the conventional GC system. The injector A and B pressure was set to 15 psi and 10 psi, respectively. A 550 V DC voltage was applied (using PS-310, Stanford Research Systems) to create the discharge and the bias voltage was set to 30 V. This value of bias voltage is selected form our previous

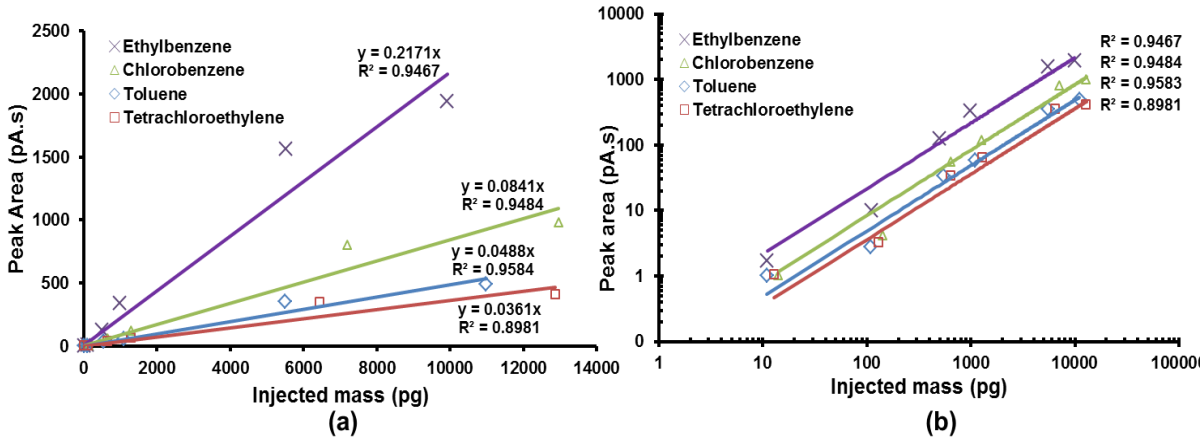

Figure 7.6 *(A) calibration curves for µDPID produced by injecting different mass (10pg-13ng) of four tests compounds and calculating the response (peak area). Each point was repeated in triplicate and the average value plotted against the injected mass. Linear regression (forced zero Y-intercept) R^2 values are shown for each compound. The slope (A.s g^{-1}) was calculated to be 0.0361, 0.0488, 0.0841 and 0.2171 for tetrachloroethylene, toluene, chlorobenzene and ethylbenzene respectively. (B) Corresponding curve plotted on log-scale for clarity.*

work showing enhanced sensitivity of the detector at 30 V [229]. Four test compounds including toluene, tetrachloroethylene, chlorobenzene and ethylbenzene were used as test compounds. Different headspace volume of test compound sealed in a vial was sampled using an autosampler (7359A) module to ensure repeatable injections. Assuming ideal gas law behavior, the mass of compound injected from a saturated vapor above the pure liquid can be calculated from the injection volume and the split ratio used for the injection. The injected mass was in the range of ~10 pg-10 ng. The response of the detector was measured in terms of peak area for each injection. The peak area has been selected as an indicator for the quantitative data analysis (instead of peak height) based on our previous results which indicate that µDPID is a mass flow rate sensitive detector (MSD) [229]. For any MSD, variation in the flow rate could give rise to the change in peak height or width; however negligible changes are observed in peak area. Therefore, the quantification of a compound in terms of peak area is comparatively more accurate. Each data point was repeated three times and the average peak area was plotted against the injected mass of each test compound (Fig. 7.6a). Since the injected mass extends over several orders of magnitude, these curves have been plotted on a log-log scale for clarity (Fig. 7.6b).

It can be deduced from these results that the response of the detector remains linear over three orders of magnitude to the injected mass of test compounds. The R-squared values and their respective slopes obtained by linear regression analysis (forced zero Y-intercept) have been indicated for each curve. The response of µDPID is relatively lower for the tetrachloroethylene due to it high ionization potential which make it difficult to ionize. The ionization potential of the remaining VOCs is reasonably close. The ionization potential for all VOCs used in this report has been indicated in Table 7.1.

The sensitivity of the detector is defined as the signal output per unit mass of the compound in the carrier gas. For MSD the sensitivity, S, is defined as

$$S = \frac{A}{W}$$

where A is the integrated peak area and W is the mass of the compound. Therefore, the slope of the curves in Fig. 7.6a indicates the sensitivity of µDPID for a particular compound under investigation. The slopes for toluene, tetrachloroethylene chlorobenzene and ethylbenzene were found to be 0.036, 0.0488, 0.0841 and 0.2171 ($A.s\ g^{-1}$) respectively, showing higher sensitivity of the µDPID towards ethylbenzene compared to other test compounds.

C. Chip-Scale GC: Chromatographic Analysis

The chip-scale GC platform was tested following the characterization of the sample injection unit and µDPID. Twelve VOCs including toluene, tetrachloroethylene, chlorobenzene, ethylbenzene, p-xylene, n-nonane, bromobenzene, n-decance, 1,2-dichlorobenzene, n-undecane, 1,2,4-trichlorobenzene and n-dodecane were selected to evaluate the performance of the chip. The purpose of the following experiments was to demonstrate the sampling, separation and detection of the compounds spanning over a boiling point range 110 ˚C-216 ˚C in the shortest possible time through the optimization of flow and temperature programming conditions.

The chip was configured as discussed in system description section (Fig. 7.1) with the carrier gas and auxiliary helium supplied by the conventional GC system. The pressure on both the supplies was set to 22 psi and 10 psi, respectively, which corresponds to the flow rate of 0.77 mL min^{-1} at the chip outlet port. The chip temperature was maintained at 40 ˚C. During the sampling, the pump was turned on to load the

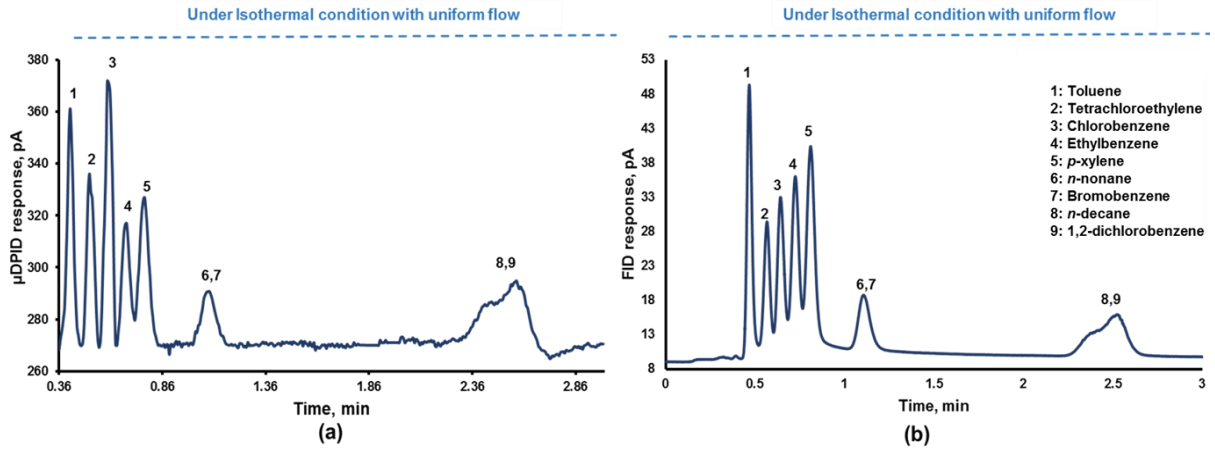

Figure 7.7 *(a) Response of the µDPID to a 3 s headspace sampling of nine-compound mixture under isothermal conditions at 40 °C and a flow rate of 0.77 mL min^{-1} at the chip outlet (b) Corresponding chromatogram generated by the FID.*

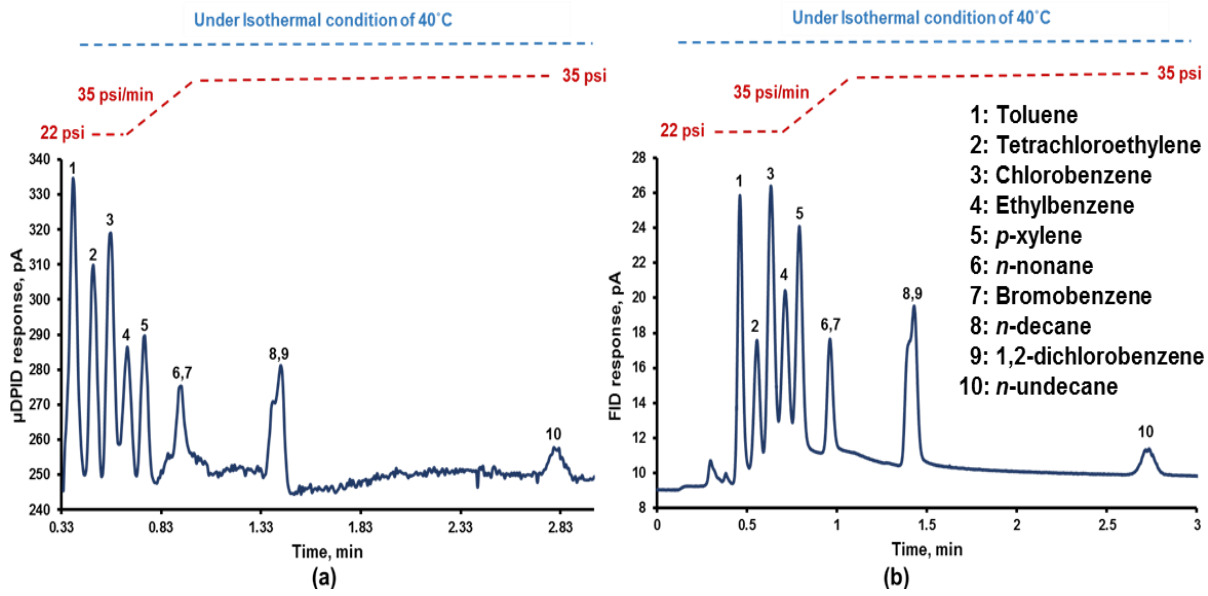

Figure 7.8 *(a) Response of the μDPID to a 3 s headspace sampling of ten-compound mixture under the flow programming and isothermal conditions at 40 °C. The initial and final flow rates through the column outlet were 0.77 mL min^{-1} and 1 mL min^{-1} at the chip outlet, respectively (b) Corresponding chromatogram generated by the FID.*

sample into the fluidic connection between the chip and the valve. A sampling time of 3 s was considered sufficient for testing the compounds. The chromatogram in Fig. 7.7 shows the successful identification of nine compounds in 2.5 min, providing good resolution and retention of the compounds. The compounds were eluted in order of decreasing vapor pressure (p_v values have been indicated in Table 7.1). The compounds with high vapor pressure tend to remain in the vapor state and thus, have more affinity for the mobile phase compared to the stationary phase which results in their early elution from the μSC. In Fig. 7.7, n-nonane and bromobenzene were not resolved due to their vapor pressure being relatively close. Similar observation was made for n-decane and 1,2-dichlorobenzene. It should be noted that the air peak detected by μDPID has been removed from the chromatogram for clarity. From the chromatograms generated by μDPID, peak width at base ($w_b = 4\sigma$) and the retention time (t_r) were calculated for every compound. For high boilers including p-xylene, C_9/bromobenzene, C_{10}/1,2-dichlorobenzene, w_b were found to be 7.2, 10 and 27 s respectively. The resolution (R_s) defined as

$$R_s = \frac{(t_r)_B - (t_r)_A}{\frac{(4\sigma)_A + (4\sigma)_B}{2}} = \frac{2d}{(4\sigma)_A + (4\sigma)_B} \qquad (1)$$

where d is the distance between the peak maxima for the two compounds, A and B. The resolution was noted to be 2.16 between p-xylene and C_9/ bromobenzene and 4.60 between C_9/bromobenzene and C_{10}.

In an effort to reduce the analysis time and improve the peak width of high boiling compounds, series of experiments were performed under flow programming conditions. The best chromatographic results have been shown in Fig. 7.8. Here the pressure was initially set to 22 psi (0.77 mL min^{-1}) for 0.7 min and

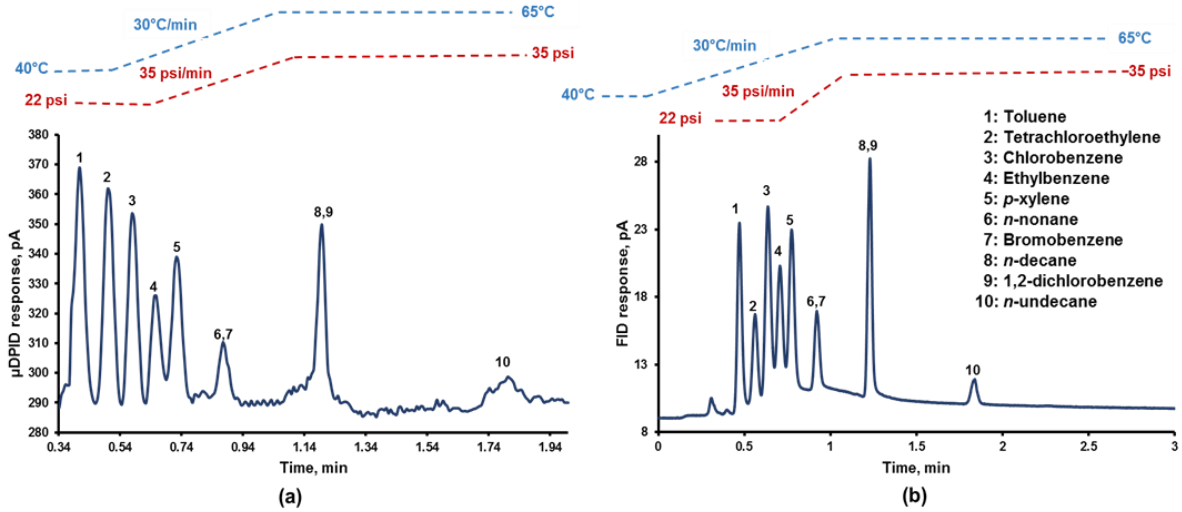

Figure 7.9 (a) *Response of the μDPID to a 3 s headspace sampling of ten-compound mixture under the flow and temperature programming conditions. The initial and final flow rates through the column were 0.77 mL min^{-1} and 0.9 mL min^{-1} at the chip outlet, respectively (b) Corresponding chromatogram generated by the FID.*

then ramped to 35 psi (1 mL min^{-1}) at the rate of 35 psi/min. The holdup time was necessary to avoid poor resolution between the first five eluting compounds. In Fig. 7.8 the first nine compounds eluted in 1.6 min which shows a reduction of 36% in the analysis time compared to the previous run. In addition, C_{11} peak was also observed at 2.8 min. The increased pressure also had a profound impact on the w_b value for high boiling compounds including p-xylene, C_9/bromobenzene and C_{10}/1,2-dichlorobenzene. A reduction of 33%, 40% and 69% in w_b was observed for these compounds respectively. This is due to the fact that at increased pressure, relatively less time is available for the longitudinal diffusion of molecules inside the μSC which results in narrower peak width. The R_s was also reduced to 2 between p-xylene and C_9/bromobenzene, 4.08 between C_9/bromobenzene and C_{10}/1,2-dichlorobenzene and 8.16 between C_{10}/1,2-dichlorobenzene and C_{11}.

Temperature is one of the most important variables in GC and an effective way of optimizing the analysis time. The superposition of temperature ($T_{initial}$ = 40 ˚C, ramp = 30 ˚C min^{-1}, T_{final} = 65 ˚C) and flow programming ($P_{initial}$ = 22 psi, ramp = 35 psi min^{-1}, P_{final} = 35psi) has been demonstrated in the chromatogram shown in Fig. 7.9. As a result the analysis was completed in 1.8 min (56% reduction in the analysis time). As expected, a further decrease of 41%, 58% and 86% in w_b was observed for p-xylene, C_9/bromobenzene and C_{10}/1,2-dichlorobenzene.

Furthermore, a separate sample containing high boilers including n-nonane, bromobenzene, n-decane, 1,2-dichlorobenzene, n-undecane, 1,2,4-trichlorobenzene and n-dodecane was also analyzed. The carrier gas pressure was increased to 35 psi while the auxiliary helium pressure was maintained at 10 psi respective, which corresponds to the flow rate of 0.9 mL min^{-1} at the chip outlet port. The chip

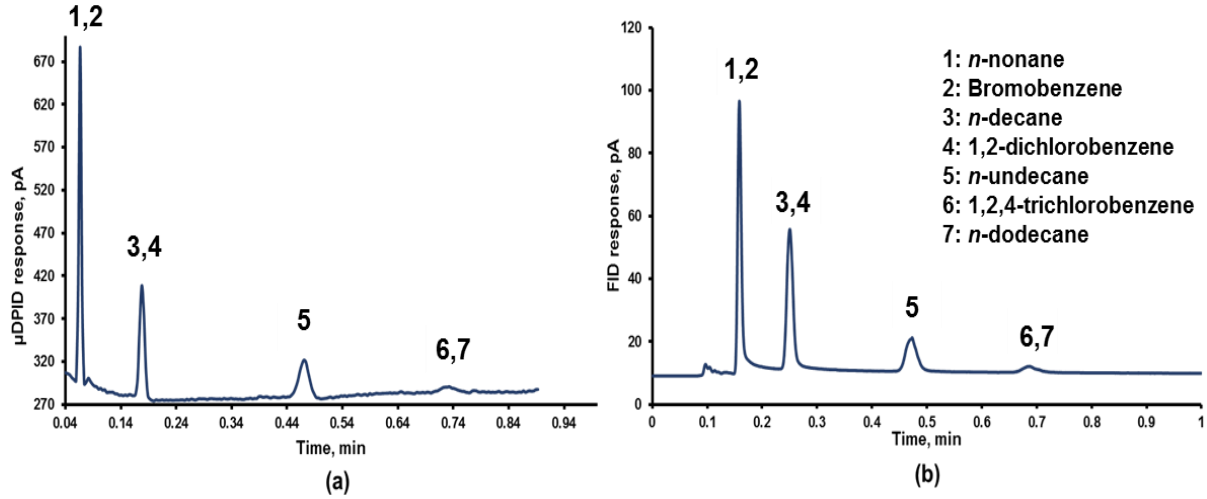

Figure 7.10 *(a) Response of the μDPID to a 6 s headspace sampling of a seven-compound mixture of high boilers under isothermal conditions at 70 °C and a flow rate of 0.9 mL min^{-1} at the chip outlet (b) Corresponding chromatogram generated by the FID.*

	Isothermal, 40 °C		Flow programmed run		Flow & Temp. programmed run		Isothermal, 70 °C	
	t_r (s)	4σ (s)	t_r (s)	4σ (s)	t_r (s)	4σ (s)	t_r (s)	4σ (s)
Toluene	24.6	4.2	24.0	6.0	24.6	4.8	—	—
Tetrachloroethylene	30.6	4.8	29.4	4.8	30	4.8	—	—
Chlorobenzene	36.0	4.8	34.2	4.8	34.8	4.2	—	—
Ethylbenzene	40.8	5.4	40.8	4.8	39.0	4.2	—	—
p-xylene	46.2	7.2	44.4	4.8	43.8	4.2	—	—
n-nonane & Bromobenzene	64.8	10	55.2	6.0	52.8	4.2	3.60	0.9
n-decane & 1,2-dichlorobenzene	150	27	84.6	8.4	66	3.6	10.8	1.5
n-undecane	—	—	168	12	108	9.0	28.2	2.4
1,2,4-trichlorobenzene & *n*-dodecane	—	—	—	—	—	—	43.2	5.4

Table 7.2 *Summary of the retention time (t_r) and peak width at the base (4σ) from the results presented in Figure 7.7-7.10 for μDPID.*

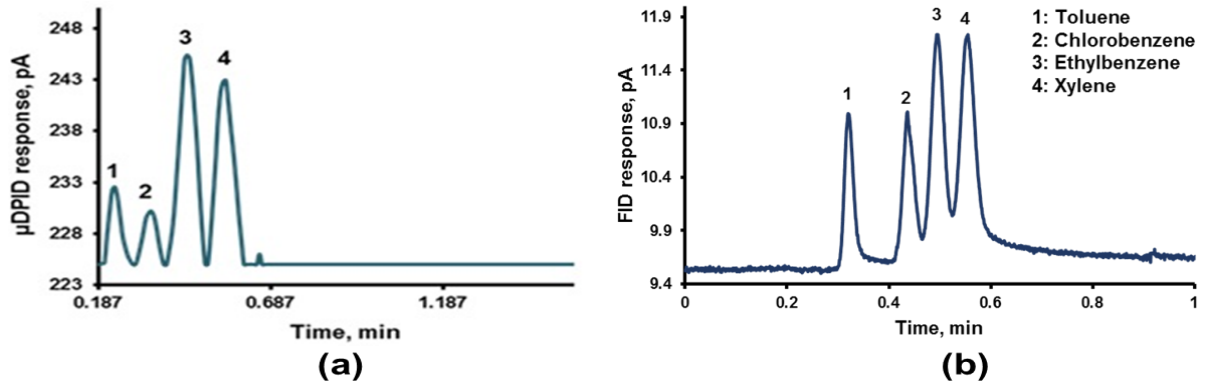

Figure 7.11 *Response of the µDPID to a 6 s headspace sampling of quaternary mixture with each compound diluted to 1 ppm concentration level in aqueous phase. Corresponding concentration in headspace using Henry's Law are 270 (toluene), 152 (chlorobenzene), 323 (ethylbenzene) and 314 ppb (p-xylene). Flow rate was set to 0.77 mL min^{-1} at the chip outlet (b) Corresponding chromatogram generated by the FID.*

temperature was raised to 70 ˚C. The loading time was increased to 6 s because of low vapor pressure of these compounds. The resulting chromatogram is shown in Fig. 7.10. The analysis was completed in 0.8 min with significantly lower values of w_b. The w_b value of 900 ms, 1.5 s, 2.4 s and 5.4 s were noted for C_9/bromobenzene, C_{10}/1,2-dichlorobenzene, C_{11} and 1,2,4-trichlorobenzene/C_{12} respectively. The data in terms of retention time (t_r), peak width (w_b) for each compounds in Fig. 7.7-7.10 has been compiled in Table 7.2. The resolution (R_s) for high boiling compounds has been listed in Table 7.3.

Aqueous Analysis

The chip performance was also evaluated for the analysis of VOCs in aqueous media. Four VOCs including toluene, chlorobenzene, ethylbenzene and p-xylene were diluted to 1 ppm (1 mg L-1) concentration level in deionized (DI) water. A small aliquot (500 µL) of the prepared sample was transferred into a 1.8 mL vial. The vial was subsequently sealed to avoid compromising the sample integrity. A sampling time of 6 s was considered sufficient for extracting VOCs from the headspace of the sample. The representative chromatogram is shown in Fig. 7.11 where the separation and detection was completed within 0.6 min. It is pertinent to mention that the United States Environmental Protection Agency (EPA) has specified the maximum contamination level (MCL) for toluene, chlorobenzene, ethylbenzene and p-xylene as 1, 0.1, 0.7 and 10 ppm, respectively.

IV. Conclusion

This is the first demonstration of an integrated µGC analysis system which has all the important features of lab-on-a-chip platform. It has a sample injection unit, a micro separation column and an ionization based detector all integrated on a 1.5 cm × 3 cm platform. The integration of µGC components on a common substrate reduces the footprint of this technology, enhances the overall performance and yields lower fabrication cost. Furthermore, each component can perform its role effectively in a quick

$$\text{Resolution} = \frac{(t_r)_B - (t_r)_A}{\frac{(4\sigma)_A + (4\sigma)_B}{2}}$$

Testing conditions	*p*-xylene-C_9	Bromobenzene-C_{10}	1,2-dichlorobenzene-C_{11}	C_{11}- 1,2,4-trichlorobenzene
Isothermal, 40 ˚C	2.16	4.60	—	—
Flow programmer run	2.0	4.08	8.16	—
Flow & Temperature programmed run	2.14	3.38	6.66	—
Isothermal, 70 ˚C	—	6.0	8.9	3.84

Table 7.3 *Peak resolution (R_s) calculated for high boilers including p-xylene, C_9/bromobenzene, C_{10}/1,2-dichlorobenzene, C_{11} and 1,2,4-trichlorobenzene in Figure 7.7-7.10. The data presented in Table 7.2 was used for the calculation.*

manner; for example, the sample injection unit requires the loading time of few seconds to produce sharp injections (FWHM ~200 ms). Similarly, the subsequent operation of the system under the temperature and flow programming conditions provide rapid analysis of complex VOC mixture. In addition, the excellent detection limit (~10 pg), response time (~200 ms) and linearity of µDPID (three orders of magnitude) augers well for its use in µGC technology. Further improvement in these properties through modification in the design of µDPID is also being considered. While the miniaturization of µGC system through integration of micro electromechanical systems (MEMS) component has been demonstrated in this work, we are also exploring its integration with electronic components to further miniaturize this technology.

Chapter 8: Summary and Outlook

I. Conclusion

The primary focus of this research was to address the critical need of developing a fully integrated lab-on-a-chip µGC platform. Such integrated µGC systems should provide all necessary steps for chemical analysis of a sample (e.g. sampling, separation and detection) on a single platform. In an effort to realize such a system, each component of the µGC system was first individually optimized to provide best performance upon integration. In collaboration with the Physics Department at Virginia Tech, nanotechnology-based solutions were explored to enhance the adsorption capacity of micro thermal pre-concentrators (µTCP). Silica nanoparticles (SNPs) were deposited using layer-by-layer (LbL) technique prior to coating Tenax TA polymer inside the µTCP chip. Here, the objective was to increase the surface-to-volume ratio (S/V) inside the µTCP chip. As a result, threefold increase in the adsorption capacity of the polymer was achieved. Selective binding of polar compounds to the SNP was also demonstrated. Moreover, in another study gold nanoparticle deposited using electroplating inside the µTCP were found to selectively capture widely used propofol compound. A comparatively simpler testing procedure was used to quantify propofol present in human breath sample eliminating the need for the separation stage.

Another contribution of this research was the development of a microfluidic chip for the extraction of volatile organic compounds (VOCs) from aqueous samples. The micro purge extractor (µPE) was fluidically integrated with the µGC modules and successfully extracted four compounds at 500 parts-per-billion concentration. Furthermore, micro discharge photo ionization detector (µDPID) was implemented in a silicon-glass architecture which provided excellent opportunity to monolithically integrate the detector with a separation column. As a result of this integration, the minimum detection limit of ~10pg was achieved. The detector response was also noted to be stable under flow and temperature programming conditions which provided rapid analysis of a wide range of compounds. In Chapter 7, an example of integrated µGC platform was demonstrated where sample injection, separation and detection were performed on a single 1.5 cm × 3 cm platform. The platform required an off-chip fluidic valve and helium as a carrier gas for the analysis. Each component of the µGC system was evaluated individually in addition to the complete integrated analytical system. The sample injection unit provided peak widths (σ) of ~200 ms and required a loading time in the order of just a few seconds. The detector response was found to be linear over four orders of magnitude. The complete µGC system separated and detected a wide variety of VOCs ranging from 110 ˚C - 216 ˚C in boiling points in less than a minute. Figure 8.1 further categorizes these key contributions in terms of adsorbent coatings, fabrication, chromatographic results and the development of fully automated zebra mini GC system.

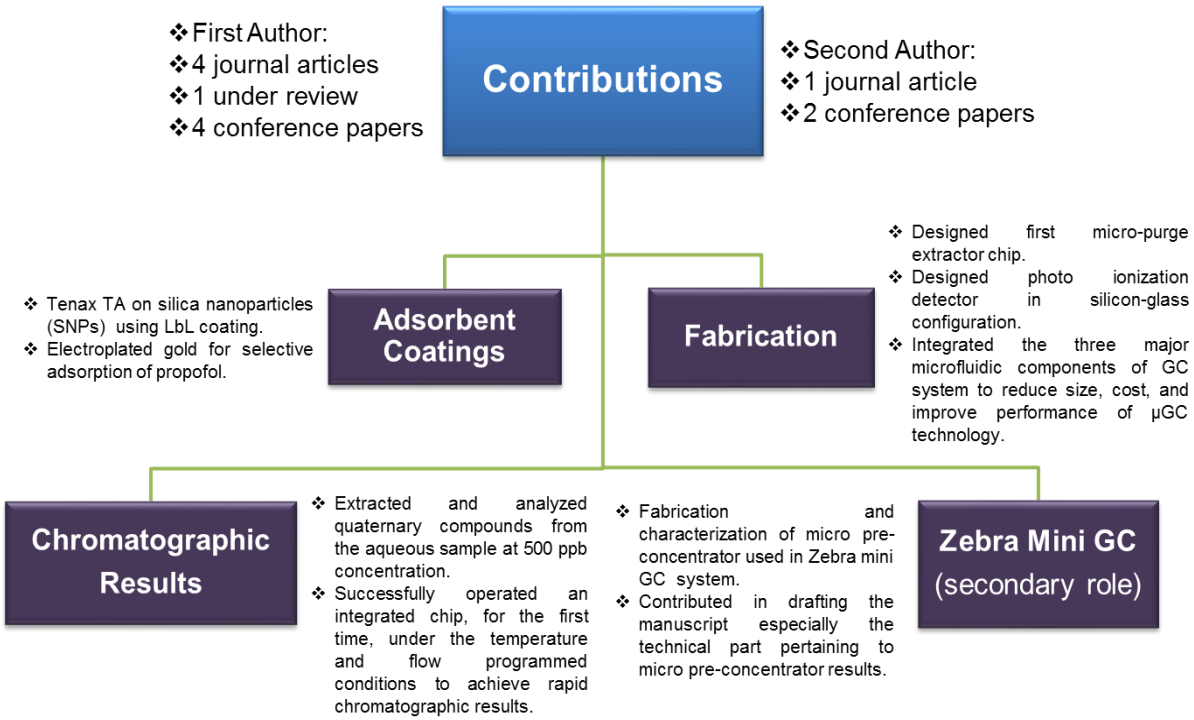

Figure 8.1 *A breakdown of contribution of this research into development of new adsorbent coatings, microfabrication techniques, chromatographic results and in the development of Zebra mini GC system.*

II. Summary of Publications

A. A Microfabricated Propofol Trap for Breath-Based Anesthesia Depth Monitoring (Chapter 2)

This publication demonstrates the selective chemical adsorption of a widely used anesthetic agent propofol (2,6-diisopropylphenol) present in the human breath sample on the surface of gold layer. The other species present in the sample are not adsorbed on the surface of gold. The fabricated silicon-glass chip is 12 mm on each side and consists of an array of high aspect ratio parabolic reflectors inside its 7 mm × 7 mm× 0.24 mm cavity. The interior surfaces of the chip are coated with an electroplated gold layer having a surface roughness of around 6.82 nm, which is an order of magnitude higher than a gold layer deposited through electron (e) beam evaporation. Our result indicates that uncoated and e-beam gold-coated chips are unable to adsorb propofol and other compounds found in human breath. In contrast, silicon-glass chips coated with Tenax TA (2,6-diphenylene oxide), a gas adsorbing polymer, captures propofol among other volatiles present in human breath. Only devices coated with an electroplated gold layer demonstrate selective affinity for the target compound propofol. The potential significance of the

chip in quantifying the propofol present in human breath samples without incorporating the gas chromatography column into the testing setup (resulting in faster analysis and reduced complexity) is also demonstrated.

B. Improved Performance of Micro-Fabricated Pre-concentrators using Silica Nanoparticles as a Surface Template (Chapter 3)

A new approach of enhancing the adsorption capability of the widely used polymer adsorbent Tenax TA poly (2,6-diphenylene oxide) through its deposition on a nano-structured template is reported. The modified Tenax TA-coated silica nanoparticles (SNP) are incorporated as an adsorbent bed in silicon based micro-thermal pre-concentrator (μTPC) chips with an array of square microposts embedded inside the cavity and sealed with a Pyrex cover. The interior surface of the chip is first modified by depositing SNP using a layer-by-layer self-assembly technique followed by coating with Tenax TA. The adsorption capacity of the SNP-Tenax TA μTPC is enhanced by as much as a factor of three compared to the one coated solely with thin film Tenax TA for the compounds tested. The increased adsorption ability of the Tenax TA is attributed to the higher surface area provided by the underlying porous SNP coating and the pores between SNPs affecting the morphology of deposited Tenax TA film by bringing nano-scale features into the polymer. In addition, the adsorption ability of the SNP coating as a pseudo-selective inorganic adsorption bed for polar compounds was also observed.

C. Purge and Trap Integrated MicroGC Platform for Chemical Identification in Aqueous Samples (Chapter 4)

The majority of current micro-scale gas chromatography (μGC) systems focus on air sampling to detect volatile organic compounds (VOCs). However, purging the VOCs from a water sample using microsystems is an unchartered territory. Various organic compounds used in everyday life find their way to water bodies. Some of these water organic compounds (WOCs) persist or degrade slowly, threatening not just human existence but also aquatic life. This article reports the first micro-purge extractor (μPE) chip and its integration with a micro-scale gas chromatography (μGC) system for the extraction and analysis of water organic compounds (WOCs) from aqueous samples. The 2 cm × 3 cm μPE chip contains two inlet and outlet ports and an etched cavity sealed with a Pyrex cover. The aqueous sample is introduced from the top inlet port while a pure inert gas is supplied from the side inlet to purge WOCs from the μPE chip. The outlets are assigned for draining water from the chip and for directing purged WOCs to the micro-thermal pre-concentrator (μTPC). The trapped compounds are desorbed from the μTPC by resistive heating using the on-chip heater and temperature sensor, are separated by a 2 m long, 80 μm wide, and 250 μm deep polydimethylsiloxane (OV-1) coated μGC separation column, and are

identified using a micro-thermal conductivity detector (μTCD) monolithically integrated with the column. The experimental results indicate that the combined system provides rapid chromatographic separation (<1.5 min) for quaternary WOCs namely toluene, tetrachloroethylene (PCE), chlorobenzene and ethylbenzene with minimum detection concentration of 500 parts-per-billion (ppb) in aqueous samples.

D. Zebra GC: A Mini Gas Chromatography System for Trace-Level Determination of Hazardous Air Pollutants (Chapter 5)

A ready-to-deploy implementation of a microfabricated gas chromatography (μGC) system characterized for detecting Hazardous Air Pollutants (HAPs) at parts-per-billion (ppb) concentrations in complex mixtures has been described. A microfabricated pre-concentrator (μPC), MEMS separation column with on-chip thermal conductivity detector (μSC-TCD), flow controller unit, and all necessary flow and thermal management as well as user interface circuitry are integrated to realize a fully functional μGC system. The work reports extensive characterization of μPC and μSC-TCD for target analytes: benzene, toluene, tetrachloroethylene, chlorobenzene, ethylbenzene, and p-xylene. A Limit of Detection (LOD) of ~1 ng was achieved, which corresponds to a sampling time of 10 min at a flow rate of 1 mL/min for an analyte present at ~25 ppbv. An innovative method using flow-manipulation generated sharp injection plugs from the μPC even in the presence of a flow-sensitive detector like a μTCD. The μGC system is compared against conventional Automated Thermal Desorption-Gas Chromatograph–Flame Ionization Detector (ATD GC-FID) system for real gasoline samples in simulated car refueling scenario. The μGC system detected five peaks, including three of the target analytes and required ~3 orders of magnitude lower sample volume as compared to the conventional system.

E. GC-on-Chip: Integrated Column and Photo Ionization Detector (Chapter 6)

This paper published in Lab on a Chip, reports a unique GC-on-chip module comprising monolithically integrated semi-packed micro separation column (μSC) and a highly sensitive micro helium discharge photo ionization detector (μDPID). While semi-packed μSC with atomic layer deposited (ALD) alumina as a stationary phase provides high separation performance, the μDPID implemented for the first time in a silicon-glass architecture inherits the desirable features of being universal, non-destructive, low power (1.4 mW), and quick response. The integrated chip is 1.5 cm × 3 cm in size and requires two-mask fabrication process. The monolithic integration alleviates the need for transfer lines between the column and the detector which improves the performance of the individual components with overall reduced fabrication and implementation costs. The chip is capable of operating under the isothermal as well as the temperature and flow programming conditions to achieve rapid chromatographic analysis. The chip performance was investigated with two samples: 1) a multi-analyte

gas mixture consisting of eight compounds ranging from 98 ˚C-174 ˚C in boiling point and 2) a mixture containing the higher alkanes (C9-C12). Our experiments indicate that the chip is capable of providing rapid chromatographic separation and detection of these compounds (<1min) through the optimization of flow and temperature programming conditions. The GC-on-chip demonstrated a minimum detection limit of ~10pg which is on par with the widely used destructive flame ionization detector (FID).

F. Chip-Scale Gas Chromatography: From Injection Through Detection (Chapter 7)

Here, we have utilized microfabrication technology to demonstrate, for the first time, the single chip integration of the key components of a μGC system in a simple two step fabrication process. The 1.5 cm × 3 cm microfluidic platform includes a sample injection unit, a micro machined semi-packed separation column (μSC) and a micro helium discharge photoionization detector (μDPID). The sample injection unit consists of a T-shaped channel operated with an equally simple setup involving a single 3-way fluidic valve, a micro-pump for sample loading and a carrier gas supply for subsequent analysis of the VOCs. The innovative sample injection technique described herein requires the loading time of a few seconds duration and produces very sharp and repeatable sample pulses (full-width-at-half-maximum ~ 200 ms) at the carrier gas flow rate compatible with efficient chromatographic separations. Furthermore, our comprehensive characterization of the chip reveals that a wide variety of VOCs ranging from 110 ˚C - 216 ˚C in boiling points can be analysed quickly (<1 min) through optimization of flow and temperature programming conditions. Moreover, the analysis of four VOCs at the concentration level of 1 parts-per-million in aqueous sample (which corresponds to the headspace concentration in lower ppb regime) was performed in a rapid manner requiring only 6 s of sampling time. The μDPID has demonstrated a linear dynamic range of four orders of magnitude and minimum detection limit of ~10pg which is comparable to the widely used flame ionization detector (FID).

III. Future Outlook

The purpose of this research was focused on the development of a truly compact μGC system. Although improvements were made on both component and integrated μGC level, there is still plenty of room for the improvement. In Chapter 3, the selective adsorption of polar compounds by SNP were attributed to the presence of hydroxyl sites on the silica surface. In future, different functionalized nanoparticles could be deposited inside μTCP to provide a unique opportunity for the selective adsorption of the species of interest. Furthermore, in Chapter 4, modifying the design of the μPE chip and integrating temperature programming ability on the μPE chip could increase the recovery of water organic compounds (WOCs). In addition to the overall chip size, the design parameters including the location of the inlets and outlets, the configuration of the fluidic ports (distributed versus single) and their widths, and the inclusion of pillars and their associated shapes and arrangements could be thoroughly studied to

improve the recovery of WOCs. Similarly, in Chapter 6 the fact that the bias voltage can increase the signal level provides excellent opportunity to improve the detector's LOD which can be realized through the modifications in the design and location of the bias electrode. The influence of the distance between the discharge and the outlet of the μSC and the size of the collector volume on the detector performance should be considered as well. A chip-scale GC platform was discussed in Chapter 7. The platform was operated with an off-chip fluidic valve and helium carrier gas supply. The operation of the μDPID using air as a carrier gas will be considered a major advancement in this regard. It will eliminate the reliance on helium carrier gas bringing down the overall operational cost of the system. In addition, the on-chip integration of a miniaturized valve and pump with chip-scale GC platform will fulfill the dream of a truly autonomous μGC system.

References

[1] K. D. Wise, "Integrated sensors, MEMS, and microsystems: Reflections on a fantastic voyage," *Sensors and Actuators A: Physical*, vol. 136, pp. 39-50, 2007.

[2] H. K. L. Chan, S. W. Pang, R. A. Veeneman, E. T. Zellers, and M. Takei, "Microfabricated preconcentrator for quantitative analysis of low concentration volatile organic compounds," *The 13th International Conference on Solid-State Sensors, Actuators and Microsystems, TRANSDUCERS '05.*, vol. 2, pp. 2091-2094, 2005.

[3] I. Gràcia, P. Ivanov, F. Blanco, N. Sabaté, X. Vilanova, X. Correig, *et al.*, "Sub-ppm gas sensor detection via spiral μ-preconcentrator," *Sensors and Actuators B: Chemical*, vol. 132, pp. 149-154, 2008.

[4] W.-C. Tian, H. K. L. Chan, L. Chia-Jung, S. W. Pang, and E. T. Zellers, "Multiple-stage microfabricated preconcentrator-focuser for micro gas chromatography system," *Microelectromechanical Systems, Journal of*, vol. 14, pp. 498-507, 2005.

[5] T. Wei-Cheng, S. W. Pang, L. Chia-Jung, and E. T. Zellers, "Microfabricated preconcentrator-focuser for a microscale gas chromatograph," *Microelectromechanical Systems, Journal of*, vol. 12, pp. 264-272, 2003.

[6] A. B. Alamin Dow and W. Lang, "A micromachined preconcentrator for ethylene monitoring system," *Sensors and Actuators B: Chemical*, vol. 151, pp. 304-307, 2010.

[7] E. H. M. Camara, P. Breuil, D. Briand, N. F. de Rooij, and C. Pijolat, "A micro gas preconcentrator with improved performance for pollution monitoring and explosives detection," *Analytica Chimica Acta*, vol. 688, pp. 175-182, 2011.

[8] A. Rydosz, W. Maziarz, T. Pisarkiewicz, K. Domański, and P. Grabiec, "A gas micropreconcentrator for low level acetone measurements," *Microelectronics Reliability*.

[9] H. Vereb, B. Alfeeli, A. Dietrich, and M. Agah, "Using MEMS-based preconcentrators to identify iron catalyzed lipid oxidation products in breath," *IEEE Sensors*, pp. 1237-1240, 2011.

[10] M. Kim and S. Mitra, "A microfabricated microconcentrator for sensors and gas chromatography," *Journal of Chromatography A*, vol. 996, pp. 1-11, 2003.

[11] E. W. Simoes, S. G. de Souza, M. L. P. da Silva, R. Furlan, and H. E. Maldonado Peres, "Study of preconcentration of non-polar compounds in microchannels with constrictions," *Sensors and Actuators B: Chemical*, vol. 115, pp. 232-239, 2006.

[12] I. Voiculescu, R. A. McGill, M. E. Zaghloul, D. Mott, J. Stepnowski, S. Stepnowski, *et al.*, "Micropreconcentrator for Enhanced Trace Detection of Explosives and Chemical Agents," *IEEE Sensors Journal*, vol. 6, pp. 1094-1104, 2006.

[13] C. E. Davis, C. K. Ho, R. C. Hughes, and M. L. Thomas, "Enhanced detection of m-xylene using a preconcentrator with a chemiresistor sensor," *Sensors and Actuators B: Chemical*, vol. 104, pp. 207-216, 2005.

[14] G. C. Frye-Mason, R. P. Manginell, E. J. Heller, C. M. Matzke, S. A. Casalnuovo, V. M. Hietala, *et al.*, "Microfabricated gas phase chemical analysis systems," *International Microprocesses and Nanotechnology Conference, Microprocesses and Nanotechnology '99.*, pp. 60-61, 1999.

[15] M. Martin, M. Crain, K. Walsh, R. A. McGill, E. Houser, J. Stepnowski, *et al.*, "Microfabricated vapor preconcentrator for portable ion mobility spectroscopy," *Sensors and Actuators B: Chemical*, vol. 126, pp. 447-454, 2007.

[16] P. R. Lewis, P. Manginell, D. R. Adkins, R. J. Kottenstette, D. R. Wheeler, S. S. Sokolowski, *et al.*, "Recent advancements in the gas-phase MicroChemLab," *Sensors Journal, IEEE*, vol. 6, pp. 784-795, 2006.

[17] B. Bae, J. Yeom, A. D. Radadia, R. I. Masel, and M. A. Shannon, "A fully-integrated MEMS preconcentrator for rapid gas sampling," *Transducers '07 & Eurosensors Xxi, Digest of Technical Papers, Vols 1 and 2*, pp. U757-U758, 2007.

[18] B. Alfeeli and M. Agah, "Toward Handheld Diagnostics of Cancer Biomarkers in Breath: Micro Preconcentration of Trace Levels of Volatiles in Human Breath," *IEEE Sensors Journal,* vol. 11, pp. 2756-62, 2011.

[19] B. Alfeeli and M. Agah, "Low Pressure Drop Micro Preconcentrators with a Cobweb Tenax-TA Film," in *Solid-State sensors, Actuators and Microsystems Workshop*, Hilton Head, SC, 2010, pp. 166-169.

[20] B. Alfeeli, D. Cho, M. Ashraf-Khorassani, L. T. Taylor, and M. Agah, "MEMS-based multi-inlet/outlet preconcentrator coated by inkjet printing of polymer adsorbents," *Sensors and Actuators B: Chemical,* vol. 133, pp. 24-32, 2008.

[21] B. Alfeeli and M. Agah, "Micro preconcentrator with embedded 3D pillars for breath analysis applications," Piscataway, NJ, USA, 2008, pp. 736-9.

[22] R. L. Grob and E. F. Barry, *Modern Practice of Gas Chromatography*, 4th ed. Hoboken, NJ: Wiley-Interscience, 2004.

[23] R. Ghijsen, H. Poppe, J. Kraak, and P. Duysters, "The Mass Loadability of Various Stationary Phases in Gas Chromatography," *Chromatographia,* vol. 27, pp. 60-66, Jan. 1989.

[24] S. Ali, M. Ashraf-Khorassani, L. T. Taylor, and M. Agah, "MEMS-based semi-packed gas chromatography columns," *Sensors and Actuators B: Chemical,* vol. 141, pp. 309-315, 2009.

[25] J. Sun, D. Cui, X. Chen, L. Zhang, H. Cai, and H. Li, "Fabrication and characterization of microelectromechanical systems-based gas chromatography column with embedded micro-posts for separation of environmental carcinogens," *Journal of Chromatography A,* vol. 1291, pp. 122-128, 2013.

[26] H. Shakeel and M. Agah, "Self-Patterned Gold-Electroplated Multicapillary Gas Separation Columns With MPG Stationary Phases," *Journal of Microelectromechanical Systems,* vol. 22, pp. 62-70, 2013.

[27] B. Alfeeli, S. Narayanan, D. Moodie, P. Zellner, M. McMillan, D. Hirtenstein, *et al.*, "Interchannel Mixing Minimization in Semi-Packed Micro Gas Chromatography Columns," *Sensors Journal, IEEE,* vol. 13, pp. 4312-4319, 2013.

[28] M. A. Zareian-Jahromi and M. Agah, "Microfabricated Gas Chromatography Columns With Monolayer-Protected Gold Stationary Phases," *Journal of Microelectromechanical Systems,* vol. 19, pp. 294-304, 2010.

[29] M. A. Zareian-Jahromi, M. Ashraf-Khorassani, L. T. Taylor, and M. Agah, "Design, modeling, and fabrication of MEMS-based multicapillary gas chromatographic columns," *Microelectromechanical Systems, Journal of,* vol. 18, pp. 28-37, 2009.

[30] J. Sun, D. Cui, F. Guan, X. Chen, and L. Zhang, "High resolution microfabricated gas chromatography column with porous silicon acting as support," *Sensors and Actuators B: Chemical,* vol. 201, pp. 19-24, 10/1/ 2014.

[31] R. Haudebourg, J. Vial, D. Thiebaut, K. Danaie, J. Breviere, P. Sassiat, *et al.*, "Temperature-Programmed Sputtered Micromachined Gas Chromatography Columns: An Approach to Fast Separations in Oilfield Applications," *Analytical chemistry,* vol. 85, pp. 114-120, 2012.

[32] J. Vial, D. Thiébaut, F. Marty, P. Guibal, R. Haudebourg, K. Nachef, *et al.*, "Silica sputtering as a novel collective stationary phase deposition for microelectromechanical system gas chromatography column: Feasibility and first separations," *Journal of Chromatography A,* vol. 1218, pp. 3262-3266, 2011.

[33] E. Covington, F. I. Bohrer, C. Xu, E. T. Zellers, and C. Kurdak, "Densely integrated array of chemiresistor vapor sensors with electron-beam patterned monolayer-protected gold nanoparticle interface films," *Lab on a Chip,* vol. 10, pp. 3058-3060, 2010.

[34] W. R. Collin, G. Serrano, L. K. Wright, H. Chang, N. Nuñovero, and E. T. Zellers, "Microfabricated Gas Chromatograph for Rapid, Trace-Level Determinations of Gas-Phase Explosive Marker Compounds," *Analytical Chemistry,* vol. 86, pp. 655-663, 2014.

[35] S. Zampolli, I. Elmi, J. Stürmann, S. Nicoletti, L. Dori, and G. C. Cardinali, "Selectivity enhancement of metal oxide gas sensors using a micromachined gas chromatographic column," *Sensors and Actuators B: Chemical,* vol. 105, pp. 400-406, 2005.

[36] P. R. Lewis, R. P. Manginell, D. R. Adkins, R. J. Kottenstette, D. R. Wheeler, S. S. Sokolowski, *et al.*, "Recent advancements in the gas-phase MicroChemLab," *Sensors Journal, IEEE,* vol. 6, pp. 784-795, 2006.

[37] D. M. Wilson, S. Hoyt, J. Janata, K. Booksh, and L. Obando, "Chemical sensors for portable, handheld field instruments," *Sensors Journal, IEEE,* vol. 1, pp. 256-274, 2001.

[38] J. Xie, H. Wang, and M. Duan, "QCM chemical sensor based on ZnO colloid spheres for the alcohols," *Sensors and Actuators B: Chemical,* vol. 203, pp. 239-244, 2014.

[39] J. H. Seo, J. Liu, X. Fan, and K. Kurabayashi, "Fabry-Pérot cavity sensor-based optofluidic gas chromatography using a microfabricated passive preconcentrator/injector," *Lab on a Chip,* vol. 13, pp. 851-859, 2013.

[40] K. Scholten, X. Fan, and E. T. Zellers, "A microfabricated optofluidic ring resonator for sensitive, high-speed detection of volatile organic compounds," *Lab on a Chip,* vol. 14, pp. 3873-3880, 2014.

[41] Y. Sun, J. Liu, D. J. Howard, G. Frye-Mason, A. K. Thompson, S.-j. Ja, *et al.*, "Rapid tandem-column micro-gas chromatography based on optofluidic ring resonators with multi-point on-column detection," *Analyst,* vol. 135, pp. 165-171, 2010.

[42] K. Reddy, Y. Guo, J. Liu, W. Lee, M. K. K. Oo, and X. Fan, "On-chip Fabry–Pérot interferometric sensors for micro-gas chromatography detection," *Sensors and Actuators B: Chemical,* vol. 159, pp. 60-65, 2011.

[43] K. Reddy, Y. Guo, J. Liu, W. Lee, M. K. K. Oo, and X. Fan, "Rapid, sensitive, and multiplexed on-chip optical sensors for micro-gas chromatography," *Lab on a Chip,* vol. 12, pp. 901-905, 2012.

[44] S. C. Terry, J. H. Jerman, and J. B. Angell, "A gas chromatographic air analyzer fabricated on a silicon wafer," *Electron Devices, IEEE Transactions on,* vol. 26, pp. 1880-1886, 1979.

[45] R. R. Reston and E. S. Kolesar, "Silicon-micromachined gas chromatography system used to separate and detect ammonia and nitrogen dioxide. I. Design, fabrication, and integration of the gas chromatography system," *Microelectromechanical Systems, Journal of,* vol. 3, pp. 134-146, 1994.

[46] S. Narayanan and M. Agah, "Fabrication and Characterization of a Suspended TCD Integrated With a Gas Separation Column," *Microelectromechanical Systems, Journal of,* vol. 22, pp. 1166-1173, 2013.

[47] S. Narayanan, B. Alfeeli, and M. Agah, "Two-port static coated micro gas chromatography column with an embedded thermal conductivity detector," *Sensors Journal, IEEE,* vol. 12, pp. 1893-1900, 2012.

[48] S. Zimmermann, P. Krippner, A. Vogel, and J. Müller, "Miniaturized flame ionization detector for gas chromatography," *Sensors and Actuators B: Chemical,* vol. 83, pp. 285-289, 2002.

[49] A. Bulbul and H. Kim, "A bubble-based microfluidic gas sensor for gas chromatographs," *Lab on a Chip,* 2015.

[50] S. Narayanan, G. Rice, and M. Agah, "A micro-discharge photoionization detector for micro-gas chromatography," *Microchimica Acta,* vol. 181, pp. 493-499, 2014.

[51] A. Manz, Y. Miyahara, J. Miura, Y. Watanabe, H. Miyagi, and K. Sato, "Design of an open-tubular column liquid chromatograph using silicon chip technology," *Sensors and actuators B: Chemical,* vol. 1, pp. 249-255, 1990.

[52] S. Shoji, M. Esashi, and T. Matsuo, "Prototype miniature blood gas analyser fabricated on a silicon wafer," *Sensors and Actuators,* vol. 14, pp. 101-107, 1988.

[53] H. Van Lintel, F. Van de Pol, and S. Bouwstra, "A piezoelectric micropump based on micromachining of silicon," *Sensors and actuators,* vol. 15, pp. 153-167, 1988.

[54] V. Gass, B. Van Der Schoot, S. Jeanneret, and N. De Rooij, "Integrated flow-regulated silicon micropump," *Sensors and Actuators A: Physical*, vol. 43, pp. 335-338, 1994.

[55] G. C. Frye-Mason, R. J. Kottenstette, E. J. Heller, C. M. Matzke, S. A. Casalnuovo, P. R. Lewis, *et al.*, "Integrated chemical analysis systems for gas phase CW agent detection," in *Micro Total Analysis Systems' 98*, 1998, pp. 477-481.

[56] R. P. Manginell, J. M. Bauer, M. W. Moorman, L. J. Sanchez, J. M. Anderson, J. J. Whiting, *et al.*, "A monolithically-integrated μGC chemical sensor system," *Sensors*, vol. 11, pp. 6517-6532, 2011.

[57] M. Agah and K. D. Wise, "Low-mass PECVD oxynitride gas chromatographic columns," *Microelectromechanical Systems, Journal of*, vol. 16, pp. 853-860, 2007.

[58] E. T. Zellers, S. A. Batterman, M. Han, and S. J. Patrash, "Optimal coating selection for the analysis of organic vapor mixtures with polymer-coated surface acoustic wave sensor arrays," *Analytical chemistry*, vol. 67, pp. 1092-1106, 1995.

[59] Q.-Y. Cai and E. T. Zellers, "Dual-chemiresistor GC detector employing monolayer-protected metal nanocluster interfaces," *Analytical chemistry*, vol. 74, pp. 3533-3539, 2002.

[60] W.-C. Tian, S. W. Pang, C.-J. Lu, and E. T. Zellers, "Microfabricated preconcentrator-focuser for a microscale gas chromatograph," *Microelectromechanical Systems, Journal of*, vol. 12, pp. 264-272, 2003.

[61] T. Sukaew, H. Chang, G. Serrano, and E. T. Zellers, "Multi-stage preconcentrator/focuser module designed to enable trace level determinations of trichloroethylene in indoor air with a microfabricated gas chromatograph," *Analyst*, vol. 136, pp. 1664-1674, 2011.

[62] G. Serrano, S. M. Reidy, and E. T. Zellers, "Assessing the reliability of wall-coated microfabricated gas chromatographic separation columns," *Sensors and Actuators B: Chemical*, vol. 141, pp. 217-226, 2009.

[63] C.-J. Lu, W. H. Steinecker, W.-C. Tian, M. C. Oborny, J. M. Nichols, M. Agah, *et al.*, "First-generation hybrid MEMS gas chromatograph," *Lab on a Chip*, vol. 5, pp. 1123-1131, 2005.

[64] W. R. Collin, G. Serrano, L. K. Wright, H. Chang, N. Nuñovero, and E. T. Zellers, "Microfabricated gas chromatograph for rapid, trace-level determinations of gas-phase explosive marker compounds," *Analytical chemistry*, vol. 86, pp. 655-663, 2013.

[65] E. Zellers, W. Steinecker, G. Lambertus, M. Agah, C. Lu, H. Chan, *et al.*, "A versatile MEMS gas chromatograph for environmental vapor mixture analysis," in *Proceedings of the Solid State Sensor, Actuator and Microsystems Workshop (Hilton Head), Hilton Head Island, SC*, 2004, pp. 61-66.

[66] S. Kim, H. Chang, and E. Zellers, "Prototype micro gas chromatograph for breath biomarkers of respiratory disease," in *Solid-State Sensors, Actuators and Microsystems Conference, 2009. TRANSDUCERS 2009. International*, 2009, pp. 128-131.

[67] S. Zampolli, I. Elmi, F. Mancarella, P. Betti, E. Dalcanale, G. Cardinali, *et al.*, "Real-time monitoring of sub-ppb concentrations of aromatic volatiles with a MEMS-enabled miniaturized gas-chromatograph," *Sensors and Actuators B: Chemical*, vol. 141, pp. 322-328, 2009.

[68] M. Nakamura, Y. Sanjo, and K. Ikeda, "Predicted sevoflurane partial pressure in the brain with an uptake and distribution model: Comparison with the measured value in internal jugular vein blood," *Journal of clinical monitoring and computing*, vol. 15, pp. 299-305, 1999.

[69] J. B. Cooper, R. S. Newbower, and R. J. Kitz, "An Analysis of Major Errors and Equipment Failures in Anesthesia Management: Considerations for," *Anesthesiology*, vol. 60, pp. 34-42, 1984.

[70] C. C. Natalini, "Sevoflurane, Desflurane, and Xenon new inhaled anesthetics in veterinary medicine," *Ciência Rural*, vol. 31, pp. 177-183, 2001.

[71] L. S. Rasmussen and J. T. Moller, "Central nervous system dysfunction after anesthesia in the geriatric patient," *Anesthesiology Clinics of North America*, vol. 18, pp. 59-70, 2000.

[72] B. Saniova, M. Drobny, and M. Sulaj, "Delirium and postoperative cognitive dysfunction after general anesthesia," *Medical Science and Technology*, vol. 15, pp. CS81-CS87, 2009.

[73] J. H. Silverstein, M. Timberger, D. L. Reich, and S. Uysal, "Central nervous system dysfunction after noncardiac surgery and anesthesia in the elderly," *Anesthesiology,* vol. 106, p. 622, 2007.

[74] B. Alfeeli and M. Agah, "MEMS-based selective preconcentration of trace level breath analytes," *Sensors Journal, IEEE,* vol. 9, pp. 1068-1075, 2009.

[75] H. Kaul and N. Bharti, "Monitoring depth of anaesthesia," *Indian J Anaesth,* vol. 46, pp. 323-332, 2002.

[76] H. Adam, E. Douglas, G. Plummer, and M. Cosgrove, "Estimation of ICI 35,868 (Diprivan R) in blood by high-performance liquid chromatography, following coupling with Gibbs' reagent," *Journal of Chromatography B: Biomedical Sciences and Applications,* vol. 223, pp. 232-237, 1981.

[77] H.-Y. Yu and J.-K. Liau, "Quantitation of propofol in plasma by capillary gas chromatography," *Journal of Chromatography B: Biomedical Sciences and Applications,* vol. 615, pp. 77-81, 1993.

[78] S.-Z. Fan, H.-Y. Yu, Y.-L. Chen, and C.-C. Liu, "Propofol concentration monitoring in plasma or whole blood by gas chromatography and high-performance liquid chromatography," *Anesthesia & Analgesia,* vol. 81, pp. 175-178, 1995.

[79] T. Kirkpatrick, I. Cockshott, E. Douglas, and W. Nimmo, "Pharmacokinetics of propofol (diprivan) in elderly patients," *British Journal of Anaesthesia,* vol. 60, pp. 146-150, 1988.

[80] P. Favetta, C. S. Degoute, J. P. Perdrix, C. Dufresne, R. Boulieu, and J. Guitton, "Propofol metabolites in man following propofol induction and maintenance," *British Journal of Anaesthesia,* vol. 88, pp. 653-658, 2002.

[81] P. Simons, I. Cockshott, E. Douglas, E. Gordon, K. Hopkins, and M. Rowland, "Disposition in male volunteers of a subanaesthetic intravenous dose of an oil in water emulsion of 14C-propofol," *Xenobiotica,* vol. 18, pp. 429-440, 1988.

[82] A. G. Doufas, N. Morioka, A. N. Mahgoub, A. R. Bjorksten, S. L. Shafer, and D. I. Sessler, "Automated responsiveness monitor to titrate propofol sedation," *Anesthesia & Analgesia,* vol. 109, pp. 778-786, 2009.

[83] H. Iwakiri, N. Nishihara, O. Nagata, T. Matsukawa, M. Ozaki, and D. I. Sessler, "Individual effect-site concentrations of propofol are similar at loss of consciousness and at awakening," *Anesthesia and analgesia,* vol. 100, p. 107, 2005.

[84] F. Bennett, D. Landry, and N. Oriol, "Analysis of heart rate dynamics during spinal and epidural anesthesia," in *Computers in Cardiology 1992, Proceedings of,* 1992, pp. 467-470.

[85] T. N. Spackman, M. D. Abel, and T. T. Schlegel, "Twelve-lead high-frequency QRS electrocardiography during anesthesia in healthy subjects," *Anesthesia & Analgesia,* vol. 100, pp. 1043-1047, 2005.

[86] M. Grossherr, A. Hengstenberg, T. Meier, L. Dibbelt, K. Gerlach, and H. Gehring, "Discontinuous monitoring of propofol concentrations in expired alveolar gas and in arterial and venous plasma during artificial ventilation," *Anesthesiology,* vol. 104, pp. 786-790, 2006.

[87] M. Grossherr, A. Hengstenberg, T. Meier, L. Dibbelt, B. Igl, A. Ziegler, *et al.*, "Propofol concentration in exhaled air and arterial plasma in mechanically ventilated patients undergoing cardiac surgery," *British journal of anaesthesia,* p. aep053, 2009.

[88] C. Hornuss, S. Praun, J. Villinger, A. Dornauer, P. Moehnle, M. Dolch, *et al.*, "Real-time monitoring of propofol in expired air in humans undergoing total intravenous anesthesia," *Anesthesiology,* vol. 106, pp. 665-674, 2007.

[89] A. Takita, K. Masui, and T. Kazama, "On-line monitoring of end-tidal propofol concentration in anesthetized patients," *Anesthesiology,* vol. 106, pp. 659-664, 2007.

[90] D. Helmig, "Air analysis by gas chromatography," *Journal of chromatography A,* vol. 843, pp. 129-146, 1999.

[91] A. Hengstenberg, M. Grossherr, T. Meier, and H. Gehring, "Breath analysis and artificial ventilation: Chemical identification and classification of volatile substances in exhaled breath during IV anesthesia," *Anesthesiology,* vol. 103, p. A808, 2005.

[92] W. Miekisch, P. Fuchs, S. Kamysek, C. Neumann, and J. K. Schubert, "Assessment of propofol concentrations in human breath and blood by means of HS-SPME–GC–MS," *Clinica chimica acta,* vol. 395, pp. 32-37, 2008.

[93] K. Schwarz, W. Filipiak, and A. Amann, "Determining concentration patterns of volatile compounds in exhaled breath by PTR-MS," *Journal of Breath Research,* vol. 3, p. 027002, 2009.

[94] B. Alfeeli, H. Vereb, A. Dietrich, and M. Agah, "Low pressure drop micro preconcentrators with cobweb Tenax-TA film for analysis of human breath," in *Micro Electro Mechanical Systems (MEMS), 2011 IEEE 24th International Conference on*, 2011, pp. 916-919.

[95] M. A. Zareian-Jahromi and M. Agah, "Microfabricated gas chromatography columns with monolayer-protected gold stationary phases," *Microelectromechanical Systems, Journal of,* vol. 19, pp. 294-304, 2010.

[96] M. Basanta, R. M. Jarvis, Y. Xu, G. Blackburn, R. Tal-Singer, A. Woodcock, *et al.*, "Non-invasive metabolomic analysis of breath using differential mobility spectrometry in patients with chronic obstructive pulmonary disease and healthy smokers," *Analyst,* vol. 135, pp. 315-320, 2010.

[97] R. A. Glaser, J. E. Arnold, and S. A. Shulman, "Direct sampling of organic solvents in expired breath with a new solid sorbent sampling device," *Scandinavian journal of work, environment & health,* pp. 63-65, 1988.

[98] M. M. Steeghs, S. M. Cristescu, and F. J. Harren, "The suitability of Tedlar bags for breath sampling in medical diagnostic research," *Physiological measurement,* vol. 28, p. 73, 2007.

[99] Y. Gong, E. Li, G. Xu, H. Wang, C. Wang, P. Li, *et al.*, "Investigation of Propofol Concentrations in Human Breath by Solid-Phase Microextraction Gas Chromatography–Mass Spectrometry," *Journal of International Medical Research,* vol. 37, pp. 1465-1471, 2009.

[100] T. Laurila, T. Sorvajärvi, J. Saarela, J. Toivonen, D. W. Wheeler, L. Ciaffoni, *et al.*, "Optical detection of the anesthetic agent propofol in the gas phase," *Analytical chemistry,* vol. 83, pp. 3963-3967, 2011.

[101] S. Baeck, T. Jaramillo, and E. McFarland, "Influence of composition and morphology on photo and electrocatalytic activity of electrodeposited Pt/WO3," *Pulse,* vol. 1, p. 17.4, 2002.

[102] G. H. A. Therese and P. V. Kamath, "Electrochemical synthesis of metal oxides and hydroxides," *Chemistry of materials,* vol. 12, pp. 1195-1204, 2000.

[103] A. Petrossians, J. J. Whalen III, J. D. Weiland, and F. Mansfeld, "Surface modification of neural stimulating/recording electrodes with high surface area platinum-iridium alloy coatings," in *Engineering in Medicine and Biology Society, EMBC, 2011 Annual International Conference of the IEEE*, 2011, pp. 3001-3004.

[104] M. Inagaki, M. Sunahara, A. Shindo, V. Vignal, and H. Konno, "Effect of oxygen plasma treatment on gas adsorption behavior and surface structure of carbon spheres derived from phenol resin," *Journal of materials research,* vol. 14, pp. 3208-3210, 1999.

[105] H. J. Lee, W. Cho, S. Jung, and M. Oh, "Morphology-selective formation and morphology-dependent gas-adsorption properties of coordination polymer particles," *Adv. Mater,* vol. 21, pp. 674-677, 2009.

[106] C. Liu, J. Shih, and Y. Ju, "Surface morphology and gas sensing characteristics of nickel phthalocyanine thin films," *Sensors and Actuators B: Chemical,* vol. 99, pp. 344-349, 2004.

[107] H. Oh and J.-J. Kim, "Influence of Surface Morphology on Adsorption Behavior in ZnO Nanowire Field-E ect Transistors," *Journal of the Korean Physical Society,* vol. 54, 2009.

[108] C. Volzone, J. G. Thompson, A. Melnitchenko, J. Ortiga, and S. R. Palethorpe, "Selective gas adsorption by amorphous clay-mineral derivatives," *Clays and Clay Minerals,* vol. 47, pp. 647-657, 1999.

[109] B. Alfeeli, "Chemical micro preconcentrators development for micro gas chromatography systems," 2010.

[110] S. K. Kim, H. Chang, and E. T. Zellers, "Microfabricated gas chromatograph for the selective determination of trichloroethylene vapor at sub-parts-per-billion concentrations in complex mixtures," *Analytical chemistry*, vol. 83, pp. 7198-7206, 2011.

[111] J. H. Seo, S. K. Kim, E. T. Zellers, and K. Kurabayashi, "Microfabricated passive vapor preconcentrator/injector designed for microscale gas chromatography," *Lab on a chip*, vol. 12, pp. 717-724, 02/ 2012.

[112] J. H. Seo, J. Liu, X. Fan, and K. Kurabayashi, "Effect of thermal desorption kinetics on vapor injection peak irregularities by a microscale gas chromatography preconcentrator," *Analytical chemistry*, vol. 84, pp. 6336-6340, 2012.

[113] E. Camara, P. Breuil, D. Briand, N. De Rooij, and C. Pijolat, "A micro gas preconcentrator with improved performance for pollution monitoring and explosives detection," *Analytica chimica acta*, vol. 688, pp. 175-182, 2011.

[114] H. K. Chan, S. W. Pang, R. Veeneman, E. T. Zellers, and M. Takei, "Microfabricated preconcentrator for quantitative analysis of low concentration volatile organic compounds," in *Solid-State Sensors, Actuators and Microsystems, 2005. Digest of Technical Papers. TRANSDUCERS'05. The 13th International Conference on*, 2005, pp. 2091-2094.

[115] A. B. A. Dow and W. Lang, "A micromachined preconcentrator for ethylene monitoring system," *Sensors and Actuators B: Chemical*, vol. 151, pp. 304-307, 2010.

[116] A. Rydosz, W. Maziarz, T. Pisarkiewicz, K. Domański, and P. Grabiec, "A gas micropreconcentrator for low level acetone measurements," *Microelectronics Reliability*, vol. 52, pp. 2640-2646, 2012.

[117] W.-C. Tian, H. K. Chan, C.-J. Lu, S. W. Pang, and E. T. Zellers, "Multiple-stage microfabricated preconcentrator-focuser for micro gas chromatography system," *Microelectromechanical Systems, Journal of*, vol. 14, pp. 498-507, 2005.

[118] H. Vereb, B. Alfeeli, A. Dietrich, and M. Agah, "Using MEMS-based preconcentrators to identify iron catalyzed lipid oxidation products in breath," in *Sensors, 2011 IEEE*, 2011, pp. 1237-1240.

[119] C. Davis, C. Ho, R. Hughes, and M. Thomas, "Enhanced detection of m-xylene using a preconcentrator with a chemiresistor sensor," *Sensors and Actuators B: Chemical*, vol. 104, pp. 207-216, 2005.

[120] G. C. Frye-Mason, R. P. Manginell, E. J. Heller, C. M. Matzke, S. Casalnuovo, V. M. Hietala, *et al.*, "Microfabricated gas phase chemical analysis systems," in *Microprocesses and Nanotechnology Conference, 1999. Digest of Papers. Microprocesses and Nanotechnology'99. 1999 International*, 1999, pp. 60-61.

[121] M. Kim and S. Mitra, "A microfabricated microconcentrator for sensors andgas chromatography," *Journal of Chromatography A*, vol. 996, pp. 1-11, 2003.

[122] E. W. Simoes, S. G. De Souza, M. L. P. Da Silva, R. Furlan, and H. E. M. Peres, "Study of preconcentration of non-polar compounds in microchannels with constrictions," *Sensors and Actuators B: Chemical*, vol. 115, pp. 232-239, 2006.

[123] I. Voiculescu, R. A. McGill, M. E. Zaghloul, D. Mott, J. Stepnowski, S. Stepnowski, *et al.*, "Micropreconcentrator for enhanced trace detection of explosives and chemical agents," *Sensors Journal, IEEE*, vol. 6, pp. 1094-1104, 2006.

[124] M. Akbar and M. Agah, "A golden micro-trap for anesthetic depth monitoring using human breath samples," in *Micro Electro Mechanical Systems (MEMS), 2012 IEEE 25th International Conference on*, 2012, pp. 906-909.

[125] M. Akbar and M. Agah, "A microfabricated propofol trap for breath-based anesthesia depth monitoring," *Microelectromechanical Systems, Journal of*, vol. 22, pp. 443-451, 2013.

[126] B. Alfeeli and M. Agah, "Toward handheld diagnostics of cancer biomarkers in breath: Micro preconcentration of trace levels of volatiles in human breath," *Sensors Journal, IEEE*, vol. 11, pp. 2756-2762, 2011.

[127] R. Borusiewicz and J. Zięba-Palus, "Comparison of the effectiveness of Tenax TA® and Carbotrap 300® in concentration of flammable liquids compounds," *Journal of forensic sciences,* vol. 52, pp. 70-74, 2007.
[128] R. Brown and C. Purnell, "Collection and analysis of trace organic vapour pollutants in ambient atmospheres: The performace of a Tenax-GC adsorbent tube," *Journal of Chromatography A,* vol. 178, pp. 79-90, 1979.
[129] A. n. Kroupa, J. Dewulf, H. Van Langenhove, and I. Víden, "Breakthrough characteristics of volatile organic compounds in the− 10 to+ 170 C temperature range on Tenax TA determined by microtrap technology," *Journal of Chromatography A,* vol. 1038, pp. 215-223, 2004.
[130] I. Maier and M. Fieber, "Retention characteristics of volatile compounds on Tenax TA," *Journal of High Resolution Chromatography,* vol. 11, pp. 566-576, 1988.
[131] E. Pellizzari, J. Bunch, R. Berkley, and J. McRae, "Collection and analysis of trace organic vapor pollutants in ambient atmospheres. The performance of a Tenax GC cartridge sampler for hazardous vapors," *Analytical Letters,* vol. 9, pp. 45-63, 1976.
[132] M. Schneider and K.-U. Goss, "Systematic investigation of the sorption properties of Tenax TA, Chromosorb 106, Porapak N, and Carbopak F," *Analytical chemistry,* vol. 81, pp. 3017-3021, 2009.
[133] S. Seshadri and J. W. Bozzelli, "Collection of vapors of selected chlorocarbons and benzene on Tenax GC," *Chemosphere,* vol. 12, pp. 809-820, 1983.
[134] V. Simon, M.-L. Riba, A. Waldhart, and L. Torres, "Breakthrough volume of monoterpenes on Tenax TA: influence of temperature and concentration for α-pinene," *Journal of chromatography A,* vol. 704, pp. 465-471, 1995.
[135] K. Ventura, M. Dostal, and J. Churáček, "Retention characteristics of some volatile compounds on Tenax GR," *Journal of Chromatography A,* vol. 642, pp. 379-382, 1993.
[136] A. Alentiev, E. Drioli, M. Gokzhaev, G. Golemme, O. Ilinich, A. Lapkin, *et al.*, "Gas permeation properties of phenylene oxide polymers," *Journal of membrane science,* vol. 138, pp. 99-107, 1998.
[137] K. Sakodynskii, L. Panina, and N. Klinskaya, "A study of some properties of Tenax, a porous polymer sorbent," *Chromatographia,* vol. 7, pp. 339-344, 1974.
[138] D. Zhao and J. J. Pignatello, "Model-aided characterization of Tenax®-ta for aromatic compound uptake from water," *Environmental toxicology and chemistry,* vol. 23, pp. 1592-1599, 2004.
[139] B. Alfeeli, V. Jain, R. K. Johnson, F. L. Beyer, J. R. Heflin, and M. Agah, "Characterization of poly (2, 6-diphenyl-p-phenylene oxide) films as adsorbent for microfabricated preconcentrators," *Microchemical Journal,* vol. 98, pp. 240-245, 2011.
[140] B. Alfeeli, L. T. Taylor, and M. Agah, "Evaluation of Tenax TA thin films as adsorbent material for micro preconcentration applications," *Microchemical Journal,* vol. 95, pp. 259-267, 2010.
[141] D. Wang, H. Shakeel, J. Lovette, G. W. Rice, J. R. Heflin, and M. Agah, "Highly stable surface functionalization of Microgas chromatography columns using layer-by-layer self-assembly of silica nanoparticles," *Analytical chemistry,* vol. 85, pp. 8135-8141, 2013.
[142] G. Decher, "Fuzzy nanoassemblies: toward layered polymeric multicomposites," *science,* vol. 277, pp. 1232-1237, 1997.
[143] E. Camara, P. Breuil, D. Briand, L. Guillot, C. Pijolat, and N. de Rooij, "Micro gas preconcentrator in porous silicon filled with a carbon absorbent," *Sensors and Actuators B: Chemical,* vol. 148, pp. 610-619, 2010.
[144] H. Föll, M. Christophersen, J. Carstensen, and G. Hasse, "Formation and application of porous silicon," *Materials Science and Engineering: R: Reports,* vol. 39, pp. 93-141, 2002.
[145] S. Xu, S. Hartvickson, and J. X. Zhao, "Increasing surface area of silica nanoparticles with a rough surface," *ACS applied materials & interfaces,* vol. 3, pp. 1865-1872, 2011.
[146] U. E. OSWER., "Draft Guidance for Evaluating the Vapor Intrusion to Indoor Air Pathway from Groundwater and Soils (Subsurface Vapor Intrusion Guidance)," ed: US Environmental Protection Agency, 2002.

[147] K. S. Betts, "Brain Drain? PBDEs Alter Development of Human Brain Cells," *Environmental Health Perspectives,* vol. 118, 2010.
[148] P. Burkhardt-Holm, T. Wahli, and W. Meier, "Nonylphenol affects the granulation pattern of epidermal mucous cells in rainbow trout, Oncorhynchus mykiss," *Ecotoxicology and environmental safety,* vol. 46, pp. 34-40, 2000.
[149] P. A. Jones, V. A. Baker, A. J. E. Irwin, and L. K. Earl, "Interpretation of the in Vitro Proliferation Response of MCF-7 Cells to Potential Oestrogens and Non-Oestrogenic Substances," *Toxicology in Vitro,* vol. 12, pp. 373-382, 8// 1998.
[150] T. Nishihara, J. Nishikawa, T. Kanayama, F. Dakeyama, K. Saito, M. Imagawa, *et al.*, "Estrogenic activities of 517 chemicals by yeast two-hybrid assay," *Journal of Health Science,* vol. 46, pp. 282-298, 2000.
[151] D. Pobel, E. Riboli, J. Cornée, H. Bertrand, and M. Guyader, "Nitrosamine, Nitrate and Nitrite in Relation to Gastric Cancer: A Case-Control Study in Marseille, France," *European Journal of Epidemiology,* vol. 11, pp. 67-73, 1995.
[152] S. R. Corporation and C. Associates, "Toxicological Profile for N-nitrosodimethylamine," vol. 755, 1989.
[153] H. Ishibashi, M. Hirano, N. Matsumura, N. Watanabe, Y. Takao, and K. Arizono, "Reproductive effects and bioconcentration of 4-nonylphenol in medaka fish (Oryzias latipes)," *Chemosphere,* vol. 65, pp. 1019-1026, 2006.
[154] M. F. Kirby, A. J. Smith, J. Rooke, P. Neall, A. P. Scott, and I. Katsiadaki, "Ethoxyresorufin-O-deethylase (EROD) and vitellogenin (VTG) in flounder (Platichthys flesus): System interaction, crosstalk and implications for monitoring," *Aquatic Toxicology,* vol. 81, pp. 233-244, 3/10/ 2007.
[155] F. Lahnsteiner, B. Berger, F. Grubinger, and T. Weismann, "The effect of 4-nonylphenol on semen quality, viability of gametes, fertilization success, and embryo and larvae survival in rainbow trout (Oncorhynchus mykiss)," *Aquatic toxicology,* vol. 71, pp. 297-306, 2005.
[156] B. Alfeeli, V. Jain, R. K. Johnson, F. L. Beyer, J. R. Heflin, and M. Agah, "Characterization of poly(2,6-diphenyl-p-phenylene oxide) films as adsorbent for microfabricated preconcentrators," *Microchemical Journal,* vol. 98, pp. 240-245, 2011.
[157] J. J. Johnston, D. A. Goldade, D. J. Kohler, and J. L. Cummings, "Determination of White Phosphorus Residues in Ducks: An Atomic Emission Detection/Compound-Independent Calibration-Based Method of Generating Residue Data for Risk Assessment and Environmental Monitoring," *Environmental Science & Technology,* vol. 34, pp. 1856-1861, 2000/05/01 2000.
[158] C.-J. Lu, W. H. Steinecker, W.-C. Tian, M. C. Oborny, J. M. Nichols, M. Agah, *et al.*, "First-generation hybrid MEMS gas chromatograph," *Lab on a Chip,* vol. 5, 2005.
[159] J. H. Seo, J. Liu, X. Fan, and K. Kurabayashi, "Fabry-Perot cavity sensor-based optofluidic gas chromatography using a microfabricated passive preconcentrator/injector," *Lab on a chip,* vol. 13, pp. 851-859, 03/ 2013.
[160] M. Akbar and M. Agah, "A Microfabricated Propofol Trap for Breath-Based Anesthesia Depth Monitoring," *Journal of Microelectromechanical Systems,* vol. 22, pp. 443-451, 2013.
[161] M. Akbar, D. Wang, R. Goodman, A. Hoover, G. Rice, J. R. Heflin, *et al.*, "Improved performance of micro-fabricated preconcentrators using silica nanoparticles as a surface template," *Journal of Chromatography A,* vol. 1322, pp. 1-7, 12/27/ 2013.
[162] M. Akbar, D. Wang, H. Shakeel, J. R. Heflin, and M. Agah, "A MEMS enabled integrated microgc platform for on-site monitoring of water organic compounds," in *The 17th International Conference on Solid-State Sensors, Actuators and Microsystems : Transducers & Eurosensors XXVII*, 2013, pp. 2759-2762.
[163] S. Narayanan, B. Alfeeli, and M. Agah, "Two-Port Static Coated Micro Gas Chromatography Column With an Embedded Thermal Conductivity Detector," *IEEE Sensors Journal,* vol. 12, pp. 1893-1900, 2012.
[164] E. R. Kuhn, "Water Injections in GC-How Wet Can You Get?," *LC GC NORTH AMERICA,* vol. 20, pp. 474-478, 2002.

[165] K. Grob and A. Habich, "Trace analysis of halocarbons in water; Direct aqueous injection with electron capture detection," *Journal of High Resolution Chromatography,* vol. 6, pp. 11-15, 1983.
[166] U. R. Bernier, C. L. Bray, and R. A. Yost, "Effect of vacuum on the performance of the flame ionization detector used for vacuum-outlet gas chromatography," *Journal of Microcolumn Separations,* vol. 12, pp. 226-235, 2000.
[167] B. Alfeeli and M. Agah, *14th International Conference on Miniaturized Systems for Chemistry and Life Sciences,* pp. 1721-1723, 2010.
[168] M. Akbar and M. Agah, "A cascaded micro preconcentration approach for extraction of volatile organic compounds in water," in *IEEE Sensors*, 2012, pp. 1-4.
[169] M. Careri, G. Mori, M. Musci, and P. Viaroli, "Evaluation of dynamic headspace and purge-and-trap techniques for the high-resolution gas chromatography analysis of nitrous oxide in seawater," *Journal of Chromatography A,* vol. 848, pp. 327-335, 1999.
[170] S. Narayanan and M. Agah, "Fabrication and Characterization of a Suspended TCD Integrated With a Gas Separation Column," *Journal of Microelectromechanical Systems,* vol. 22, pp. 1166-1173, 2013.
[171] H. M. McNair and J. M. Miller, *Basic gas chromatography*: John Wiley & Sons, 2011.
[172] C.-W. Lee and C. P. Weisel, "Determination of Methyl tert-Butyl Ether and tert-Butyl Alcohol in Human Urine by High-Temperature Purge-and-Trap Gas Chromatography-Mass Spectrometry," *Journal of Analytical Toxicology,* vol. 22, pp. 1-5, January 1, 1998 1998.
[173] E. Martínez, S. l. Lacorte, I. Llobet, P. Viana, and D. Barceló, "Multicomponent analysis of volatile organic compounds in water by automated purge and trap coupled to gas chromatography–mass spectrometry," *Journal of Chromatography A,* vol. 959, pp. 181-190, 2002.
[174] J. M. Warner and R. K. Beasley, "Purge and trap chromatographic method for the determination of acrylonitrile, chlorobenzene, 1,2-dichloroethane, and ethylbenzene in aqueous samples," *Analytical Chemistry,* vol. 56, pp. 1953-1956, 1984/09/01 1984.
[175] A. N. Irwin, C. D. Mowry, and T. T. Borek III, "Research into the variables affecting purge and trap collection for a portable field trihalomethane testing unit," 2006.
[176] S. T. Vater, S. F. Velazquez, and V. J. Cogliano, "A case study of cancer data set combinations for PCBs," *Regulatory Toxicology and Pharmacology,* vol. 22, pp. 2-10, 1995.
[177] L. Gao, Q. Song, G. E. Patterson, R. G. Cooks, and Z. Ouyang, "Handheld rectilinear ion trap mass spectrometer," *Analytical chemistry,* vol. 78, pp. 5994-6002, 2006.
[178] L. Li, T.-C. Chen, Y. Ren, P. I. Hendricks, R. G. Cooks, and Z. Ouyang, "Mini 12, Miniature Mass Spectrometer for Clinical and Other Applications Introduction and Characterization," *Analytical chemistry,* vol. 86, pp. 2909-2916, 2014.
[179] A. N. Freedman, "The photoionization detector: Theory, performance and application as a low-level monitor of oil vapour," *Journal of Chromatography A,* vol. 190, pp. 263-273, 1980.
[180] M. Dubois, K. A. Gilles, J. K. Hamilton, P. Rebers, and F. Smith, "Colorimetric method for determination of sugars and related substances," *Analytical chemistry,* vol. 28, pp. 350-356, 1956.
[181] Agilent 490 Micro GC Product Information Page; available via the internet at: http://www.chem.agilent.com/en-US/products-services/Instruments-Systems/Gas-Chromatography/490-Micro-GC/Pages/default.aspx.
[182] Inficon 3000 Micro GC Gas Analyzer Product Information Page; available via the Internet at: http://products.inficon.com/en-us/nav-products/Product/Detail/3000_Micro_GC_Gas_Analyzer?path=Products%2Fpg_ChemicalDetection.
[183] W. C. Tian, H. K. L. Chan, S. W. Pang, C. J. Lu, and E. T. Zellers, "High sensitivity three-stage microfabricated preconcentrator-focuser for micro gas chromatography," 2003, pp. 131-134.
[184] H. H. Hill and D. G. McMinn, *Detectors for capillary chromatography*: Wiley New York, 1992.
[185] R. Pecsar, R. DeLew, and K. Iwao, "Performance of a reduced volume thermal conductivity detector," *Analytical Chemistry,* vol. 45, pp. 2191-2198, 1973.

[186] S. Zimmermann, S. Wischhusen, and J. Müller, "Micro flame ionization detector and micro flame spectrometer," *Sensors and Actuators B: Chemical,* vol. 63, pp. 159-166, 2000.
[187] S. Martin, G. Frye, J. Spates, and M. Butler, "Gas sensing with acoustic devices," in *Ultrasonics Symposium, 1996. Proceedings., 1996 IEEE*, 1996, pp. 423-434.
[188] C. Chen, F. Tsow, K. D. Campbell, R. Iglesias, E. Forzani, and N. Tao, "A wireless hybrid chemical sensor for detection of environmental volatile organic compounds," *Sensors Journal, IEEE,* vol. 13, pp. 1748-1755, 2013.
[189] R. A. Iglesias, F. Tsow, R. Wang, E. S. Forzani, and N. Tao, "Hybrid Separation and Detection Device for Analysis of Benzene, Toluene, Ethylbenzene, and Xylenes in Complex Samples," *Analytical Chemistry,* vol. 81, pp. 8930-8935, 2009/11/01 2009.
[190] Y. Mohsen, H. Lahlou, J.-B. Sanchez, F. Berger, I. Bezverkhyy, G. Weber, *et al.*, "Development of a micro-analytical prototype for selective trace detection of orthonitrotoluene," *Microchemical Journal,* vol. 114, pp. 48-52, 2014.
[191] H. Shakeel and M. Agah, "Self-Patterned Gold-Electroplated Multicapillary Gas Separation Columns With MPG Stationary Phases," *Microelectromechanical Systems, Journal of,* vol. 22, pp. 62-70, 2013.
[192] A Guide to Interpreting Detector Specifications for Gas Chromatographs; available via the Internet at: https://www.chem.agilent.com/Library/technicaloverviews/Public/5989-3423EN.pdf.
[193] M. Akbar, S. Narayanan, M. Restaino, and M. Agah, "A purge and trap integrated microGC platform for chemical identification in aqueous samples," *Analyst,* vol. 139, pp. 3384-3392, 2014.
[194] P. P. Egeghy, R. Tornero-Velez, and S. M. Rappaport, "Environmental and biological monitoring of benzene during self-service automobile refueling," *Environmental Health Perspectives,* vol. 108, pp. 1195-1202, 2000.
[195] F. L. Dorman, J. J. Whiting, J. W. Cochran, and J. Gardea-Torresdey, "Gas Chromatography," *Analytical Chemistry,* vol. 82, pp. 4775-4785, 2010.
[196] A. Boots, A. Smolinska, J. van Berkel, R. Fijten, E. Stobberingh, M. Boumans, *et al.*, "Identification of microorganisms based on headspace analysis of volatile organic compounds by gas chromatography–mass spectrometry," *Journal of breath research,* vol. 8, p. 027106, 2014.
[197] A. Wilson, "Electronic-nose Applications in Forensic Science and for Analysis of Volatile Biomarkers in the Human Breath," *J Forensic Sci Criminol,* vol. 1, p. S103, 2014.
[198] S. Giannoukos, B. Brkić, S. Taylor, and N. France, "Membrane Inlet Mass Spectrometry for Homeland Security and Forensic Applications," *Journal of The American Society for Mass Spectrometry,* pp. 1-9, 2014.
[199] Y.-S. Lin, C.-Y. Kuo, W.-C. Tian, T.-H. Wu, H.-J. Sheen, H.-Y. Kuo, *et al.*, "Batch fabrication of micro preconcentrator with thin film microheater using Tollen's reaction," in *The 17th International Conference on Solid-State Sensors, Actuators and Microsystems (TRANSDUCERS & EUROSENSORS XXVII),* , 2013, pp. 2025-2028.
[200] Y. Mohsen, J.-B. Sanchez, F. Berger, H. Lahlou, I. Bezverkhyy, V. Fierro, *et al.*, "Selection and characterization of adsorbents for the analysis of an explosive-related molecule traces in the air," *Sensors and Actuators B: Chemical,* vol. 176, pp. 124-131, 2013.
[201] B.-X. Chen, T.-Y. Hung, R.-S. Jian, and C.-J. Lu, "A multidimensional micro gas chromatograph employing a parallel separation multi-column chip and stop-flow μGC× μGCs configuration," *Lab on a Chip,* vol. 13, pp. 1333-1341, 2013.
[202] H. Shakeel, G. W. Rice, and M. Agah, "Semipacked columns with atomic layer-deposited alumina as a stationary phase," *Sensors and Actuators B: Chemical,* vol. 203, pp. 641-646, 2014.
[203] H. Shakeel, D. Wang, R. Heflin, and M. Agah, "Width-modulated microfluidic columns for gas separations," *IEEE Sensors Journal,* vol. 14, pp. 3352 - 3357 2014.
[204] A. Wang, S. Hynynen, A. R. Hawkins, S. E. Tolley, H. D. Tolley, and M. L. Lee, "Axial thermal gradients in microchip gas chromatography," *Journal of Chromatography A,* vol. 1374, pp. 216-223, 2014.

[205] E. Covington, F. Bohrer, C. Xu, E. Zellers, and C. Kurdak, "Densely integrated array of chemiresistor vapor sensors with electron-beam patterned monolayer-protected gold nanoparticle interface films," *Lab on a Chip,* vol. 10, pp. 3058-3060, 2010.

[206] C. Chen, F. Tsow, K. D. Campbell, R. Iglesias, E. Forzani, and N. Tao, "A wireless hybrid chemical sensor for detection of environmental volatile organic compounds," *IEEE sensors journal,* vol. 13, p. 1748, 2013.

[207] A. Garg, M. Akbar, E. Vejerano, S. Narayanan, L. Nazhandali, L. C. Marr, *et al.*, "Zebra GC: A mini gas chromatography system for trace-level determination of hazardous air pollutants," *Sensors and Actuators B: Chemical,* vol. 212, pp. 145-154, 2015.

[208] Y. Mohsen, H. Lahlou, J.-B. Sanchez, F. Berger, I. Bezverkhyy, G. Weber, *et al.*, "Development of a micro-analytical prototype for selective trace detection of orthonitrotoluene," *Microchemical Journal,* vol. 114, pp. 48-52, 2014.

[209] B. C. Kaanta, H. Chen, and X. Zhang, "A monolithically fabricated gas chromatography separation column with an integrated high sensitivity thermal conductivity detector," *Journal of Micromechanics and Microengineering,* vol. 20, p. 055016, 2010.

[210] S. Narayanan, G. Rice, and M. Agah, "Characterization of a micro-helium discharge detector for gas chromatography," *Sensors and Actuators B: Chemical,* vol. 206, pp. 190-197, 2015.

[211] Q. Zhong, W. H. Steinecker, and E. T. Zellers, "Characterization of a high-performance portable GC with a chemiresistor array detector," *Analyst,* vol. 134, pp. 283-293, 2009.

[212] M. C. Pietrogrande, M. G. Zampolli, F. Dondi, C. Szopa, R. Sternberg, A. Buch, *et al.*, "In situ analysis of the Martian soil by gas chromatography: Decoding of complex chromatograms of organic molecules of exobiological interest," *Journal of Chromatography A,* vol. 1071, pp. 255-261, 4/15/ 2005.

[213] C. R. Oliveira, A. A. Ferreira, C. J. Oliveira, D. A. Azevedo, E. V. S. Neto, and F. R. A. Neto, "Biomarkers in crude oil revealed by comprehensive two-dimensional gas chromatography time-of-flight mass spectrometry: depositional paleoenvironment proxies," *Organic Geochemistry,* vol. 46, pp. 154-164, 2012.

[214] G. Song, T. Qin, H. Liu, G.-B. Xu, Y.-Y. Pan, F.-X. Xiong, *et al.*, "Quantitative breath analysis of volatile organic compounds of lung cancer patients," *Lung Cancer,* vol. 67, pp. 227-231, 2010.

[215] C. Sottani, B. Porro, M. Comelli, M. Imbriani, and C. Minoia, "An analysis to study trends in occupational exposure to antineoplastic drugs among health care workers," *Journal of Chromatography B,* vol. 878, pp. 2593-2605, 2010.

[216] F. James, P. Breuil, C. Pijolat, M. Camara, D. Briand, A. Bart, *et al.*, "Development of a MEMS Preconcentrator for Micro-gas Chromatography Analyses," *Procedia Engineering,* vol. 87, pp. 500-503, 2014.

[217] M. Camara, P. Breuil, D. Briand, J.-P. Viricelle, C. Pijolat, and N. F. De Rooij, "Preconcentration modeling for the optimization of a micro gas preconcentrator applied to environmental monitoring," *Analytical chemistry,* vol. 87, pp. 4455-4463, 2015.

[218] A. Manz, D. J. Harrison, E. M. Verpoorte, J. C. Fettinger, A. Paulus, H. Lüdi, *et al.*, "Planar chips technology for miniaturization and integration of separation techniques into monitoring systems: capillary electrophoresis on a chip," *Journal of Chromatography A,* vol. 593, pp. 253-258, 1992.

[219] D. J. Harrison, A. Manz, Z. Fan, H. Luedi, and H. M. Widmer, "Capillary electrophoresis and sample injection systems integrated on a planar glass chip," *Analytical chemistry,* vol. 64, pp. 1926-1932, 1992.

[220] S. C. Jacobson, R. Hergenroder, L. B. Koutny, R. Warmack, and J. M. Ramsey, "Effects of injection schemes and column geometry on the performance of microchip electrophoresis devices," *Analytical Chemistry,* vol. 66, pp. 1107-1113, 1994.

[221] M. Li, E. Myers, H. Tang, S. Aldridge, H. McCaig, J. Whiting, *et al.*, "Nanoelectromechanical resonator arrays for ultrafast, gas-phase chromatographic chemical analysis," *Nano letters,* vol. 10, pp. 3899-3903, 2010.

[222] P. Lewis, R. Manginell, D. Adkins, R. Kottenstette, D. Wheeler, S. Sokolowski, *et al.*, "RG manley and GC Frye-Mason," *IEEE Sensors Journal*, vol. 6, pp. 784-795, 2006.
[223] E. Snow, F. Perkins, E. Houser, S. Badescu, and T. Reinecke, "Chemical detection with a single-walled carbon nanotube capacitor," *Science*, vol. 307, pp. 1942-1945, 2005.
[224] D. Janasek, J. Franzke, and A. Manz, "Scaling and the design of miniaturized chemical-analysis systems," *Nature*, vol. 442, pp. 374-380, 2006.
[225] P. J. Chapman, F. Vogt, P. Dutta, P. G. Datskos, G. L. Devault, and M. J. Sepaniak, "Facile hyphenation of gas chromatography and a microcantilever array sensor for enhanced selectivity," *Analytical chemistry*, vol. 79, pp. 364-370, 2007.
[226] A. Bulbul and H. Kim, "A bubble-based microfluidic gas sensor for gas chromatographs," *Lab on a Chip*, vol. 15, pp. 94-104, 2015.
[227] B. Bae, J. Kim, J. Yeom, Q. Chen, C. Ray, and M. Shannon, "Development of a portable gas analyzer using a micro-Gas Chromatograph/Flame Ionization Detector (micro-GC/FID) for NASA's environmental missions," in *42nd International Conference on Environmental Systems, San Diego, California*, 2012, pp. 15-19.
[228] F.-Y. Chen, W.-C. Chang, R.-S. Jian, and C.-J. Lu, "Novel Gas Chromatographic Detector Utilizing the Localized Surface Plasmon Resonance of a Gold Nanoparticle Monolayer inside a Glass Capillary," *Analytical chemistry*, vol. 86, pp. 5257-5264, 2014.
[229] M. Akbar, H. Shakeel, and M. Agah, "GC-on-chip: integrated column and photoionization detector," *Lab on a Chip*, vol. 15, pp. 1748-1758, 2015.

Appendix A: List of Publications

Journal Publications:

1. **M. Akbar**, H. Shakeel and M. Agah, "GC-on-chip: Integrated column and photoionization detector," Lab on a Chip, vol. 15, no. 7, Feb 2014, pp. 1748-1758.
2. A. Garg, **M. Akbar**, E. Vejerano, S. Narayanan, L. Nazhandali, L. Marr and M. Agah, "Zebra GC: A mini gas chromatography system for trace-level determination of hazardous air pollutants," Sensors and Actuator B: Chemical, vol. 212, June 2015, pp. 145-154.
3. **M. Akbar**, S. Narayanan, M. Restaino and M. Agah, "Purge and trap integrated microGC platform for chemical identification in aqueous samples," Analyst, vol. 139, no. 13, June 2014, pp. 3384-3392.
4. **M. Akbar*,** D. Wang*, R. Goodman, A. Hoover, G. W. Rice, J. R. Heflin and M. Agah, "Improved performance of micro-fabricated preconcentrators using silica nanoparticles as a surface template," Journal of Chromatography A, vol. 1322, December 2013, pp. 1-7.
5. **M. Akbar** and M. Agah, "A micro-fabricated propofol trap for breath based anesthesia depth monitoring," IEEE Journal of Microelectromechanical Systems, vol. 22, no. 2, April 2013, pp. 443-451.

Conference Proceedings:

1. **M. Akbar**, H. Shakeel and M. Agah, "An integrated chromatography chip for rapid gas separation and detection" IEEE MEMS 2015-Estoril, Portugal, pp. 771-774.
2. A. Garg, **M. Akbar**, S. Narayanan, L. Nazhandali and M. Agah, "Zebra GC: a fully integrated micro gas chromatography system," IEEE Sensors 2014, October 2014, Valencia, Spain, pp. 673-676.
3. **M. Akbar**, D. Wang, H. Shakeel, J. R. Heflin, and M. Agah "A MEMS enabled integrated micro GC platform for on-site monitoring of water organic compounds," Transducers and EurosensorsXXVII, Barcelona (Spain), June 2013, pp. 2759-2762.
4. D. Wang, **M. Akbar**, J. R. Heflin, and M. Agah "Novel layer by layer silica nanoparticles as an adsorbent bed for micro-fabricated preconcentrators," IEEE Sensors, October 2012, Taipei, Taiwan, pp. 119-122.
5. **M. Akbar** and M. Agah, "A cascaded micro-preconcentration approach for extraction of volatile organic compounds in water," IEEE Sensors, October 2012, Taipei, Taiwan, pp. 915-918.
6. **M. Akbar** and M. Agah, "A golden micro-trap for anesthetic depth monitoring using human breath samples," IEEE MEMS 2012-Paris, France, pp. 906-909.

Appendix B: Attribution

Several colleagues aided in writing and research behind three of my chapters presented in this dissertation. **Dr. Masoud Agah** has served as a principle investigator (PI) throughout the course of this research project. All of these chapters have been written by the author of this dissertation (Muhammad Akbar) except Chapter 3 and Chapter 5. A brief description of different students/professors and their contributions are included here.

Chapter 3: Improved Performance of Micro-Fabricated Pre-concentrators using Silica Nanoparticles as a Surface Template

Chapter 3 was submitted to Journal of Chromatography A. Dr. Dong Wang (currently a postdoctoral student at Electrical Engineering department, Virginia Tech) from Dr. Randy Heflin's group developed LbL process for coating silica nanoparticle inside micro pre-concentrator. Dr. Rice group demonstrated the selective adsorption of polar compounds on silica nanoparticle surface. Dr. Gary Rice helped shape technical discussion for the journal article and also provided valuable editorial comments.

Chapter 4: A Purge and Trap Integrated MicroGC Platform for Chemical Identification in Aqueous Samples

Chapter 4 was submitted to RSC, Analyst. Dr. Shree Narayanan (currently employed at Intel, Inc.) used his previously developed monolithic integrated column and thermal conductivity detector chip for the separation and detection of volatile organic compounds.

Chapter 5: Zebra GC-A Mini Gas Chromatography System for Trace-Level Determination of Hazardous Air Pollutants

Chapter 5 was submitted to Sensors and Actuators B: Chemical. Mr. Apoorva Garg was lead author of this chapter (currently employed at Bloomberg). The role of the author of this dissertation (Muhammad Akbar) was to fabricate the microfabricated pre-concentrator, its characterization and writing technical discussion for explaining the results.

Chapter 6: GC-on-Chip: Integrated Column and Photo Ionization Detector

Chapter 6 was submitted RSC, Lab on a Chip. Previously developed atomic layer deposition (ALD) technique by Dr. Hamza Shakeel (NIST) was used for the separation purpose.